KONINKLIJKE NEDERLANDSE AKADEMIE
VAN WETENSCHAPPEN

PROCEEDINGS

SERIES B

PHYSICAL SCIENCES

VOLUME LXII

No. 5

1959
NORTH-HOLLAND PUBLISHING COMPANY
(N.V. NOORD-HOLLANDSCHE UITGEVERS MAATSCHAPPIJ)
AMSTERDAM

The complete Proceedings consist of three Series, viz.:

SERIES A: MATHEMATICAL SCIENCES

SERIES B: PHYSICAL SCIENCES

SERIES C: BIOLOGICAL AND MEDICAL SCIENCES

Articles for these Series cannot be accepted unless formally communicated for publication by one of the members of the Royal Neth. Academy of Sciences.

CRYSTALLOGRAPHIC STUDIES ON SOME "COENZYMES Q"

BY

CAROLINE H. MacGILLAVRY

(Communicated at the meeting of September 26, 1959)

1. A few years ago, Dr. R. L. LESTER of Wisconsin University sent me for X-ray investigation a number of samples of substances, isolated from various sources, to which the collective name of coenzymes Q has been given (LESTER c.s. 1958). At the time, little was known about these compounds, and in particular, their molecular weights were still doubtful.

The crystals are orange-yellow coloured, of tabular habit and irregular shape; two prevalent edges are nearly perpendicular.

Although the quality of the tiny crystals was mostly poor, it was possible to make some single crystal X-ray diagrams in a Weissenberg camera, from which the cell constants could be determined. The crystals were found to be triclinic, pseudo-monoclinic, and frequently twinned. Densities were measured by the flotation method and from these data and the cell constants the molecular weights of the substances were found, assuming two molecules per unit cell. Preliminary values of these molecular weights have been reported by LESTER e.a. (1958, 1959). The cell constants have since been refined by least-squares; the results are given in Table I.

TABLE I

Cell constants, densities and molecular weights of Coenzymes *Q* from different sources

	Beef Heart mitochondria	Torula utilis	Azotobacter vinelandii
a	6.19 ± 0.08 A	6.2 ± 0.15 A	6.18 ± 0.08 A
b	59.5 ± 0.4 A	54.85 ± 0.9 A	50.1 ± 0.6 A
c	7.8 ± 0.1 A	7.78 ± 0.04 A	7.79 ± 0.04 A
d_{010}	56.9 ± 0.4 A	52.45 ± 0.9 A	47.9 ± 0.6 A
α	(91°) *	91 ± 1°	91 ± 1°
β	(89°)	89 ± 1°	89 ± 1°
γ	73 ± 1°	(73°)	73 ± 3°
density . . .	1.09	1.085	1.083 gr/cm^3
molecular weights:			
$M_{X\text{-rays}}$ . . .	900	820	750
$M_{calc.}$	863	795	727

* values between brackets are by analogy rather than actually measured.

(Since d_{010} is by far the largest spacing, the b-axis could have been chosen in such a way that the cell would be more nearly an orthogonal parallelepiped. The axes in Table I were chosen so as to obtain as close a relation as possible to the subcell discussed below.)

It is seen that the molecular weights thus determined are consistently somewhat higher than the values calculated from the structure formula I which has since been established for coenzyme Q (Wolf e.a. 1958, Morton e.a. 1958).

(I)

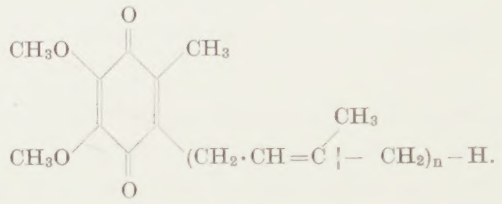

In this formula, n, the number of isoprene groups in the long chain, can have values varying from 6 to 10, dependent on the source from which the coenzyme is isolated. For the substances described in this study, the following values for n have been given.

Beef heart mitochondria	n = 10
Torula utilis	n = 9
Azotobacter vinelandii	n = 8.

2. From the cell constants of the three compounds studied by us, it is seen that their crystal structures must be very similar. This is also evident directly from the X-ray diagrams which show similar very characteristic intensity distributions. Moreover, all films indicate that the contents of the unit cells have a very pronounced pseudo-periodicity. The clusters of strong reflections define a "subcell" (Patterson, 1931, Vand, 1951) which bears the following relation to the cells defined in Table I.

subcell	true cell
[100]	[100]
[010]	[021]/p, where p is such that $b_{subcell}$ is about 4.8 A.
[001]	[001]
(100)	(100)
(010)	(0, p/2, 0)
(001)	(0, —1/2, 1)

This subcell, which is common to the three compounds, reveals the periodicity of their isoprene chains. It can thus be concluded that practically all the isoprene units have the same configuration and even conformation.

It is interesting to compare the dimensions of this subcell with those of β-guttapercha (Bunn, 1942), Table II.

The very close relation of the cell dimensions suggests a stacking of the same elements. This would mean that the isoprene chains in coenzyme

TABLE II

Comparison of cell dimensions etc. of

	Coenzyme Q subcell	β guttapercha
a	6.18 A	11.78 A
d_{100}	5.92 A	5.89 A (1/2 a)
b	4.8 A	4.72 A
c	7.79 A	7.78 A
α	87°	90°
β	89°	90°
γ	73°	90°
space group .	$P\bar{1}$ (?)	$P2_12_12_1$
number of molecules per cell . .	2	4

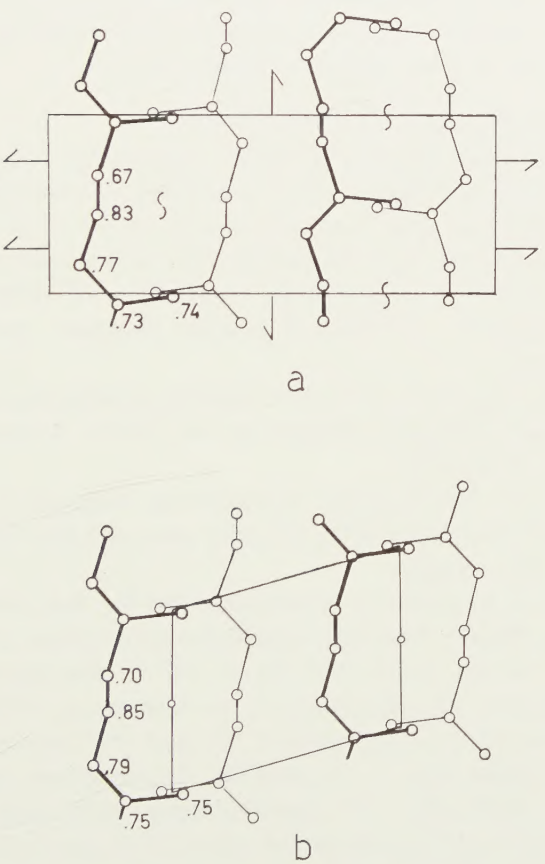

Fig. 1. *a*. Structure of β guttapercha according to Jeffrey (1944), with origin shifted so as to conform with *b*. *b*. Proposed structure for the subcell of coenzyme *Q*.

Q have the same configuration and conformation as those in β-guttapercha, i.e. *all-trans* across the double bonds and non-planar with respect to the single bonds. Taking the coordinates of the atoms in the β-gutta unit as given by JEFFREY (1944), a tentative structure for the subcell of coenzyme Q was set up (fig. 1*a* and *b*), and subcell structure factors were calculated for a number of reciprocal nodes corresponding to this subcell. The agreement with experiment is only fair, as could be expected since the whole quinone part of the molecule is neglected in these calculations. But it seems that the model could be approximately correct for the "tails" of the molecules. In any case, there is little doubt about the *all-trans* configuration in the isoprene chains of these compounds. It is known that in rubber, with cis-configuration, the overall length of the isoprene unit is markedly shorter than 4.7 A. It is suggested that an X-ray investigation of the compounds described as ubiquinones by MORTON e.a. (see for example MORTON, 1958a) might reveal whether they have the same chain-configuration as the coenzymes Q. With respect to this it may be of interest that a "ubiquinone" prepared by Professor E. C. SLATER of this University gave a powder diagram undistinguishable from that of the coenzyme Q from beef heart mitochondria.

3. *Experimental details* (with A. KREUGER).

Q 275 from beef heart [1]). Crystals repeatedly twinned on (010). Abnormal interference figure under polarising microscope. Weissenberg diagrams of zero and first layer about axis of 7.8 A (c-axis).

M 4 from beef heart. Less frequently twinned, unmistakably triclinic. Identity with Q 275 was proved by comparison of (010) reflections on Weissenberg diagram, and also of powder diagrams made in Guinier–de Wolff camera.

Weissenberg diagrams as for Q 275. The long spacing d_{010} was determined from an oscillation diagram flanked by two Debye Scherrer diagrams of Al-powder for calibration.

1–30–4 B 4 from Torula utilis. Weissenberg diagrams of only slightly twinned crystal about axis 6.2 A (a-axis), zero and first layer line. Optics the same as next sample.

3–4–3 L from Azotobacter vinelandii. By far the best crystals, but still very tiny. Optics: Vibration directions in the plane (010) at an angle of about 17° to the a-axis and about 16° to the c-axis respectively. Interference figure: one binormal at the border, n_γ within the field of vision (aperture 0.85), at azimuths of 80° and $-9°$ respectively from the a-axis. From these data it is possible to construct the axial plane. (010): $n_\gamma = 33°$, (010): $Bn^I = 37°$ approximately. Axial angle 2V about 90°. X-rays: Weissenberg diagrams about axis 6.18 A, zero and first layer line.

The X-ray apparatus used was put at the disposal of the author by the Netherlands Organisation for Pure Research (Z.W.O.).

[1]) Sample numbers as given by R. L. LESTER.

REFERENCES

Bunn, C. A., Proc. Roy. Soc. A **180**, 40 (1942).

Jeffrey, G. A., Trans. Far. Soc. **40**, 517 (1944).

Lester, R. L., F. L. Crane and Y. Hatefi, J. Am. Chem. Soc. **80**, 4751 (1958).

————, Y. Hatefi, C. Widmer and F. L. Crane, Biochim. Biophys. Acta **33**, 169 (1959).

Morton, R. A., U. Gloor, O. Schindler, G. M. Wilson, L. H. Chopard-dit-Jean, F. W. Hemming, O. Isler, W. M. F. Leat, J. F. Pennock, R. Ruegg, U. Schwieter and O. Wiss, Helv. Chim. Acta **41**, 2343 (1958).

————, Nature **182**, 1764 (1958*a*).

Patterson, A. L., Z. Kristallogr. **76**, 187 (1931).

Vand, V., Acta Cryst. **4**, 104 (1951).

Wolf, D. E., C. H. Hoffman, N. R. Trenner, B. H. Arison, G. H. Shunk, B. O. Linn, J. F. McPherson and K. Folkers, J. Am. Chem. Soc. **80**, 4752 (1958).

INFLUENCE OF THE IRRADIATION TEMPERATURE ON THE POSITION OF THE F-BAND IN MIX-CRYSTALS OF KCl AND NaCl

BY

E. OTTENS, A. J. ELAND [1]) AND W. G. BURGERS

(Communicated at the meeting of September 26, 1959)

Summary

The position of the F-band is measured for mix-crystals of NaCl and KCl, obtained by quenching from the homogeneous state. Measurements are made on crystals X-rayed both at room temperature and at the temperature of liquid air. Also the absorption is measured at both temperatures. A special attachment for the Beckman-spectrophotometer is described, which enables such measurements to be carried out.

It was found that for the mix-crystals the position of the F-band is dependent on the temperature at which the crystals are irradiated, the maximum lying at shorter wave-length (difference about 10–15 mμ) for irradiation at liquid air temperature as compared to irradiation at room temperature. Such a shift is *not* observed for the pure crystals: here the position of the band is independent of the irradiation temperature.

For mix-crystals irradiated at liquid air temperature the F-band lies between that for pure NaCl and pure KCl. The "anomalous" position of the maximum of a 10 NaCl/90 KCl crystal irradiated at room temperature as observed by Gnaedinger (position at a longer wave-length than that for pure KCl) disappears for irradiation at liquid air temperature.

1. *Introduction*

For some years the decomposition of mix-crystals of NaCl and KCl has been studied in this laboratory. It is well-known that below 500° C the mutual solubility is limited and decreases with decreasing temperature. X-ray and thermodynamic investigations concerning the phenomena accompanying the decomposition were carried out by several investigators, in particular by TICHELAAR (1956), who also discussed literature up to that time.

We have started an examination of F-centers in mix-crystals, because such centers may be expected to be sensitive to changes in ion configuration in their immediate neighbourhood [2]). On the other hand it

[1]) Now at Philips Research Laboratories, Eindhoven.

[2]) See e.g. the theoretical considerations of GNAEDINGER (1953) on the "structure" of F-bands, in which the author considered them to be built up of seven "elementary" bands, due to halogen vacancies with different surroundings, viz. 6 $Na^{\bullet}$, 5 $Na^{\bullet}$ + 1 $K^{\bullet}$, 4 $Na^{\bullet}$ + 2 $K^{\bullet}$, . . . 6 $K^{\bullet}$.

may be concluded from Tichelaar's work that at temperatures slightly under the solubility line the decomposition takes place by displacements of the cations without essentially breaking up the single crystal structure. In its first stages such a process would involve an enrichment in number of equal ions (either Na or K) in small lattice regions [1]). This would influence the energy levels of the electrons in the F-centers and therefore the position of the corresponding F-bands. For this reason it seems possible that the behaviour of the F-bands might lead to a closer understanding of the decomposition mechanism.

Up to now, however, we have only studied the formation and the position of F-bands in the homogeneous mix-crystals. The only author, as far as we know, who reported on the subject, is GNAEDINGER (1953). In this paper measurements are given concerning the position of the F-band in mix-crystals of KCl and RbCl, which salts form a continuous series of stable solid solutions. It was found that the positions of the maxima were intermediate between those of the pure components. This is what one would expect on account of a rule given by MOLLWO (1933), according to which the position of the maximum of the F-band, at a given temperature of the crystal, only depends on the lattice constant d according to the relation $\lambda_{max} = \text{const. } d^2$. Gnaedinger's paper also contains measurements concerning a metastable quenched mix-crystal of NaCl and KCl of composition 10 NaCl/90 KCl (mol. %). Most remarkably for this crystal, the F-band was situated on the "wrong" side of the F-band of pure KCl, viz. at a longer wave-length and therefore outside the range between the F-band of pure NaCl and pure KCl.

It should be noted that in these experiments the crystals were X-rayed at room temperature. We thought it of interest to irradiate also at lower temperatures. For this purpose a special attachment to a Beckman-spectrophotometer was constructed, the description of which is given in the following section.

2. *Experimental*

The spectrophotometer used was a Beckman-instrument, model DU. The cell-holder of this instrument was replaced by a special attachment (cf. fig. 1) in order to adapt the instrument to our measurements. This apparatus had to meet the following requirements:

a) Irradiation and measurement had to be possible at any temperature between that of liquid air and of about 150° C.

b) Condensation of water vapour on the crystal had to be avoided absolutely, because even traces of water have a decomposing effect on the metastable mix-crystals.

---

[1]) Indications based on X-ray diffraction effects, obtained by KLOOTWIJK and TIEDEMA (1958), made it probable that a certain degree of ordening is present in the distribution of the Na- and K-ions in a decomposed 50–50 crystal.

This necessitated irradiation of the crystal in vacuum. In fig. 2 a sectional view of the apparatus is given. The vacuum cryostat consists of a stainless steel dewar flask A, mounted on a square metal plate B. By means of this plate it is possible to position the cryostat accurately in the photometer as well as in the irradiation-house attached to the X-ray tube.

The original cell compartment of the photometer is replaced by the metal box C. As will be described in section 3, for each measuring-point it is necessary to adjust the intensity of the incident light-beam. For this purpose the sample has to be taken out of the light-beam and replaced by a calibrating opening. To make this possible the cryostat is fastened to a carriage D, rolling on a number of steel balls E lying in "V" grooves.

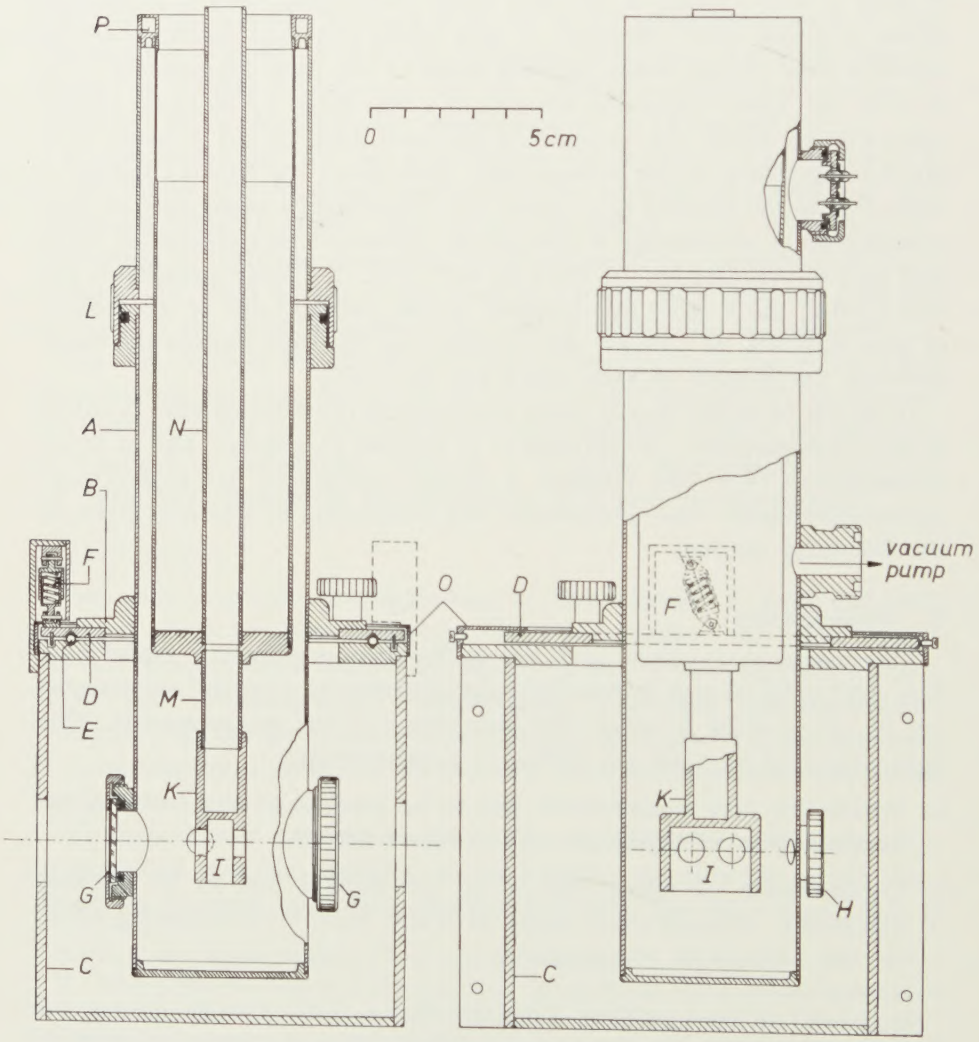

Fig. 2. Sectional view of the apparatus.

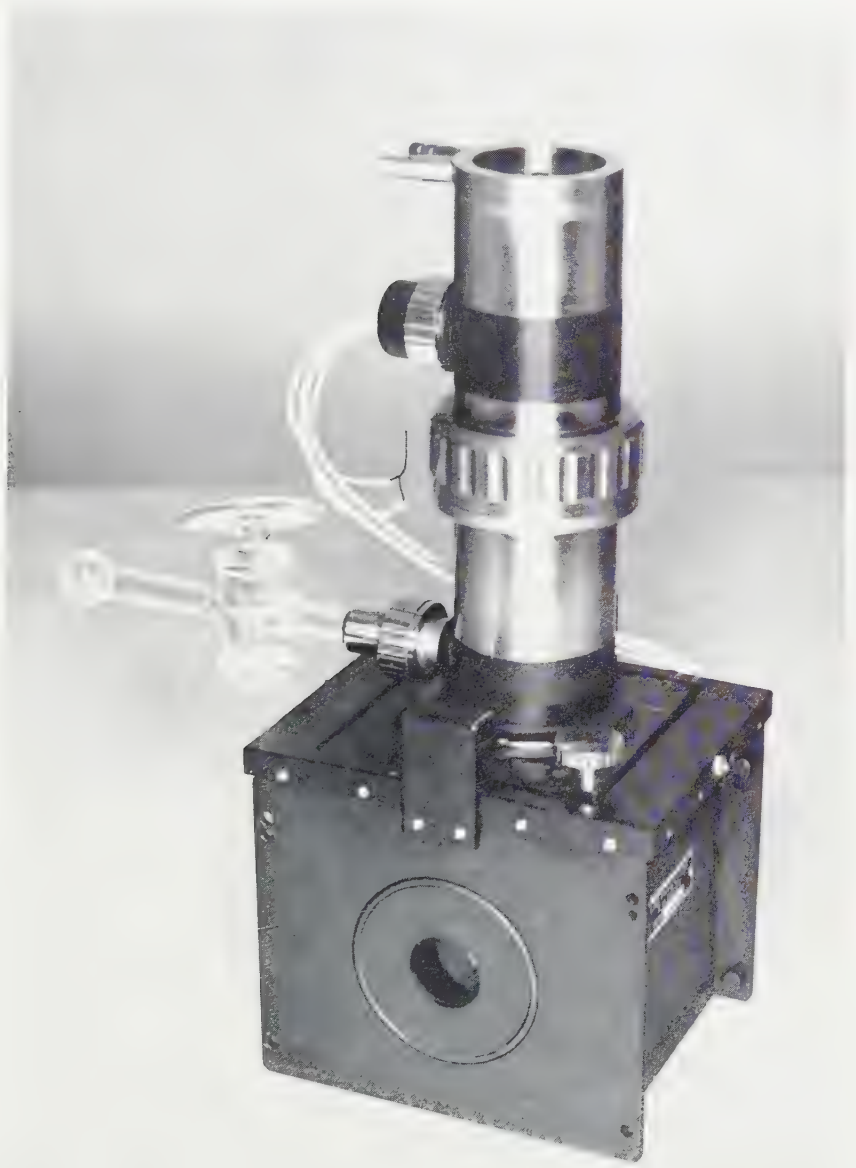

Fig. 1. Attachment adapted to the Beckman-spectrophotometer for X-ray irradiation and absorption measurement of crystals at various temperatures.

The slide is pressed down on the steel balls by two spiral springs F. In this way a "tumbler-action" is obtained giving two reproducible positions bringing either the crystal or the calibrating opening in the light-beam. At the bottom the dewar flask is equipped with two quartz windows G, allowing light transmission through the crystal. The holder with the crystal (cf. fig. 3) is inserted in opening I of the copper house K and locked with a small screw.

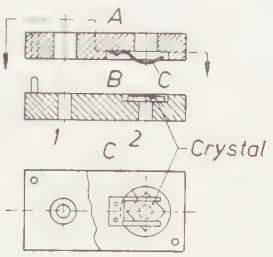

Fig. 3. Crystal-holder.

The crystal can be irradiated through the plastic-foil window H by rotating the crystal-holder 90 degrees by means of the joint at L (sealed by an "O" ring).

The copper house K is fixed to the bottom of the liquid-air container by means of a stainless steel tube M, while, in a straight line with M, a brass tube N is fitted. By inserting a copper rod in this tube down to the bottom, a good heat-exchange is obtained between the copper house K and the liquid air. By replacing the copper rod by a small electric furnace (a glass tube containing a small heating-element at the bottom) any temperature from $-180°$ C to about 150° C can be obtained in a few minutes. The low thermal conductivity of the stainless steel tube M keeps heat-loss down. E.g. only 5 watts are required for maintaining a temperature of 0° C.

The temperature was measured by a copper-constantane thermocouple, the leads of which were brought out uninterrupted through kovar seals with hollow inlets, thus preventing undesired thermal potentials. Because the photometer was fitted out with a photomultiplyer tube, which was light-sensitive to a high degree, it was important to keep out any light. This was achieved by enveloping slide D, as it were, in a flat box O having a play of a few tenths of mms. Moreover all internal parts were painted black with camera lacquer.

The inner mantle of the dewar flask was made as thin as possible at its top in order to keep heat-supply through the metal cylinder as low as possible. Nevertheless a circular chamber P, containing a small heating-element, was necessary to keep the temperature of the top of the dewar flask above 0° C.

The crystal-holder (cf. fig. 3) consists of two brass blocks A and B, each

containing two openings, 1 and 2, of equal diameters. The crystal plate is laid upon opening 2. Then block A is placed as a cover on B. The crystal is fixed by two small springs C. In order to insert the crystal-holder in the copper house K (cf. fig. 2), the dewar is dismounted at L.

3. *Measurement*

As we wanted to measure the absorption caused by the F-centers, the absorption of the non irradiated crystal had to be subtracted from the absorption of the coloured crystal. To achieve this for a chosen wave-length, slide D is first placed in the position in which the light passes through opening 1 of the specimen holder (intensity $I_0 = 100$). D is then shifted to its other position in which the light passes opening 2, and thus passes through the crystal (intensity I). In this way the absorption, given by the optical density $D = \ln I_0/I$, is determined both for the non-irradiated and for the irradiated crystal. At the same time a possible difference in the diameters of the openings 1 and 2 is eliminated from the measurement.

The X-radiation originated from a tungsten tube, run at 47 KV and 17 mA. The duration of each exposure was 30 minutes. The crystal plates had dimensions of approximately $4 \times 3 \times 0.5$ mm^3.

4. *Preparation of crystals*

The mix-crystals were prepared in the same way as described by Tichelaar (1956). Known quantities of NaCl and KCl (Brocades p.a.) were mixed in the pulverized state and then melted in a porcelain crucible in an electric furnace. The melt was cooled slowly to a temperature close below the solidus-line and kept there for about two days to homogenize. It was then cooled slowly to about 550° C (the top of the solubility curve lies at about 500° C) and finally quenched to room temperature. The cleaved parts thus obtained were single crystals; they were kept in an exsiccator with P_2O_5. All further manipulations were carried out in dry air, to prevent decomposition. For a short time the crystals can be protected against humidity by immersion in zapon varnish, diluted with amylacetate, by which process they become covered by a thin layer of lacquer. The compositions were determined by X-rays, using the relationship between lattice parameter and composition as given by Bunk and Tichelaar (1953). Crystals were prepared with the following compositions (in mol. % NaCl/KCl): 100/0, 88/12, 65/35, 53/47, 39/61, 18/82, 9/91, 0/100.

5. *Results*

Distinct bands, lying in the range of wave-lengths expected for F bands, were observed for mix-crystals with compositions not too far from the pure components, namely for 9/91, 18/82 and 88/12 NaCl/KCl. Crystals with compositions nearer to the aequimolecular composition

either did not show such bands or they were very unstable [1] [2].

As an example we show in fig. 4 the absorption spectrum for the composition 88 NaCl/12 KCl. The figure shows four curves, obtained with two crystals. Crystal I was X-rayed at room temperature (about 20° C), crystal II at −180° C. For both crystals the absorption was measured at −180° C and at 20° C.

The figure first of all shows the well-known fact, characteristic for an F-band, that its maximum shifts to a longer wave-length with increasing

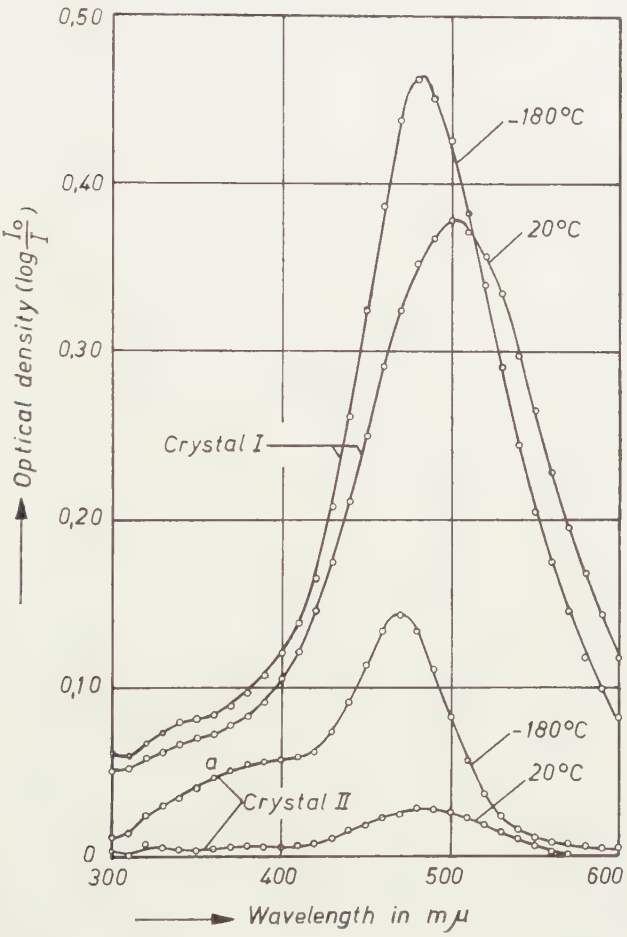

Fig. 4. Absorption spectrum of two X-rayed mix-crystals with composition 88 NaCl/12 KCl. Crystal I: X-rayed at 20° C. Crystal II: X-rayed at —180° C. The absorption of both crystals was measured at —180° C and at 20° C.

---

[1] For the system KCl-RbCl it was found by Gnaedinger (1953) that the more the composition approaches 50-50, the larger the half-width of the F-band.

[2] Moreover, most crystals showed an "abnormal" band at about 420 mμ, discussed by Halperin and Schlesinger (1959) and by Ottens *et al.* (1959). As shown in the last-mentioned paper, the intensity of this band was lower when irradiated at room temperature.

temperature of the absorption measurement, while at the same time the band-width increases. The first fact is a direct consequence of Mollwo's rule (cf. section 1) in connection with the thermal dilation of the crystal lattice, the second is due to the increased thermal lattice vibrations.

Moreover it appears that the position of the maximum is dependent on the temperature at which the crystal is irradiated, the maximum lying at a shorter wave-length for the crystal X-rayed at $-180°$ C as compared with the crystal X-rayed at room temperature. The shift due to this cause amounts to about 10–15 mμ. A similar dependence of the maximum on the temperature of irradiation is *not* found for the crystals of the pure components and it is therefore characteristic for the solid solution state.

In fig. 5 a graph is given of all the maxima measured as a function of composition, and the data are put together as well in Table I.

TABLE I

Wave-length of the maxima in the F-bands in NaCl-KCl mix-crystals as function of composition, temperature of irradiation and temperature of measurement

Composition mol. % NaCl	X-rayed at	Measured at 20° C	Measured at —180° C
100 (NaCl)	20° C	462	450
	—180° C		
88	20° C	495	480
	—180° C	485	470
18	20° C	565	540
	—180° C	550	532
9	20° C	567	544
	—180° C	552	534
0 (KCl)	20° C	557	540
	—180° C		

6. *Discussion*

An inspection of fig. 5 and Table I learns that for crystals X-rayed at liquid air temperature the positions of the maxima found for the mix-crystals lie *between* those of the pure components. This holds good independent of the temperature of measurement. The "anomaly" observed by Gnaedinger (cf. section 1) does not occur for irradiation at low temperature. Our results confirm Gnaedinger's finding for crystals irradiated at room temperature: under these circumstances both the crystals with composition 9 NaCl/91 KCl and those with 18 NaCl/82 KCl have an F-band with a maximum wave-length larger than that belonging to pure KCl.

It seems therefore that irradiation at liquid air temperature produces a different state in a mix-crystal, possibly different surroundings of the

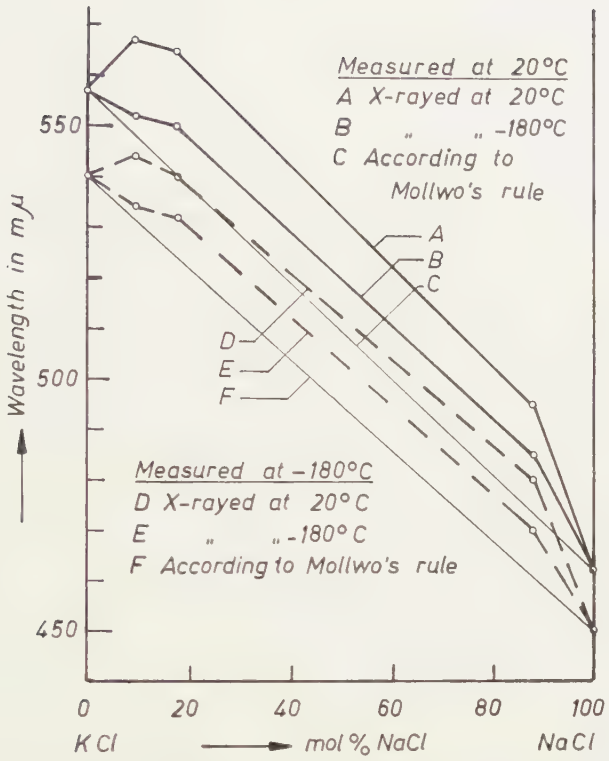

Fig. 5. Position of the maxima in the F-bands in X-rayed NaCl-KCl mix-crystals as function of composition, temperature of irradiation and temperature of measurements.

F-center, as compared with the state produced by irradiation at higher temperature [1]). As mentioned in section 1, it might be expected that such a change influences the position of the F-band.

As already stated in section 1, an intermediate position of the F-band maxima for the mix-crystals, relative to that of the components, can be expected on account of Mollwo's rule in connection with the continuous increase of lattice constant from pure NaCl to pure KCl. If this rule would be the only determining factor, then, considering the linear increase of the lattice constant and the fact that the total change amounts to only 10 %, one might expect that in first approximation the position of the maximum of the F-band would also vary in a linear way with the composition (cf. fig. 5). It is evident that the actually observed maxima do not coincide with the calculated ones: the former all lie at longer wavelengths. This again is an indication that for the mix-crystals the lattice constant is not the only determining factor and points anew to an influence of the actual surroundings of the F-centers.

In this connection it is of interest to notice that Mollwo's rule cor-

[1]) In a discussion with Professor W. Dekeyser of Ghent this possibility was raised by him.

responds fairly well with the change in position of the F maximum found for various pure alkali salts at normal concentrations of F-centers. However, measurements of KAISER (1952) on evaporated salt films show that for excessive concentrations of halogen-vacancies the F-band shifts over about 120 Å (12 mμ) in the direction of shorter wave-length. According to SEITZ (1954) one may assume in such a case that already in the first shell of halogen ions, surrounding a given halogen-vacancy, a halogen-ion is missing. The surroundings of each F-center would be disturbed in this way and this might be the cause of the observed shift.

From fig. 4 it may be concluded that the percentage of F-centers, disappearing by thermal bleaching (by increasing the temperature of the crystal from liquid air temperature up to room temperature), is much larger for the crystal X rayed at $-180°$ C (crystal II) than for the crystal X rayed at 20° C (crystal I). As it may be assumed that the disappearance is mainly due to the recombination with V_1-centers (positive ion-vacancy plus an electron-hole) and as the number of recombinations will be proportional to the number of V_1 centers present, it seems probable that irradiation at $-180°$ C produces more V_1-centers than irradiation at room temperature. This is actually observed for KCl crystals (DORENDORF (1950) (1951)). For mix-crystals the "shoulder" (a) in fig. 4 at about 360 mμ points to the same conclusion.

Laboratory of Physical Chemistry,
Technological University, Delft,
The Netherlands

REFERENCES

BUNK, A. J. H. and G. W. TICHELAAR, Proc. Kon. Ned. Akad. v. Wetensch., Amsterdam **B 56**, 375 (1953).

CASLER, R., P. PRINGSHEIM and P. YUSTER, J. Chem. Phys. **18**, 887 (1950).

DORENDORF, H., Z. Phys. **128**, 166 (1950); **129**, 317 (1951).

GNAEDINGER Jr., R. J., J. Chem. Phys. **21**, 323 (1953).

HALPERIN, A. and M. SCHLESINGER, J. Chem. Phys. **30**, 339 (1959).

KAISER, R., Z. Phys. **132**, 482 (1952).

KLOOTWIJK, P. H. and T. J. TIEDEMA, Proc. Kon. Ned. Akad. v. Wetensch., Amsterdam **B 61**, 188 (1958).

MOLLWO, E., Z. Phys. **85**, 56 (1933); according to H. F. IVEY, Phys. Rev. **72**, 341 (1941), $\lambda_{max} = \text{const.}\ d^{1.84}$.

OTTENS, E., A. J. ELAND, H. B. ZEEDIJK and W. G. BURGERS, these Proceedings **B 62**, 277 (1959).

SEITZ, F., Rev. Mod. Physics **26**, 42–43 (1954).

TICHELAAR, G. W., Thesis Delft 1956. See also W. G. BURGERS and G. W. TICHELAAR, Proc. Kon. Ned. Akad. v. Wetensch., Amsterdam **B 57**, 73 (1954).

ABSORPTION BAND AT 420 mμ IN X-RAY COLOURED KCl-CRYSTALS AND IN MIX-CRYSTALS OF KCl AND NaCl

BY

E. OTTENS, A. J. ELAND [1]), H. B. ZEEDIJK AND W. G. BURGERS

(Communicated at the meeting of September 26, 1959)

Summary

In X-rayed crystals of KCl and in mix-crystals of NaCl and KCl an absorption band has been observed at a wave-length of about 420 mμ. The presence of this band is probably due to some unknown impurity in the crystals. The measurements confirm the observation of HALPERIN and SCHLESINGER (1959) that the intensity of the band is highly dependent on the thermal pre-treatment of the crystals; moreover it is unstable at room temperature.

1. Recently HALPERIN and SCHLESINGER (1959) reported the appearance of a thus far not-observed absorption band at about 420 mμ in X-rayed KCl-crystals which had been heat-treated (kept at 500° C during several hours) before irradiation. The intensity of the band, as compared with the normal F-band, was markedly dependent on the thermal pre-treatment. The band could be bleached by irradiation at its own wave-length under formation of additional F-centers, and vice versa. Thermal bleaching has been observed as well. According to the authors, a correlation seems to exist between the new absorption band and the thermoluminescence of the crystals.

2. Apparently we had come across the same band in the course of an investigation of F-centers in X-ray coloured mix-crystals of NaCl and KCl [2]). As an example fig. 1 shows the absorption of a mix-crystal with composition (in mol. %) 9NaCl/91KCl, obtained after melting the components together in a porcelain crucible and after quenching from a temperature above the solubility curve (cf. TICHELAAR (1956). The crystal was irradiated and the absorption measured at −180° C. In this case a maximum is present at about 420 mμ, which is much higher than that at 530 mμ, due to the F-centers.

---

[1]) Now at Philips Research Laboratory at Eindhoven.

[2]) Cf. OTTENS, ELAND and BURGERS (1959). In this paper also details of the experimental method are given.

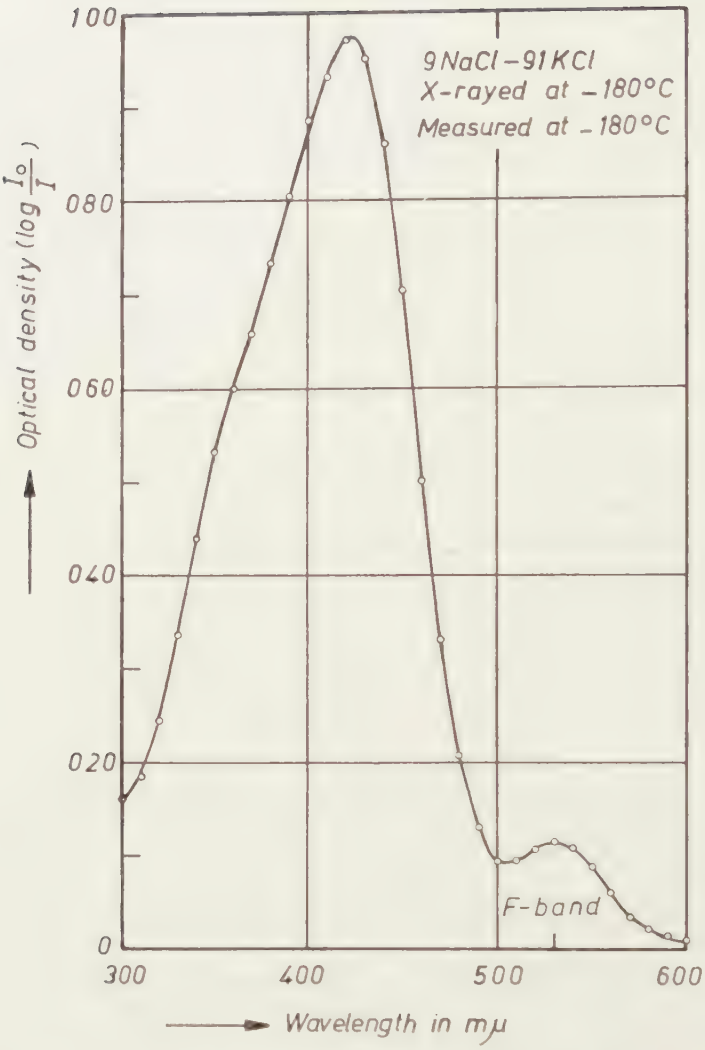

Fig. 1. Absorption-curve of mix-crystal 9 NaCl/91 KCl (mol. %). X-rayed and measured at —180° C. Strong 420 mμ band.

As mix-crystals with various other compositions, prepared from the same material (Brocades p.a.), showed a band at approximately the same wave-length, we thought at first that its occurrence was characteristic for the solid solution state. This, however, appeared not to be the case. The band was also observed in crystals of KCl used for the preparation of the mix-crystals. This is shown in fig. 2, again for irradiation and measurement at —180° C. The two curves correspond to a) a crystal quenched from 550 C and b) a slowly cooled crystal. The pronounced difference between the two curves confirms the conclusions of Halperin and Schlesinger that the intensity of the band is strongly dependent on the thermal pre-treatment of the crystals. It also confirms the existence

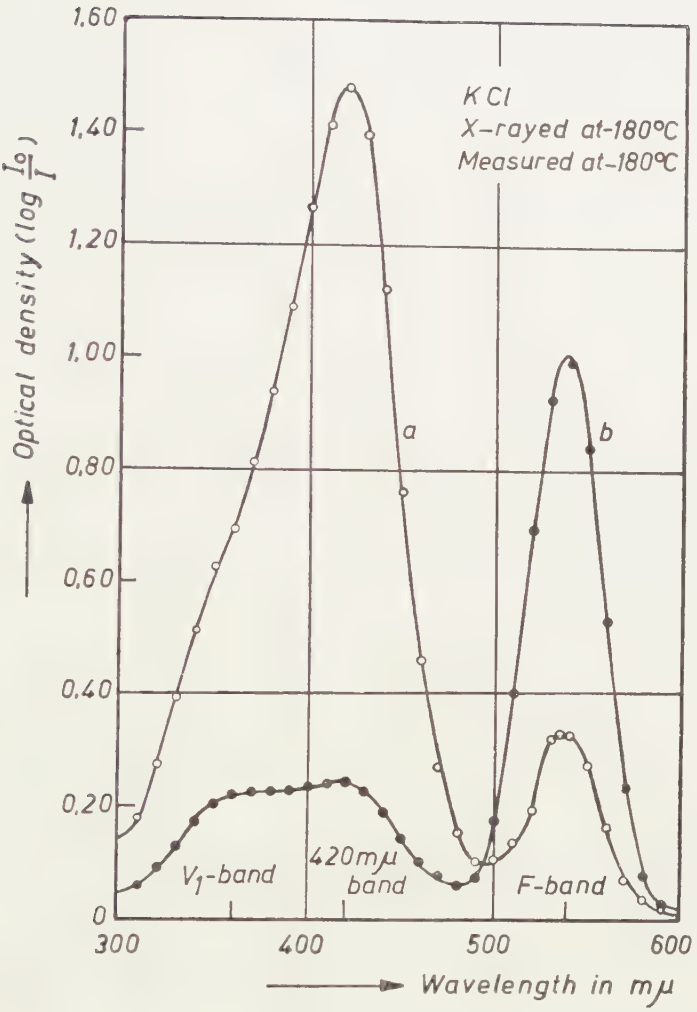

Fig. 2. Absorption-curve of two X-rayed KCl-crystals. X-rayed and measured at —180° C. Curve *a*: crystal quenched from 550° C: 420 mμ band strong, F-band weak. Curve *b*: crystal slowly cooled: 420 mμ band weak, F-band strong.

of an interrelation between the 420 mμ-band and the F-band, in the sense that the one is stronger in case the other is weaker.

3. In the course of our work we had also obtained KCl-crystals (prepared from material of unknown origin) which did not show a trace of the new band, although the crystals were quenched from 500° C. This raised the question whether its presence was solely an effect of thermal pre-treatment, or whether also the purity of the material played a part. In our method of preparation the possibility could not be wholly excluded that some "impurity" might have been introduced into the melt. We therefore prepared crystals (from KCl, Brocades p.a.) under such pre-

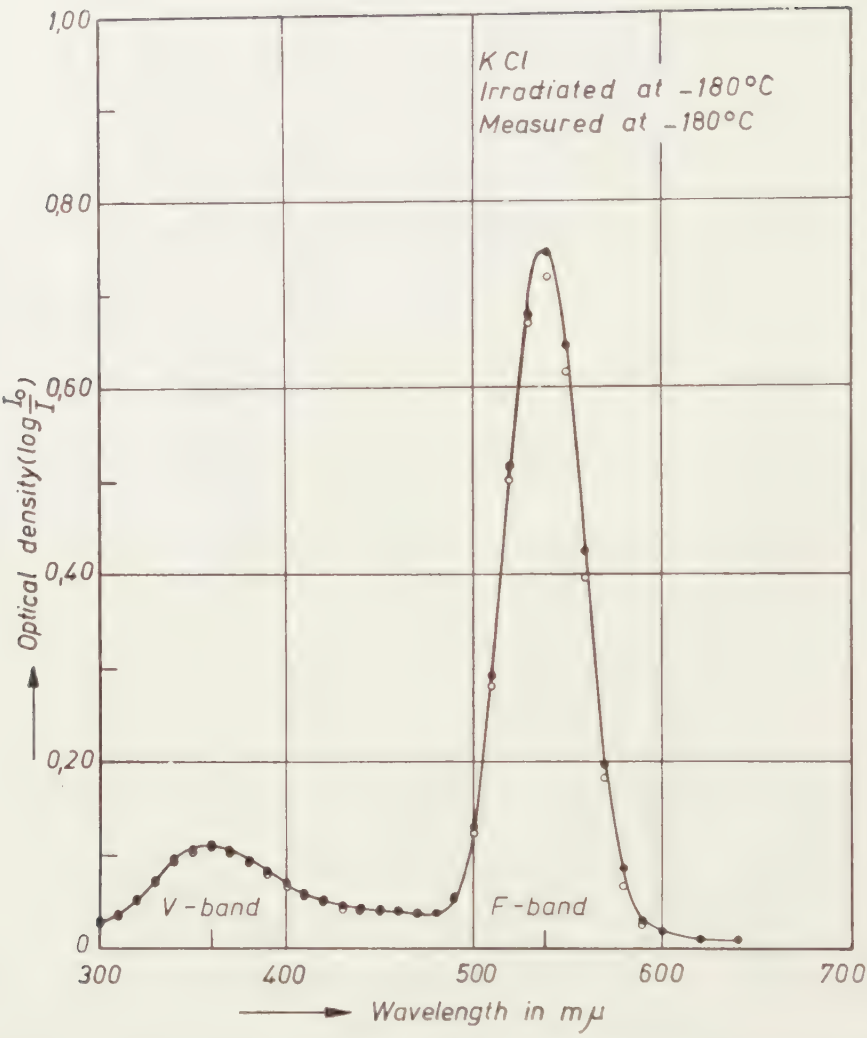

Fig. 3. Absorption-curve of two "pure" KCl-crystals cleared out of the same block and both heated at 500° C for 5 hours. X-rayed and measured at —180° C. ●: crystal slowly cooled. ○: crystal quenched. 420 mμ band absent.

cautions as would prevent or at least reduce to a minimum the occurrence of an impurity, e.g. the porcelain crucible in which the salt was melted was cleaned beforehand in boiling aqua regia, the crucible was covered during melting and the cover was not once lifted in the course of the preparation etc. Crystals prepared in this way did *not* show the 420 mμ-band, neither could it be produced afterwards by a heat-treatment, as applied by HALPERIN and SCHLESINGER. This is obvious from fig. 3, which shows the absorption curves of two crystals cleaved out of the same block. Both crystals were heated at 500° C for 5 hours, then one (●) slowly cooled, the other (○) quenched. This result strengthens our

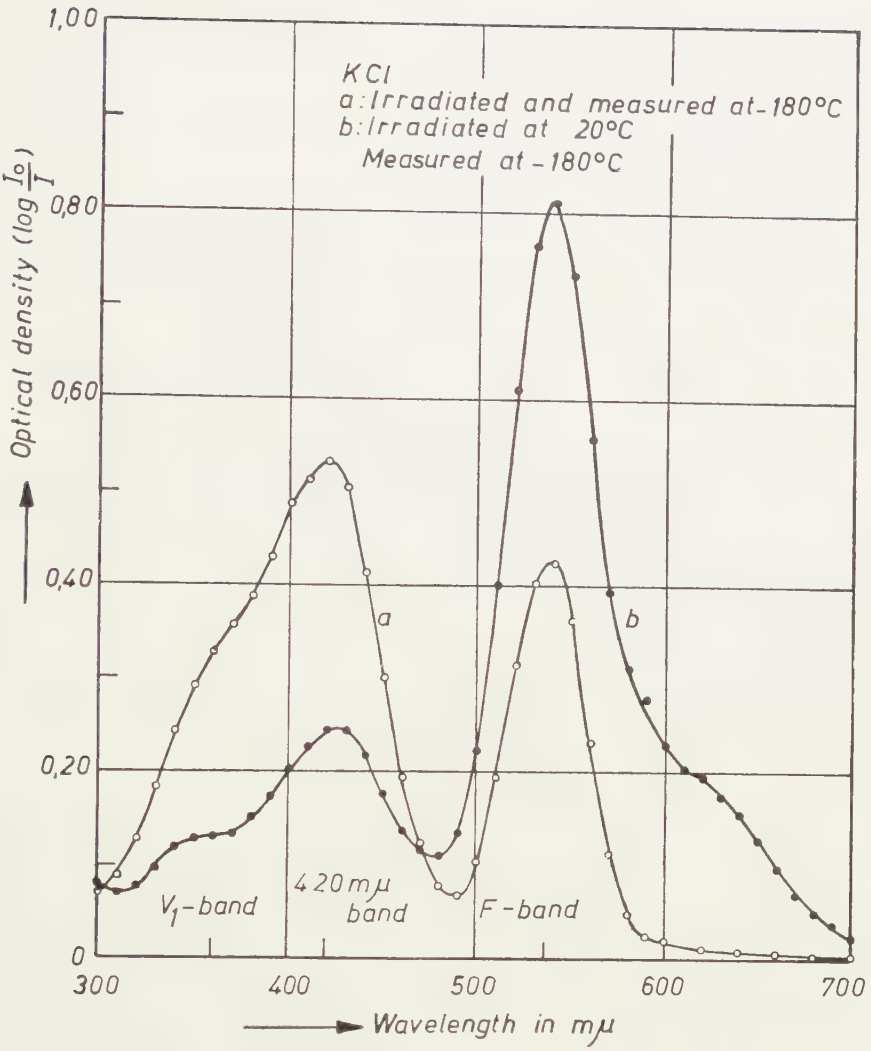

Fig. 4. Influence of temperature of irradiation on the 420 mμ band of a KCl-crystal. Curve a: X-rayed and measured at —180° C. Crystal then bleached at 100° C for $\frac{1}{2}$ hour. Curve b: X-rayed at 20° C, measured at —180° C. 420 mμ band weaker, F-band stronger.

supposition that the band is primarily due to some "impurity" in the KCl used by us. At present we do not know its nature. In a recent paper Ishiguro and Okuno (1959) report a band at 425 mμ for silver-doped KCl. They call this the E-band. According to the authors it is due to the presence of neutral silver atoms. It is remarkable that also the E-band shows a "strong-weak" relation with regard to the F-band, as may be seen from Ishiguro and Okuno's paper.

4. Finally we refer to the observation of Halperin and Schlesinger that the 420 mμ-band can be bleached at about 250° K. This makes it

probable that the band is unstable at room-temperature. In fact, keeping an irradiated crystal at room-temperature for some time makes it disappear completely. Moreover, irradiation at this temperature causes a much weaker intensity than irradiation at liquid-air temperature, in favour of the F-band. This is shown in fig. 4.

We intend to continue this investigation.

Laboratory of Physical Chemistry,
Technological University, Delft,
The Netherlands

REFERENCES

HALPERIN, A. and M. SCHLESINGER, J. Chem. Phys. **30**, 339 (1959).
ISHIGURO, M. and T. OKUNO, Mem. Inst. Scient. Ind. Res., Osaka Univ. **16**, 37 (1959).
OTTENS, E., A. J. ELAND and W. G. BURGERS, Proc. Kon. Ned. Akad. v. Wetensch., Amsterdam **B 62**, 268 (1959).
TICHELAAR, G. W., Thesis Delft 1956; W. G. BURGERS and G. W. TICHELAAR, Proc. Kon. Ned. Akad. v. Wetensch., Amsterdam **B 57**, 73 (1954).

AN OCCURRENCE OF CORUNDUM IN THE PRECAMBRIAN OF GHANA

BY

A. F. J. SMIT AND J. E. J. M. VAN LANDEWIJK

(Communicated by Prof. G. H. R. VON KOENIGSWALD at the meeting of Sept. 26, 1959)

Corundum has occasionally been found in placer deposits in Ghana but as far as we know there are no records of the mineral *in situ* in the country. This preliminary note records the discovery of an occurrence of corundum *in situ*, together with a brief account of the geology and mineralogy of the occurrence. A more detailed account will be published later.

The rock containing corundum was found near Nebiewale in N. Ghana. The geographical position of this village is 1° 40′ W. Long. 10° 35′ 20″ N. Lat. (sheet Navrongo 1944, Topographical map of Ghana 1 : 250,000) [1].

The Nebiewale region is underlain by granite-gneisses of the so-called Cape Coast complex (Geological map of Ghana, 1955) which is intrusive into Middle Precambrian Birrimian regional metamorphic rocks, among others sedimentary and volcanic schists and metamorphosed basic intrusions.

In the Nebiewale area granite-gneiss, cut by numerous pegmatite veins, predominates. The corundum occurs in lenses of muscovite-gneiss of varying size in the country rock. All transitions are found from clearly defined inclusions to ghost inclusions, only recognizable by the mineral composition. The rock around the inclusions is probably endomorphically contaminated.

The country rock has the following mean composition: quartz 30–35 %; microcline, orthoclase, perthite, 10–30 %; albite, 0–32 %; oligoclase, 0–50 %; biotite, 2.5–3.5 %; muscovite, 1–1.5 %; and epidote 0.5–1 %. If the country rock can be regarded as an igneous rock, it is a leuco-sodaclase adamellite (17″ P), according to JOHANSSEN. Most of the rock is porphyritic and heterogeneous, but the composition varies normally within the above-mentioned limits. It is possible that the enclosing rock is a migmatite, probably in contact with an intrusion in the N.E.

[1] In the literature Nebiewale has been mentioned in a paper by ROHLEDER who believes that the village is situated in an old volcanic crater, which he called the Nebiewale Caldera.

We intend to discuss this problem in a separate publication in due course.

The quartz is partly myrmekitic, microcline as well as isomicrocline is probably present, the plagioclase is untwinned or albite-twinned. The biotite is pleochroic light to dark brown with many pleochroic haloes, some with a zircon core. The myrmekite seems to replace the plagioclase, the microcline the quartz; the muscovite seems to replace the biotite and the plagioclase. Dark inclusions, sometimes with corundum, and veins of pegmatite and aplite are present.

Part of the enclosing rock has a quartz content of 10–20 %, and an albite content of 50–60 %. This rock is probably contaminated by digestion of the inclusions.

In parts where corundum remnants are still found, the average composition is: quartz, 35–40 %; oligoclase, 40 %; biotite 20–25 %.

The endomorphose seems to be: biotite, oligoclase and quartz giving rise to the formation of alkali feldspars and muscovite, which evolve to quartz, alkali feldspars and oligoclase.

The nearly digested corundum inclusions contain andesine and a high percentage of biotite and no alkali feldspars. The corundum is partly altered into small muscovite flakes, lying at random, which form larger crystals at some distance from the corundum.

Some corundum crystals are poikilitic, enclosing small specks of biotite oriented in one direction. The biotite seems to be older than the corundum which, in its turn, is altered to muscovite.

The biotite around the corundum has no pleochroic haloes and is partly smaller and not so well oriented as in the rest of the inclusions. The clearly bounded corundum-bearing inclusions, up to 6 sq. feet, have a white zone of one foot around them, mainly consisting of feldspars (quartz, 0.5 %; oligoclase-andesine, 91 %; biotite, 3.5 %; muscovite, 5 %, some corundum relics).

A zone rich in biotite or composed of nearly-digested biotite-rich inclusions sometimes surrounds the white feldspathic rim.

The inclusion itself is greenish in colour and has abundant, large crystals of grey, speckled, barrel shaped emery and opaque to translucent corundum crystals (up to 2″), which are fluorescent, violet, red-violet and grey-blue.

The corundum is generally arranged in lines, parallel to the orientation of the inclusions (biotite-muscovite). The crystals sometimes contain inclusions of iron ore or biotite and are partly replaced by muscovite as outlined above.

The corundum is sometimes uniaxial, sometimes biaxial; it has a good cleavage and shows polygonal growth lines around a more massive core. The mineral is sometimes twinned.

Muscovite, iron ore, oligoclase-andesine and some small biotite crystals accompany the corundum.

We acknowledge the financial support from the University College of Ghana which enables us to carry out this research.

REFERENCES

Ghana Geological Survey, Geological map of Ghana (1955).

Johanssen, A., A Descriptive Petrography of the Igneous Rocks, University of Chicago Press (1955).

Rohleder, P. T., The Nebiewale Caldera, Gold Coast, The Geographical Journal, XC, 546 (1937).

Survey Dept., Gold Coast, Topographical map of Ghana, sheet Navrongo, (1944).

APPLICATION OF LIFTING SURFACE THEORY TO SHIP SCREWS

BY

J. A. SPARENBERG

(Communicated by Prof. W. P. A. VAN LAMMEREN at the meeting of Sept. 26, 1959)

Summary

The problem of determining the relation between the geometrical form of a propeller blade and its pressure distribution is reduced to a two dimensional integral equation. This has been done by extending the existing lifting surface theory for airplane wings to rotating helicoidal surfaces. The essential tool is the acceleration potential.

1. *Introduction*

The theory of lifting surfaces has been applied extensively to airplane wings of finite span (for instance [1][1]), [2] and [3]). In this article we discuss the adaptation of this theory to rotating screw propellers. Such a theory is needed especially for screws of fast ships, because the aspect ratio of their blades becomes rather small.

These screws are generally designed by using the vortex line theory. This theory takes care of a mean value of the induced velocity at the profile. For a blade with a small aspect ratio however the variation of the values of the induced velocities along the chord are also important. In order to allow for this, several types of corrections (so called vortex line-vortex sheet corrections) are suggested ([4] and [5]). Recent measurements of VAN MANEN and CROWLEY [6] gave rise to some doubt about the prevailing types of corrections. In order to obtain an insight into the accuracy which is arrived at by the calculations just mentioned, numerical results from an exact lifting surface theory are necessary.

Before doing this it is desirable to have at our disposal a more general treatment of the screw. To some extent this has already been given by GUILLOTON [7] and STRSCHELETZKY [8]. These authors replace the propeller blade by a layer of bound vortices. The lifting forces are calculated by the law of Kutta–Joukowski.

The point of departure used in this article is the theory of the acceleration potential as described by PRANDTL [9]. Theoretically this yields a more satisfactory approach because then we start from the basic equations of hydrodynamics and do not need laws which proceed from

[1]) Numbers between square brackets refer to the bibliography at the end of this article.

these equations by integration. The given theory results into two equivalent integral equations both of which can be chosen as a basis for further numerical calculations.

2. *Formulation of the problem*

The propeller blades are assumed to be infinitely thin and the influences of the ship and the propeller boss are neglected. First we consider the theory of a one bladed screw, which already contains all the specific mathematical complications. In the last paragraph of this paper reference is made to screws with more blades.

The one bladed screw rotates with an angular velocity ω around the x axis (fig. 1). The undisturbed velocity of the non-viscous and incompressible fluid has the magnitude U and is in the direction of the positive x axis.

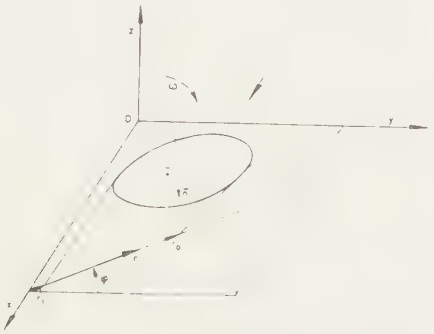

Fig. 1. Scheme for a one bladed screw.

We consider a rotating helicoidal surface

$$H(x, r, \varphi, t) \stackrel{\text{def}}{=} \varphi + \omega t - ax = 0, \qquad a = \frac{\omega}{U} \tag{2.1}$$

where t represents the time and x, r and φ form a system of cylindrical coordinates. The domain of x and r can be described by

$$x_l(r) \leqslant x \leqslant x_t(r), \quad r_i \leqslant r \leqslant r_0, \tag{2.2}$$

the functions $x_l(r)$ and $x_t(t)$ determine respectively the leading edge and the trailing edge of the blade, r_i and r_0 are the inner and the outer radius of the blade. For $a = \omega/U$ (2.1) the rotating surface $H = 0$ does not disturb the incoming uniform flow.

Next we consider a screw blade $F = 0$ which lies in the neighbourhood of $H = 0$,

$$F(x, r, \varphi, t) \stackrel{\text{def}}{=} \varphi + \omega t - ax + \varepsilon f(x, r) = 0. \tag{2.3}$$

The function $f(x, r)$, which is a measure for the deviation of the screw blade from the helicoidal surface, is some reasonable smooth function. ε is a small constant. This deviation (angle of attack and camber) induces

disturbances of the uniform flow, which are supposed to be small with respect to U. The components of the velocity of the fluid are denoted by

$$U+u,\ v,\ w \tag{2.4}$$

respectively in the x, r and φ direction.

For an arbitrary surface $G(x, r, \varphi, t)=0$ moving in a non-viscous and incompressible fluid the formula

$$\frac{\partial G}{\partial t}+(U+u)\frac{\partial G}{\partial x}+v\frac{\partial G}{\partial r}+w\frac{\partial G}{r\partial \varphi}=0, \tag{2.5}$$

holding on $G=0$ provides the condition for the velocity to be tangential to the surface. The disturbance velocities u, v and w have to be taken all at the same side of the surface. Substituting (2.3) into (2.5) and taking into account only first order terms in u, v and w we obtain

$$\varepsilon U\frac{\partial f}{\partial x}=au-\frac{w}{r}. \tag{2.6}$$

This equation can also be derived by considering the relative velocity of the fluid with respect to the screw blade.

Thus we need to determine velocities u, v and w which meet the equations of motion (discussed in the next paragraph) and equation (2.6). Besides this, u, v and w have to vanish for $x\to-\infty$.

3. *The screw blade as a pressure dipole layer*

The equations of motion of a linearised time dependent flow in cylindrical coordinates are

$$U\frac{\partial u}{\partial x}+\frac{\partial u}{\partial t}=-\frac{1}{\mu}\frac{\partial p(x, r, \varphi, t)}{\partial x}, \tag{3.1}$$

$$U\frac{\partial v}{\partial x}+\frac{\partial v}{\partial t}=-\frac{1}{\mu}\frac{\partial p(x, r, \varphi, t)}{\partial r}, \tag{3.2}$$

$$U\frac{\partial w}{\partial x}+\frac{\partial w}{\partial t}=-\frac{1}{\mu}\frac{\partial p(x, r, \varphi, t)}{r\partial \varphi}, \tag{3.3}$$

where μ is the specific density and p the pressure. The equation of continuity and the potential equation are

$$\frac{\partial u}{\partial x}+\frac{1}{r}\frac{\partial rv}{\partial r}+\frac{1}{r}\frac{\partial w}{\partial \varphi}=0 \tag{3.4}$$

$$\left(\frac{\partial^2}{\partial x^2}+\frac{1}{r}\frac{\partial}{\partial r}r\frac{\partial}{\partial r}+\frac{1}{r^2}\frac{\partial^2}{\partial \varphi^2}\right)\psi(x, r, \varphi)=0. \tag{3.5}$$

Adding the derivatives of $r\cdot(3.1)$, $r\cdot(3.2)$ and (3.3) with respect to x, r and φ respectively and observing the equation of continuity, we find that $p(x, r, \varphi, t)$ satisfies the potential equation (3.5). Hence the pressure can be represented by a distribution of pressure poles and pressure dipoles on the screw blade. The dipoles have their axes normal to the surface of the blade. We shall show that only the pressure dipole layer is needed.

We consider the screw blade $F = 0$ which slightly disturbs the incoming homogeneous flow with undisturbed velocity U. The unit normal to this surface has the components

$$(3.6)\qquad \left\{\left(\frac{\partial F}{\partial x}\right)^2+\left(\frac{\partial F}{\partial r}\right)^2+\left(\frac{\partial F}{r\partial\varphi}\right)^2\right\}^{-1/2}\left\{\frac{\partial F}{\partial x},\frac{\partial F}{\partial r},\frac{\partial F}{r\partial\varphi}\right\}\overset{\text{def}}{=}C\left\{\frac{\partial F}{\partial x},\frac{\partial F}{\partial r},\frac{\partial F}{r\partial\varphi}\right\},$$

respectively in the x, r and φ direction.

The normal acceleration A_n of a fluid particle in the neighbourhood of $F=0$ becomes

$$(3.7)\qquad \begin{cases} A_n = C\left\{\frac{\partial F}{\partial x}\left(U\frac{\partial u}{\partial x}+\frac{\partial u}{\partial t}\right)+\frac{\partial F}{\partial r}\left(U\frac{\partial v}{\partial x}+\frac{\partial v}{\partial t}\right)+\frac{\partial F}{r\partial\varphi}\left(U\frac{\partial w}{\partial x}+\frac{\partial w}{\partial t}\right)\right\}= \\ \qquad = C\left(U\frac{\partial}{\partial x}+\frac{\partial}{\partial t}\right)\left(u\frac{\partial F}{\partial x}+v\frac{\partial F}{\partial r}+w\frac{\partial F}{r\partial\varphi}\right)-C\left(u\frac{\partial}{\partial x}+v\frac{\partial}{\partial r}+w\frac{\partial}{r\partial\varphi}\right)\left(U\frac{\partial}{\partial x}+\frac{\partial}{\partial t}\right)F. \end{cases}$$

From (2.5) it follows that within terms of the first order in u, v and w

$$(3.8)\qquad A_n = -C\left(U\frac{\partial}{\partial x}+\frac{\partial}{\partial t}\right)^2 F.$$

This formula is independent of the side of the surface, it only depends on the point which we consider. Hence the normal acceleration A_n is equal at both sides of the blade. From (3.1), (3.2) and (3.3) it follows that the same holds for the normal derivative of the pressure. This implies that the pressure in the fluid can be represented by a pressure dipole layer on the screw blade [10]. Because our theory is linearised this dipole layer can be taken to coincide with the helicoidal surface.

4. *The velocity field induced by a rotating pressure dipole*

A pressure pole of strength S, situated at the point ξ, ϱ, θ has the pressure field

$$(4.1)\quad P(x,r,\varphi,\xi,\varrho,\theta)\overset{\text{def}}{=}\frac{S}{4\pi\{(x-\xi)^2+r^2+\varrho^2-2r\varrho\cos(\theta-\varphi)\}^{1/2}}\overset{\text{def}}{=}\frac{S}{4\pi R(x,r,\varphi,\xi,\varrho,\theta)}.$$

Differentiation of this expression with respect to ξ, ϱ and θ in the direction of the unit normal $\vec{n}$ of $H=0$ (fig. 1), yields the pressure field of a pressure dipole with axis normal to the helicoidal surface. The unit normal $\vec{n}$ has, in accordance with (3.6), the components.

$$(4.2)\qquad \vec{n}=\left(a^2+\frac{1}{\varrho^2}\right)^{-1/2}\left(a,\,o,\,-\frac{1}{\varrho}\right).$$

Herwith the pressure field of a pressure dipole attached to the rotating surface $H=0$ becomes

$$(4.3)\qquad \begin{cases} D(x,r,\varphi,\xi,\varrho,\theta)\overset{\text{def}}{=}\frac{S\varrho}{4\pi(1+a^2\varrho^2)^{1/2}}\left(a\frac{\partial}{\partial\xi}-\frac{1}{\varrho^2}\frac{\partial}{\partial\theta}\right)P(x,r,\varphi,\xi,\varrho,\theta)|_{\theta=a\xi-\omega t}= \\ \qquad =\frac{S}{4\pi(1+a^2\varrho^2)^{1/2}}\,\frac{\{a\varrho(x-\xi)+r\sin(a\xi-\omega t-\varphi)\}}{R^3(x,r,\varphi,\xi,\varrho,a\xi-\omega t)}. \end{cases}$$

The external force exerted by this pressure field can be determined by calculating the resultant pressure on a small closed surface which surrounds the point of singularity. It turns out that this force has the magnitude S and is directed along $\vec{n}$.

The equations of motion (3.1), (3.2) and (3.3) determine the velocities which belong to the rotating pressure field (4.3). The right hand sides of these equations become

$$-\frac{1}{\mu}\frac{\partial D}{\partial x}-\frac{S}{4\pi\mu(1+a^2\varrho^2)^{1/2}}\left[\frac{3\{a\varrho(x-\xi)+r\sin(a\xi-\omega t-\varphi)\}(x-\xi)}{R^5(x,r,\varphi,\xi,\varrho,a\xi-\omega t)}-\frac{a\varrho}{R^3}\right], \tag{4.4}$$

$$\frac{1}{\mu}\frac{\partial D}{\partial r}-\frac{S}{4\pi\mu(1+a^2\varrho^2)^{1/2}}\left[\frac{3\{a\varrho(x-\xi)+r\sin(a\xi-\omega t-\varphi)\}\{r-\varrho\cos(a\xi-\omega t-\varphi)\}}{R^5}-\frac{\sin(a\xi-\omega t-\varphi)}{R^3}\right]. \tag{4.5}$$

$$-\frac{1}{\mu}\frac{\partial D}{r\partial\varphi}=\frac{S}{4\pi\mu(1+a^2\varrho^2)^{1/2}}\left[\frac{3\{a\varrho(x-\xi)+r\sin(a\xi-\omega t-\varphi)\}\varrho\sin(a\xi-\omega t-\varphi)}{R^5}+\frac{\cos(a\xi-\omega t-\varphi)}{R^3}\right]. \tag{4.6}$$

The solution of

$$U\frac{\partial\psi}{\partial x}+\frac{\partial\psi}{\partial t}=L(x,r,\varphi,t), \tag{4.7}$$

where $L(x,r,\varphi,t)$ is some prescribed function, which tends to zero for $x\to-\infty$, is

$$\psi=\frac{1}{U}\int_{-\infty}^{x-\xi}L\left(\tau+\xi,r,\varphi,t+\frac{(\tau-x+\xi)}{U}\right)d\tau. \tag{4.8}$$

From this equation we find for the velocity field induced by the rotating pressure dipole at time $t=0$

$$(u,v,w)=\frac{S}{4\pi\mu U(1+a^2\varrho^2)^{1/2}}\int_{-\infty}^{x-\xi}\cdot\left[\frac{3\{a\varrho(x-\tau)+r\sin(a(x-\tau)-\varphi)\}\{\tau,r-\varrho\cos(a(x-\tau)-\varphi),-\varrho\sin(a(x-\tau)-\varphi)\}}{\{\tau^2+r^2+\varrho^2-2r\varrho\cos(a(x-\tau)-\varphi)\}^{5/2}}+-\frac{\{a\varrho,\sin(a(x-\tau)-\varphi),-\cos(a(x-\tau)-\varphi)\}}{\{\tau^2+r^2+\varrho^2-2r\varrho\cos(a(x-\tau)-\varphi)\}^{3/2}}\right]d\tau. \tag{4.9}$$

This can be written as follows,

$$\begin{aligned}(u,v,w)=&\\ &\frac{S}{4\pi\mu U(1+a^2\varrho^2)^{1/2}}\Big(\frac{\{-r\sin(a\xi-\varphi),(x-\xi)\sin(a\xi-\varphi),-(x-\xi)\cos(a\xi-\varphi)\}}{\{(x-\xi)^2+r^2+\varrho^2-2r\varrho\cos(a\xi-\varphi)\}^{3/2}}+\\ &-\frac{d}{d\varrho}\int_{-\infty}^{x-\xi}\Big[\{ar\varrho\cos(a(x-\tau)-\varphi)-a\varrho^2,-a\varrho\tau\cos(a(x-\tau)-\varphi)+\\ &-\varrho\sin(a(x-\tau)-\varphi),-r+\varrho\cos(a(x-\tau)-\varphi)+\\ &-a\varrho\tau\sin(a(x-\tau)-\varphi)\}\{\tau^2+r^2+\varrho^2-2r\varrho\cos(a(x-\tau)-\varphi)\}^{-3/2}\Big]d\tau\Big).\end{aligned} \tag{4.10}$$

The proof of this statement is rather lengthy and needs only elementary analysis, therefore it will not be discussed here.

In expression (4.9) the highest exponent of the two numerators, under the sign of integration is 5/2, while in expression (4.10) it is 3/2. This mathematical reduction has also physical meaning. From the equality of (4.9) and (4.10) follows the equivalence of a rotating pressure dipole and a vortex system. This system consists of a rotating bound vortex element of length $d\varrho$ stretched along the radius ϱ and of trailing vortices

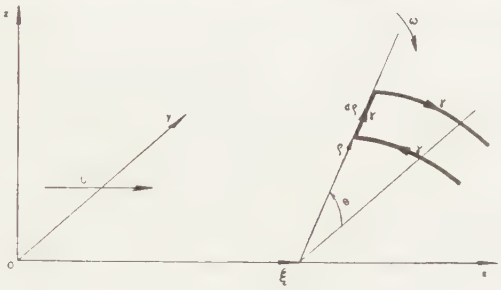

Fig. 2. The rotating vortex element.

along helicoidal lines (fig. 2). The first term in (4.10) originates from the bound vortex element which, in order to induce the correct velocities, must have the strength

$$\gamma = \frac{S}{\mu U(1+a^2\varrho^2)^{1/2}\, d\varrho}. \tag{4.11}$$

The second term is caused by the two trailing vortices with strength $\pm\gamma$, which are close to each other. Their resulting induced velocity can be obtained by differentiating the induced velocity of the outmost trailing vortex with respect to ϱ.

When the velocity fields of both representations (pressure dipole (4.9) and bound vortex with trailing vortices (4.10) are equal, then also the external forces exerted by these entities must be the same. We know that the external force exerted by the pressure dipole (4.3) has the magnitude S. From this and from (4.11) it follows that the force T on the rotating bound vortex with intensity γ is

$$T = \gamma\mu U(1+a^2\varrho^2)^{1/2}\, d\varrho. \tag{4.12}$$

The quantity $U(1+a^2\varrho^2)^{1/2}$ can be interpreted as the local velocity of the bound vortex.

Equation (4.12) states the law of Kutta–Joukowski for a rotating bound vortex element.

5. *The integral equation for the distribution of pressure dipoles*

It is our aim to formulate some integral equations which have to be satisfied at the blades of the screw. First we will derive such an equation

from the point of view of the pressure dipole layer. Then we have to introduce the velocities induced by a pressure dipole (4.9) into condition (2.6). The strength S of the dipole becomes a function of the coordinates ξ and ϱ. After integrating over the blade we obtain

$$
(5.1)\quad \begin{cases} 4\pi\varepsilon\mu U^2 r\,\dfrac{\partial f}{\partial x} = \\ \lim\limits_{\varphi\to ax}\iint\limits_{0} S(\xi,\varrho)\int\limits_{-\infty}^{x-\xi}\Big[\dfrac{3\{a\varrho\tau - r\sin(a(\tau-x)+\varphi)\}\{ar\tau - \varrho\sin(a(\tau-x)+\varphi)\}}{\{\tau^2+r^2+\varrho^2-2r\varrho\cos(a(\tau-x)+\varphi)\}^{5/2}} - \\ \qquad - \dfrac{\{a^2r\varrho+\cos(a(\tau-x)+\varphi)\}}{\{\tau^2+r^2+\varrho^2-2r\varrho\cos(a(\tau-x)+\varphi)\}^{3/2}}\Big]\,d\tau d\xi d\varrho \overset{\text{def}}{=} \\ \lim\limits_{\varphi\to ax}\iint\limits_{0} S(\xi,\varrho)\int\limits_{-\infty}^{x-\xi} F(x,r,\varphi,\varrho,\tau)\,d\tau d\xi d\varrho \overset{\text{def}}{=} \\ \qquad\qquad \lim\limits_{\varphi\to ax}\iint\limits_{0} S(\xi,\varrho)\,K^*(x,r,\varphi,\xi,\varrho)\,d\xi d\varrho. \end{cases}
$$

The limit $\varphi\to ax$ means that the point x, r, φ, in which we consider the induced velocities, tends to the helicoidal surface $H=0$. When we simply put the value φ equal to ax into $K^*(x,r,\varphi,\xi,\varrho)$ we find

$$
(5.2)\quad \begin{cases} K(x,r,\xi,\varrho) \overset{\text{def}}{=} K^*(x,r,ax,\xi,\varrho) = \\ \qquad \displaystyle\int_{-\infty}^{x-\xi}\Big[\frac{3(a\varrho\tau - r\sin a\tau)(ar\tau - \varrho\sin a\tau)}{\{\tau^2+r^2+\varrho^2-2r\varrho\cos a\tau\}^{5/2}} - \frac{(a^2r\varrho - \cos a\tau)}{\{\tau^2+r^2+\varrho^2-2r\varrho\cos a\tau\}^{3/2}}\Big]\,d\tau. \end{cases}
$$

It can be seen that for $\xi<x$ and $\varrho\to r$ this function becomes infinite. The singularity arises from a small part of the range of integration in the neighbourhood of $\tau=0$. For the study of this singular behaviour the range of integration in (5.2) may be changed into $-\alpha\leqslant\tau\leqslant\alpha$, where α is some sufficiently small but fixed positive number. Putting $\varrho=r+\nu$ where ν is a small quantity it is valid to expand the numerators with respect to τ and ν. We obtain integrals of the form

$$
(5.3)\qquad \nu^l\int_{-\alpha}^{+\alpha}\frac{\tau^m d\tau}{\{\tau^2+r^2+(r+\nu)^2-2r(r+\nu)\cos a\tau\}^{q/2}} \leqslant (q=3 \text{ or } 5)
$$

$$
(5.4)\qquad \leqslant \nu^l\int_{-\alpha}^{+\alpha}\frac{\tau^m d\tau}{\{\tau^2(1+ka^2r^2)+\nu^2\}^{q/2}}, \qquad 0<k<1,
$$

where l and m are integers. It can easily be shown that for $l+m\geqslant q-1$ this expression remains finite when $\nu\to 0$. Hence in (5.2) we have to expand the numerators of the first and the second fraction up to and including terms of the third and first order respectively. By doing this we find, after an estimation of the resulting integrals the following first two terms of $K(x,r,\xi,\varrho)$

$$
(5.5)\quad K(x,r,\xi,\varrho)\approx\frac{-2(1+a^2r^2)^{1/2}}{(r-\varrho)^2}+\frac{ra^2}{(1+a^2r^2)^{1/2}(r-\varrho)}, \qquad \xi<x,\ \varrho\to r.
$$

This singularity however cannot be integrated and hence we have to follow a different method for giving a meaning to the limit stated in (5.1). This will be discussed in the following.

We divide the area of the blade into three regions (fig. 3). The strip O_1 defined by $x_l(r) \leqslant \xi \leqslant x-\gamma$, $|\varrho - r| \leqslant \beta$, the rectangle O_2 defined by $|x-\xi| \leqslant \gamma$, $|\varrho - r| \leqslant \beta$ and the remaining part O_3. In this definition γ and β are arbitrarily small positive quantities.

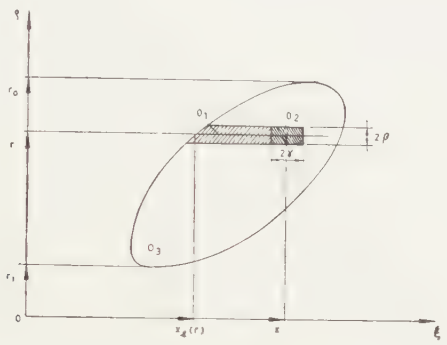

Fig. 3. The domains of integration.

The domain O_3 does not yield any difficulty in the limiting process $\varphi \to ax$ because the point ξ, ϱ remains at a finite distance of the point x, r.

The integration over O_1 when first $\varphi \to ax$ and then $\beta \to 0$ can be written as

$$\lim_{\varphi \to ax} \int_{x_l(r)}^{x-\gamma} \int_{r-\beta}^{r+\beta} S(\xi, \varrho) \{ \int_{-\alpha}^{+\alpha} F(x, r, \varphi, \varrho, \tau)\, d\tau \}\, d\xi d\varrho, \tag{5.6}$$

where α is again a sufficiently small but fixed quantity. This is valid since only the singular part of the kernel can yield a contribution to the integral over the strip of vanishing width. $\beta \to 0$. Then it is possible to expand the function $S(\xi, \varrho)$ and the numerators of $F(x, r, \varphi, \varrho, \tau)$ with respect to the small quantities

$$\delta = \varphi - ax, \quad \nu = \varrho - r, \quad \tau. \tag{5.7}$$

The integrals which appear are of the type (5.3), only now a factor δ^n arises in the numerator. They can easily be estimated. It turns out that again a finite number of terms need to be considered which for the limiting case, first $\delta \to 0$ and then $\beta \to 0$, yield a contribution. After this it is possible to expand the denominators where also a finite number of terms need to be taken into account. In this way we find after a complicated but elementary calculation for the contribution of (5.6)

$$\frac{4\sqrt{1+a^2r^2}}{\beta} \int_{x_l(r)}^{x-\gamma} S(\xi, r)\, d\xi, \qquad \beta \to 0. \tag{5.8}$$

The integration over the small rectangle O_2 can be treated in a similar way. Its contribution can be written as

$$\lim_{\varphi \to ax} \int_{x-\gamma}^{x+\gamma} \int_{r-\beta}^{r+\beta} S(\xi, \varrho) \left\{ \int_{-\gamma}^{x-\xi} F(x, r, \varphi, \varrho, \tau)\, d\tau \right\} d\xi d\varrho. \tag{5.9}$$

The lower boundary $-\infty$ for the integration over τ is replaced by the fixed value $-\gamma < 0$ because the range of integration $-\infty \leqslant \tau \leqslant -\gamma$ does not yield a finite contribution when $\beta \to 0$. We now expand $S(\xi, \varrho)$ by a Taylor expansion for two variables and integrate partially with respect to ξ. Then we arrive at similar formulae as we found for the region O_1. It turns out that the contribution of the integral over O_2 becomes

$$\frac{4\sqrt{1+a^2r^2}}{\beta} \int S(\xi, r)\, d\xi, \qquad \beta \to 0. \tag{5.10}$$

This is the extension of the range of integration in (5.8) from $x-\gamma$ to x.

Using (5.8) and (5.10) we obtain for (5.1)

$$\left.\begin{aligned} 4\pi\mu U^2 r \frac{\partial f}{\partial x} = \lim_{\beta \to 0} \Big[\Big(\int_{r_i}^{r-\rho} + \int_{r+\beta}^{r_0} \Big) \int_{x_i(\varrho)}^{x_t(\varrho)} \cdot \\ \cdot S(\xi, \varrho)\, K(x, r, \xi, \varrho)\, d\xi d\varrho + \frac{4\sqrt{1+a^2r^2}}{\beta} \int_{x_i}^{x} S(\xi, r)\, d\xi \Big], \end{aligned}\right\} \tag{5.11}$$

where $K(x, r, \xi, \varrho)$ is defined in (5.2) and its singular behaviour is given in (5.5). This is called the Hadamard principal value of the integral.

For the case $a = 0$ we have no rotation of the blade and hence our formulae must reduce to those of the lifting surface theory for wings. The coordinates x and r, resp. ξ and ϱ on the blade of the screw then become cartesian coordinates. From (5.2) it follows that (5.11) reduces to

$$\left.\begin{aligned} 4\pi\mu U^2 \Phi = -\lim_{\beta \to 0} \Big[\Big(\int_{r_i}^{r-\beta} + \int_{r+\beta}^{r_0} \Big) \int_{x_i(\varrho)}^{x_t(\varrho)} \cdot \\ \cdot \frac{S(\xi, \varrho)}{(r-\varrho)^2} \left\{ 1 - \frac{x-\xi}{\{(x-\xi)^2 + (r-\varrho)^2\}^{1/2}} \right\} d\xi d\varrho - \frac{4}{\beta} \int_{x_i(r)}^{x} S(\xi, r)\, d\xi \Big], \end{aligned}\right\} \tag{5.12}$$

where the function $\Phi = r(\partial f / \partial x)$ is the angle of attack of a surface element of the wing. This formula agrees with the basic equation in [1].

6. *The integral equation for the distribution of bound vortices.*

Here we start from the second formulation of the induced velocities (4.10). These have to be substituted into equation (2.6). After performing

a partial integration with respect to ϱ we obtain

$$
(6.1)\quad \left.\begin{aligned} 4\pi\varepsilon\mu U^2 r\,\frac{\partial f}{\partial x} = \lim_{\varphi \to ax}\Big[\iint_{O} S(\xi,\varrho)\,\frac{\{ar^2\sin(\varphi-a\xi)+(x-\xi)\cos(\varphi-a\xi)\}}{\{(x-\xi)^2+r^2+\varrho^2-2r\varrho\cos(\varphi-a\xi)\}^{3/2}}\,d\xi d\varrho - \\ -\iint_{O}\frac{\partial S(\xi,\varrho)}{\partial\varrho}\,M(x,r,\varphi,\xi,\varrho)\,d\xi d\varrho + \int_{x_v}^{x_a}\{S(\xi,\varrho_u(\xi))\,M(x,r,\varphi,\xi,\varrho_u(\xi)) + \\ - S(\xi,\varrho_\alpha(\xi))\,M(x,r,\varphi,\xi,\varrho_\alpha(\xi))\}\,d\xi\Big] \end{aligned}\right\}
$$

where

$$
(6.2)\quad \left.\begin{aligned} M(x,r,\varphi,\xi,\varrho) = \\ -\int_{-\infty}^{(x-\xi)}\frac{\{(1-a^2r^2)\varrho\cos(a(\tau-x)+\varphi)+a\varrho\tau\sin(a(\tau-x)+\varphi)-r(1-a^2\varrho^2)\}}{\{\tau^2+r^2+\varrho^2-2r\varrho\cos(a(\tau-x)+\varphi)\}^{3/2}}\,d\tau, \end{aligned}\right\}
$$

x_a and x_v denote the largest and smallest value of the ξ coordinate and $\varrho_u(\xi)$ and $\varrho_d(\xi)$ describe the circumference as function of ξ (fig. 4).

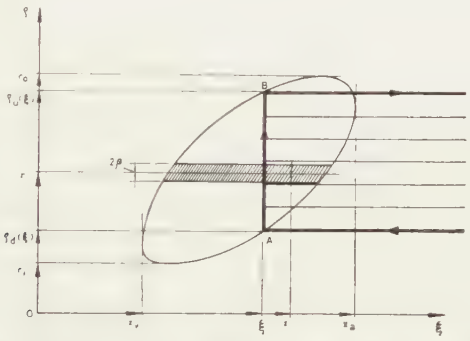

Fig. 4. A typical vortex system on the blade of the screw.

When we consider the case $\varphi = ax$ the kernels in (6.1) possess singularities which can easily be estimated. We find for the kernel of the first integral

$$
(6.3)\quad \left.\begin{aligned} \lim_{\substack{\xi\to x\\ \varrho\to r}}\Big[\frac{ar^2\sin(\varphi-a\xi)+(x-\xi)\cos(\varphi-a\xi)}{\{(x-\xi)^2+r^2+\varrho^2-2r\varrho\cos(\varphi-a\xi)\}^{3/2}}\Big]_{\varphi=ax} \approx \\ \approx \frac{-(1+a^2r^2)(\xi-x)}{\{(1+a^2r^2)(\xi-x)^2+(\varrho-r)^2\}^{3/2}}. \end{aligned}\right\}
$$

The singular behaviour of the function $M(x, r, \varphi, \xi, \varrho)$ is given by

$$
(6.4)\qquad \lim_{\varrho\to r} M(x,r,ax,\xi,\varrho) \approx \frac{+2(1+a^2r^2)^{1/2}}{(\varrho-r)}, \qquad \xi < x.
$$

By excluding the strip $|r-\varrho|<\beta$ from the domain of integration, it is possible to carry out the integrations in (6.1).

From the formulae (6.3) and (6.4) for the singularities it follows that the limit $\beta \to 0$ exists. However when the integrals can be interpreted in this way, we are not sure that the result is correct. There remains a

possibility of contributions of functions which for $\varphi = ax$ are zero everywhere except for $\varrho = r$ (δ functions of Dirac or its derivatives). That this does not happen follows from a more carefull passing to the limit, first $\varphi \to ax$ and then $\beta \to 0$.

The last integral in (6.1) is one dimensional with ξ as the variable of integration. It is more natural to introduce ϱ instead of ξ because then for $r_i \leqslant \varrho \leqslant r_0$ (fig. 4) we cover the whole leading edge and the whole trailing edge separately.

Ultimately we come to the following form for equation (6.1).

$$
\begin{aligned}
4\pi\varepsilon\mu U^2 r \frac{\partial f}{\partial x} = \lim_{\beta \to 0} \Bigg[& \Bigg(\int_{r_i}^{r-\beta} + \int_{r+\beta}^{r_0} \Bigg) \int_{\xi_l(\varrho)}^{\xi_t(\varrho)} \cdot \\
& \cdot S(\xi, \varrho) \, \frac{\{ar^2 \sin a(x-\xi) + (x-\xi)\cos a(x-\xi)\}}{\{(x-\xi)^2 + r^2 + \varrho^2 - 2r\varrho \cos a(x-\xi)\}^{3/2}} \, d\xi d\varrho + \\
& - \Bigg(\int_{r_i}^{r-\beta} + \int_{r+\beta}^{r_0} \Bigg) \int_{\xi_l(\varrho)}^{\xi_t(\varrho)} \frac{\partial S(\xi, \varrho)}{\partial \varrho} \, M(x, r, ax, \xi, \varrho) \, d\xi d\varrho + \\
& + \Bigg(\int_{r_i}^{r-\beta} + \int_{r+\beta}^{r_0} \Bigg) S(\xi_l(\varrho), \varrho) \, M(x, r, ax, \xi_l(\varrho), \varrho) \left(\frac{d\xi_l(\varrho)}{d\varrho} \right) d\varrho + \\
& - \int_{r_i}^{r_0} S(\xi_t(\varrho), \varrho) \, M(x, r, ax, \xi_t(\varrho), \varrho) \left(\frac{d\xi_t(\varrho)}{d\varrho} \right) d\varrho \Bigg].
\end{aligned}
\tag{6.5}
$$

We shall now discuss shortly the well known physical meaning of the different parts of the right hand side of equation (6.5). The first integral represents the velocities induced by the bound vortices of which in fig. 4 a typical one is drawn, the thick line AB. The second integral provides the velocities induced by free vortices, lying on screw lines, caused by variations in the ϱ direction of the bound vortices. In the figure these free vortices are drawn as horizontal lines starting at AB and stretching to the right. The last two integrations in (6.5) give the velocities induced by the free vortices which arise by the ending of the bound vortices at the circumference, point A or B. The strength of such a free vortex, denoted in fig. 4 by a thick horizontal line, is equal to the strength of the bound vortex at the circumference. The relative rotation with respect to the bound vortex is indicated by arrows.

7. *Final remarks*

In lifting surface theory there are two main types of problems. First, the problem of determining the shape of the surface for a given load distribution. Second, the inverse problem where the surface is given and it is asked to determine the pressures exerted by the fluid. In contrast to the lifting surface theory for airplane wings, the first problem is more

interesting from the point of view of ship screws. Mathematically it means that in our integral equations (5.11) and (6.5) the function $S(\xi, \varrho)$ is known. In order to calculate the function $f(x, r)$ which determines the angle of attack and the camber of the blade sections, we have to carry out the indicated integrations. This is rather cumbersome owing to the complicated nature of the kernels. Equation (5.11) looks more simple than (6.5). However in this last equation the kernel functions involved are integrations over velocities induced by bound vortices along straight lines and free vortices on screw lines. These induced velocities have been studied rather intensively (induction factors) [5]. Hence it seems recommendable for numerical calculations to start from equation (6.5).

Another point which has to be discussed is the extension of the theory to more bladed screws. Here we have to consider also the velocities induced by the other blades. We assume that the pressure distributions on the N equally spaced blades are identical. Then we can simply replace (5.1) for instance by

$$4\pi\varepsilon U^2 r \frac{\partial f}{\partial x} = \lim_{\varphi \to ax} \iint_O S(\xi, \varrho) \sum_{n=0}^{N-1} K^*\left(x, r, \varphi + \frac{2\pi n}{N}, \xi, \varrho\right) d\xi d\varrho. \tag{7.1}$$

The added part of the kernel has no singularities, because the points of one blade are at a finite distance of the points of the other blades. From this it follows that all our limit considerations and statements about integrability remain valid. The same can be done with equation (6.1).

Summarizing the results of this paper, we can state that we have derived, for the one blade propeller, two equivalent expressions (5.11) and (6.5) which give the relation ship between the pressure distribution and the geometrical form of the propeller blade. It is easy to modify these equations so that they become valid for the screw with more blades. In general it may be expected that for an accurate numerical treatment of the two problems, stated in the beginning of this paragraph, electronic computers will be essential.

Netherlands Ship Model Basin,
Wageningen

REFERENCES

1. Multhopp, H., Methods of calculating the lift distribution of wings (subsonic lifting surface theory). R.A.E. Rep. Aero 2353 (1950).
2. Truckenbrodt, E., Tragflächentheorie bei inkompressibler Strömung. Jahrbuch der Wiss. Ges. für Luftfahrt (1953).
3. Spiegel, E. van, Boundary problems in lifting surface theory. Thesis, Delft, Holland (1959).
4. Ginzel, J., Theory of the broad-bladed propeller. Admiralty Research Laboratory, Teddington, Middlesex (1952).

5. Lerbs, H., Ergebnisse der angewandten Theorie des Schiffspropellors. Jahrbuch der Schiffbautechnischen Gesellschaft 49 (1955).
6. Manen, J. D. van and J. D. Crowley, Some applications of the circulation theory of screw propellers. Metropolitan-section of the S.N.A.M.E. (to be published).
7. Guilloton, R., Applications de la courbure induite aux calculs des hélices marines. Association Technique Maritime, Session (1955).
8. Strscheletzky, M., Hydrodynamische Grundlagen zur Berechnung der Schiffsschrauben. Verlag G. Braun, Karlsruhe (1950).
9. Prandtl, L., Beitrag zur Theorie der tragende Fläche. Z.A.M.M. 16 (1936).
10. Kellog, D. D., Foundations of potential theory. New York (1953).

A COMPARISON OF AN EMPIRICAL AND OF A KINETIC EQUATION, BOTH DESCRIBING A SELECTIVE CATALYTIC PROCESS

BY

R. J. A. M. VAN DER BORG

(Communicated by Prof. J. H. DE BOER at the meeting of September 26, 1959)

1. INTRODUCTION

Recently a method for simplifying process development has been proposed by WEBER [1]. Analysing a great number of selective chemical, mostly catalytic, processes he discovered a graphical statistical method by means of which all the examined processes could be described.

In this method an isosceles rectangular diagram is used, in which the result of each individual experiment is indicated as an experimental point, (x, y), in such a way that the fraction (y) of the starting material A which is transformed into the desired product B is plotted vertically and the fraction (x) of A which is converted into an undesired by-product C is plotted horizontally. WEBER discovered that all points (x, y) of a series of experiments, in which only one reaction parameter was varied, as e.g. the contact time, could be described by an equation:

$$y = \frac{x(1-x)}{a+bx} \tag{1}$$

a and b being empirical constants. As, apparently, all series of practical experiments may be described by this equation, each series giving one set of the empirical constants a and b, the number of experiments of each series may be drastically reduced, as is most clearly brought forward by WATERMAN [2]. This graphical tracing method, together with the empirical equation (1), therefore, makes it possible to determine the optimum process conditions after far less experimental observations than before.

2. COMPARISON OF THE EMPIRICAL EQUATION WITH A KINETIC APPROACH

In discussing various applications WATERMAN [2] and WEBER [1] compare, in some cases, equation (1) with equations which are derived from kinetic considerations. The main example they give is the catalytic hydrogenation of linoleic esters, which reaction has been investigated, in earlier years [3], in Waterman's laboratory, and which can be described as a consecutive first order reaction [4]:

$$\text{linoleic ester } (L) \xrightarrow{k_1} \text{oleic ester } (O) \xrightarrow{k_2} \text{stearic ester } (S).$$

In a selective hydrogenation oleic ester is the desired product B and stearic ester the undesired by-product C. In discussing various types of selectivity WHEELER [5], indicating this type as type III selectivity, derives, from kinetic considerations the following equation:

$$\alpha_B = \frac{S}{S-1}(1-\alpha_A)\left[(1-\alpha_A)^{-[1-(1/S)]}-1\right] \tag{2}$$

where α_B is the fraction of initial A converted into B, α_A is the fraction of A reacted and S is the so-called selectivity factor k_1/k_2.
Applying both equations (1) and (2) to their hydrogenation experiments of linoleic ester, WEBER [1] and WATERMAN [2] derive the conclusion that the hydrogenation experiments at high temperatures (180° C) can be described by both equations. The hydrogenation experiments at low temperature (20° C–90° C), may also well be covered by the empirical equation (1), equation (2), however, fails in this case.

3. A NEW APPROACH

Equation (2) as derived by Wheeler contains only one reaction constant, S. Equation (1) is characterised by two empirical constants, a and b. A slight extension of the kinetic scheme, underlying (2), may introduce a second kinetic reaction constant.

Instead of this scheme:

(A) $$L \xrightarrow{k_1} O \xrightarrow{k_2} S$$

another scheme will be used, allowing a *direct* conversion of L into S:

(B)

If all reactions may be described as first order reactions, the following rate equations hold:

$$dL/dt = -k_1 L - k_3 L \tag{3}$$

$$dO/dt = k_1 L - k_2 O \tag{4}$$

$$dS/dt = k_2 O + k_3 L \tag{5}$$

whereas, when weight or mole fractions are used:

$$L + O + S = 1 \tag{6}$$

$$O = y \tag{7}$$

$$S = x. \tag{8}$$

Initially

$$L = 1 \tag{9}$$

and finally

$$S = 1. \tag{10}$$

As shown in the mathematical derivations at the end of this paper, this set of equations leads to:

$$(1-x-y)^l = 1-x-my \tag{11}$$

where

$$l = \frac{k_2/k_1}{1+k_3/k_1} \tag{12}$$

and

$$m = k_2/k_1 - k_3/k_1. \tag{13}$$

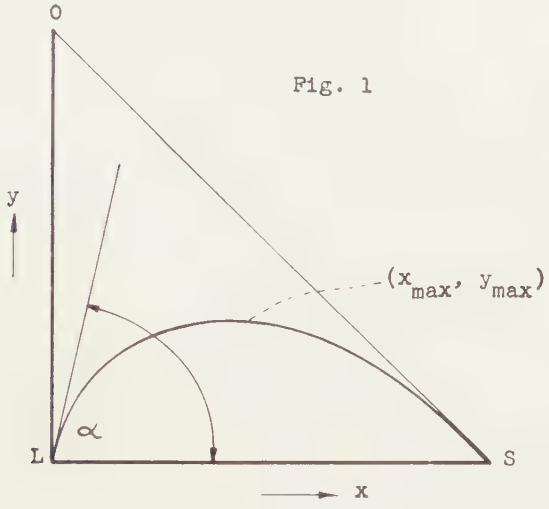

Fig. 1

4. Evaluation of equation (11)

The constants l and m may be evaluated in the following way. The experimental data are plotted in a rectangular diagram, as indicated in the introduction and, as a first approximation, a curve is drawn in the way it is expected to run. The values of x and y in the maximum (see fig. 1) of the (real) curve give k_2/k_1 (mathematical derivations):

$$\frac{k_2}{k_1} = \frac{1-x_{\max}-y_{\max}}{y_{\max}}. \tag{14}$$

The direction of the curve in the origin (mathematical derivations) gives k_3/k_1:

$$k_3/k_1 = \operatorname{cotg} \alpha. \tag{15}$$

The provisional curve gives provisional values for l and m. The exact values may be estimated from two experimental points (x_1, y_1) and (x_2, y_2) as follows. Elimination of m in equation (11) gives:

$$(1-x_1-y_1)^l = \frac{y_1}{y_2}(1-x_2-y_2)^l - \frac{y_1}{y_2}(1-x_2) + (1-x_1). \tag{16}$$

Both the left hand side of (16) and the right hand side of this equation are then drawn as functions of l (values of l round the approximate one).

The intersection of both curves (see fig. 2), $f(l)_{\text{left}}$ and $f(l)_{\text{right}}$ respectively, gives the exact value of l, whereupon that of m can be calculated.

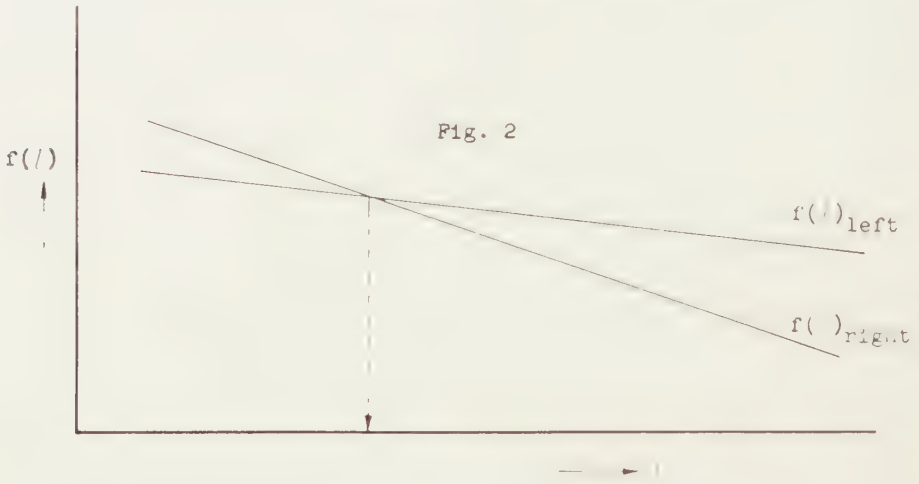

Fig. 2

5. Some examples

Some of the curves of low-temperature hydrogenation, which cannot be described by Wheeler's equation (2), but which can be described by the empirical equation (1) are taken from the figures of Weber [1] (his fig. 28) and Waterman [2] (his fig. 93) and shown in fig. 3. The constants a and b of the drawn lines are given in table I; they are taken from table VIII of Weber [1] or from table XVII of Waterman [2].

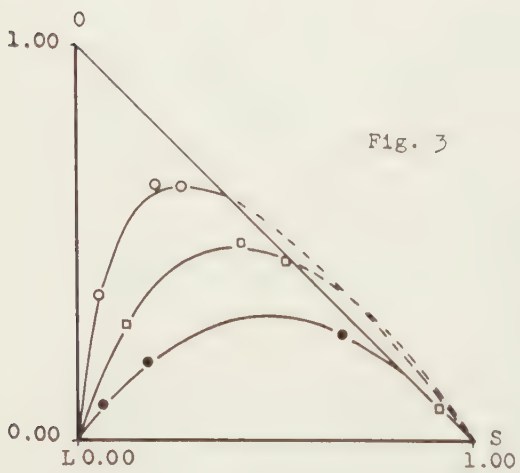

Fig. 3

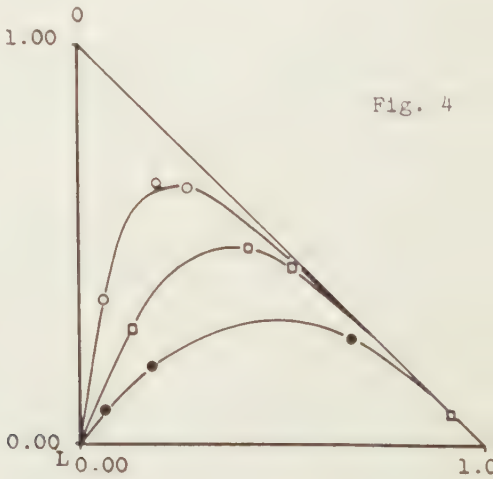

Fig. 4

o 2.5 % Ni-guhr 90 °C, 1 atm
□ 10 % Pt-carbon 30 °C, 1 atm
● 10 % Pt-carbon 20 °C, 100 atm

Table I also gives the values of l and m calculated along the lines of section 4 of the present article.

TABLE I

Symbol	Catalyst	Pressure atm H_2	Temp. ° C	a	b	l	m	k_2/k_1	k_3/k_1
○	2.5 % Ni-guhr	1	90	0.117	0.712	0.150	+0.049	0.17	0.12
□	10 % Pt-carbon	1	30	0.340	0.398	0.178	—0.142	0.25	0.39
●	10 % Pt-carbon	100	20	0.747	0.128	0.373	—0.110	0.65	0.76

With the aid of the values l and m fig. 4 is drawn. Moreover k_2/k_1 and k_3/k_1 can be calculated; these values are also given in table I.

6. Comparison between equations (1) and (11)

Figs. 2 and 4 show great similarity. An advantage of the curves derived from (11) is that they remain inside the triangle. (1) describes the observations only in so far as the curve remains inside the triangle, the hypothenuse being the continuation of the curve.

A comparison of the numerical values derived from (11) and (1) is shown in table II.

TABLE II

x	○		□		●	
	y (11)	y (1)	y (11)	y (1)	y (11)	y (1)
0.062	0.362	0.362	—	—	—	—
0.100	0.486	0.479	0.226	0.236	0.117	0.118
0.174	—	—	0.352	0.352	—	—
0.183	—	—	—	—	0.194	0.194
0.200	0.627	0.618	0.385	0.382	0.207	0.207
0.277	0.637	0.637	—	—	—	—
0.300	0.632	0.634	0.475	0.458	0.270	0.267
0.400	0.576	0.597	0.495	0.481	0.306	0.301
0.419	—	—	0.493	0.480	—	—
0.500	0.493	(0.500)	0.460	0.464	0.314	0.308
0.600	0.398	(0.400)	0.388	(0.400)	0.294	0.292
0.671	—	—	—	—	0.265	0.265
0.700	0.300	(0.300)	0.298	(0.300)	0.250	0.250
0.850	0.150	(0.150)	0.150	(0.150)	0.142	0.149

Where (1) falls outside the figure the values of the hypothenuse are given in brackets.

The y-values have been calculated from the x-values with the help of the parameters given in table I.

Despite the similarity between the two series of numerical values we have not succeeded in reducing (1) and (11) to each other.

7. Mathematical derivations

a) *Derivation of equation* (11)

From the equations

(6) $L = 0 \ldots S \ldots 1$

(7) $O = y$

(8) $S = x$

it follows:

$$L = 1 - x - y.$$

We put

(8a) $$1 - x = u.$$

For equation (3) we can write:

(17) $$\frac{d(u-y)}{dt} = -k_1(u-y) - k_3(u-y)$$

equation (4) becomes:

(18) $$dy/dt = k_1(u-y) - k_2 y$$

and as $dx/dt = -du/dt$, we obtain from (5):

(19) $$du/dt = -k_2 y - k_3(u-y).$$

Division of (18) by (19) gives:

(20) $$\frac{dy}{du} = \frac{k_1 u - k_1 y - k_2 y}{-k_3 u - k_2 y + k_3 y}$$

Suppose

(21) $$y = vu$$

hence

$$dy/du = u(dv/du) + v.$$

Substituting this into (20) we obtain:

$$u\frac{dv}{du} = \frac{k_1 - k_1 v - k_2 v + k_3 v + k_2 v^2 - k_3 v^2}{-k_3 - k_2 v + k_3 v}.$$

The variables can now be separated and the equation be integrated:

(22) $$\int \frac{-k_3 + (k_3 - k_2)v}{-(k_3 - k_2)v^2 - (k_1 + k_2 - k_3)v + k_1} dv = \int \frac{du}{u}.$$

The left hand side of (22) can be simplified and be split up into partial fractions, leading to:

$$\frac{k_2}{k_1-k_2+k_3}\int\frac{dv}{v-1}-\frac{k_1+k_3}{k_1-k_2+k_3}\int\frac{dv}{v+k_1/(k_3-k_2)}=\int\frac{du}{u}$$

$$\frac{k_2}{k_1-k_2+k_3}\ln|v-1|-\frac{k_1+k_3}{k_1-k_2+k_3}\ln|v+k_1/(k_3-k_2)|=\ln u+\ln P_1$$

$$\frac{|v-1|^{k_2/(k_1+k_3)}}{|v+k_1/(k_3-k_2)|}=(P_1u)^{(k_1-k_2+k_3)/(k_1+k_3)}=P_2u^{[1-k_2/(k_1+k_3)]}=P_2\frac{u}{u^{k_2/(k_1+k_3)}}$$

hence

$$\frac{|uv-u|^{k_2/(k_1+k_3)}}{u|v+k_1/(k_3-k_2)|}=P_2. \tag{23}$$

Substituting (8a) and (21) into (23) we obtain:

$$\frac{|y-1+x|^{k_2/(k_1+k_3)}}{|y+(1-x)k_1/(k_3-k_2)|}=P_2.$$

Because the curve must remain inside the triangle, the equation can be written:

$$(1-x-y)^{k_2/(k_1+k_3)}=P_3[1-x-y(k_2-k_3)/k_1].$$

The initial condition $(x;y)=(o;o)$ gives $P_3=1$.

Substituting (12) and (13) we finally obtain:

$$(1-x-y)^l=1-x-my. \tag{11}$$

b) *Another derivation of equation* (11) *by* H. A. G. Chermin

Equation (17) immediately leads to:

$$u-y=\exp\{-(k_1+k_3)t\}. \tag{24}$$

Substituting (24) into (18) we obtain:

$$dy/dt+k_2y=k_1\ \exp\{-(k_1+k_3)t\}$$

which leads to

$$y=\exp(-\int_0^t k_2dt)[C+\int_0^t k_1\exp\{-(k_1+k_3)t\}\exp(\int_0^t k_2dt)dt].$$

When $t=o$, $y=o$, hence $C=o$, hence

$$y=\exp(-k_2t)\int_0^t k_1\exp\{(k_2-k_1-k_3)t\}\,dt$$

$$y=\exp(-k_2t)\frac{k_1}{k_2-k_1-k_3}[\exp\{(k_2-k_1-k_3)t\}-1]$$

$$y=\frac{k_1}{k_2-(k_1+k_3)}[\exp\{-(k_1+k_3)t\}-\exp(-k_2t)]. \tag{25}$$

Putting

$$(k_1+k_3)t = \tau \tag{26}$$

and using equations (12) and (13) for l and m, we obtain

$$y = 1/(m-1)\{\exp(-\tau)-\exp(-l\tau). \tag{27}$$

(24) together with (26) gives:

$$1-x-y = \exp(-\tau). \tag{28}$$

Substituting this into (27) we obtain

$$\begin{aligned}(m-1)y &= (1-x-y)-\exp(-l\tau)\\ \exp(-l\tau) &= 1-x-my.\end{aligned} \tag{29}$$

As

$$\exp(-l\tau) = \{\exp(-\tau)\}^l$$

we obtain from (28) and (29):

$$(1-x-y)^l = 1-x-my. \tag{11}$$

This derivation has the advantage that also y and $(u-y)$ are obtained as functions of t (equations (24) and (25) respectively).

c) *Derivation of equation* (14)

In the maximum of the curve the first derivative is equal to zero. Division of (4) by (5) gives

$$\frac{dO}{dS} = \frac{k_1L-k_2O}{k_2O+k_3L} \tag{30}$$

hence

$$k_1L_{\max}-k_2O_{\max} = 0$$

$$\frac{k_2}{k_1} = \frac{1-x_{\max}-y_{\max}}{y_{\max}}. \tag{14}$$

d) *Derivation of equation* (15)

Equation (15) likewise follows from (30). For $L = 1$ and $O = 0$, we obtain

$$dO/dS = k_1/k_3 = \operatorname{tg}\alpha$$

$$k_3/k_1 = \operatorname{cotg}\alpha. \tag{15}$$

The author wishes to thank Prof. J. H. DE BOER and Prof. G. MEYER for their valuable stimulation and comments, and especially also Mr. H. A. G. CHERMIN for his contribution towards the mathematical derivations.

LITERATURE

1. Weber, A. B. R., Hydro-isomerization of parafin wax, thesis, Delft 41–75 (1957).
2. Waterman, H. I., Anal. Chim. Acta, **18**, 395, 498 (1958); H. I. Waterman, Correlation between Physical Constants and Chemical Structure, Elsevier Publishing Company, Amsterdam, London, New York, Princeton, 104–113 (1958).
3. Vlodrop, C. van, Katalytische hydrogenering van vette oliën, thesis Delft 1938.
4. Boelhouwer, C., J. Snelderwaard and H. I. Waterman, J. Am. Oil Chemists' Soc., **33**, 143 (1956).
5. Wheeler, A., Advances in Catalysis, **III**, 249, 317; Academic Press Inc., New York, 1951.

THE KINETICS OF THE SELECTIVE FORMATION OF THE INTERMEDIATE PRODUCT IN TWO CONSECUTIVE REACTIONS

BY

J. H. DE BOER AND R. J. A. M. VAN DER BORG

(Communicated at the meeting of September 26, 1959)

1. INTRODUCTION

In a previous article [1], one of us (VAN DER BORG) has shown that the formulation of a selective catalytic process:

(α) $$A \xrightarrow{k_1} B \xrightarrow{k_2} C$$

where B is a desired intermediate, which can react further to give an undesired by-product C, may substantially be improved when also a direct transformation of A into C is taken into consideration:

(β)

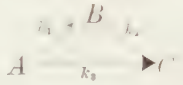

It could be proved that a kinetic equation based on scheme (β) describes the experimental data equally well as an empirical equation which is recommended for its universal use [2]. In such a case the equation which is based on kinetic considerations is to be recommended in favour of the empirical one, because its constants have a physical significance.

In the present article the physical meaning of schemes (α) and (β) and of the equations, which are based on these schemes will be discussed.

2. EQUATIONS

a. *The general equation*

If the three all-over reactions, for practical purposes, can be described as first order reactions, scheme β leads [1] to the following equation:

(1) $$(1-x-y)^l = 1-x-my$$

where x is the fraction of A which is converted into C and y is the fraction which is converted into B and where:

(2) $$l = \frac{k_2/k_1}{1+k_3/k_1}$$

and

(3) $$m = k_2/k_1 - k_3/k_1.$$

The parameters of equation (1), therefore, are the relations between the rate constants, k_2/k_1 and k_3/k_1 respectively.

b. The special case of $k_3 = 0$

If $k_3 \to 0$, scheme (β) reduces to scheme (α), which is, therefore, a special case of the more general scheme (β). Substituting $k_3 = 0$ in equations (2) and (3), we obtain:

$$l = m = k_2/k_1,$$

and equation (1) reduces to:

$$(1-x-y)^{k_2/k_1} = 1-x-\frac{k_2}{k_1}y \tag{4}$$

Equation (4) is identical with the equation which WHEELER [3] derived from the kinetics of scheme (α), viz.:

$$\alpha_B = \frac{S}{S-1}(1-\alpha_A)\ [(1-\alpha_A)^{(1-S/S)} - 1] \tag{5}$$

where α_B is the fraction of A, converted into B,
α_A is the fraction of A which has reacted,
and S is the so-called selectivity factor; $S = k_1/k_2$.

The identity of (4) and (5) can easily be seen, when we note that:

$$\alpha_B = y \text{ and } \alpha_A = x+y.$$

c. The special case of $k_2 = 0$

If $k_2 = 0$, we obtain:

$$l = 0,$$

$$m = -k_3/k_1.$$

and equation (1) reduces to:

$$x = \frac{k_3}{k_1}y \tag{6}$$

Scheme (β), in such a case, reduces to scheme (γ)

$$A \begin{matrix} \xrightarrow{k_1} B \\ \xrightarrow[k_3]{} C \end{matrix} \tag{γ}$$

Wheeler's equation (7), derived [3] from scheme (γ), viz.:

$$\alpha_B = S\alpha_C, \tag{7}$$

where: $S = k_1/k_3$,
is identical with (6), when we note that in this case

$$\alpha_B = y \text{ and } \alpha_C = x.$$

3. THE PHYSICAL MEANING OF SCHEME (β)

Suppose A to be a molecule, which, on a heterogeneous catalyst, can react with a molecule M to form a product B, whilst this reaction may

be followed by another reaction with M, on the same catalyst, to give product C. To give an example, A may be an organic aromatic compound, such as benzene or naphthalene, and M may be oxygen. On a vanadium oxide catalyst product B may then be maleic anhydride or phthalic anhydride, respectively and C is carbon dioxyde. In a hydrogenation process, A may be an acetylenic compound, B the corresponding ethylenic compound and C the saturated compound, or, if A is linoleic ester, B may be oleic ester and C stearic ester. In all these hydrogenation processes, M is hydrogen and the catalyst is e.g. nickel or platinum in a suitable form.

In order to execute the partial process $A \rightarrow B$ molecules of A and of M have to move to the surface of the catalyst (diffusion to the outer surface and, if necessary, diffusion into the pores), they have to be adsorbed on that surface, whereupon they can react to form adsorbed B, which has to be desorbed, followed by a diffusion of B from the surface of the catalyst to the bulk of the homogeneous (liquid or gaseous) phase.

Apart from all diffusion processes and apart from the chemisorption process of M, the partial process $A \rightarrow B$ involves:

a) chemisorption of A,
b) reaction of chemisorbed A and M to chemisorbed B,
c) desorption of B.

The partial process $B \rightarrow C$, treated similarly, involves:

d) chemisorption of B,
e) reaction of chemisorbed B and M to chemisorbed C,
f) desorption of C.

The direct route $A \rightarrow C$ of scheme (β), however, comprises:

a) chemisorption of A,
b) reaction of chemisorbed A and M to chemisorbed B,
e) reaction of chemisorbed B and M to chemisorbed C,
f) desorption of C.

We assume that the chemisorbed state of B, produced in reaction b) is identical with that which results from the chemisorption process d); in that case step e) in the partial process $B \rightarrow C$ is the same as in the direct route $A \rightarrow C$.

The essential difference between $A \rightarrow B \rightarrow C$ and $A \rightarrow C$, therefore, is the behaviour of the intermediate B.

In the latter, direct, route, the intermediate B is not desorbed, and, consequently, does not contribute to the content of B in the bulk phase. If, during its time of adsorption [4a] a molecule M can react with the adsorbed intermediate, step e) is performed. If, however, its time of adsorption is so short that step e) does not take place, B is desorbed. The time of adsorption depends on the activation energy for desorption and on the degree of mobility of the adsorbed species [4b]. The rate of reaction of the intermediate depends on similar entities.

4. The fate of the adsorbed molecule B

In order to get an idea about the fate of the chemisorbed molecule B after step b) is performed, we shall apply some equations of the theory of absolute reaction rates [5] to this problem.

a. *Localized adsorption of B and M*

If we suppose both B and M to be adsorbed on definite adsorption sites, without translatory movement across the surface and without rotational freedom, the rate, v_c, of step c) may be given as follows:

$$v_c = C_B \times \frac{kT}{h} \times \frac{F_{\neq}}{F_B} e^{-E_d/kT} \tag{8}$$

where C_B is the surface concentration of B, $F_{\neq}$ is the partition function of the activated complex for desorption per cm², F_B is the partition function of the adsorbed molecules B per cm², E_d is the activation energy for desorption (per molecule), k Boltzmann's constant, h Planck's constant and T the absolute temperature.

Similarly the rate, v_e, of step e) following b) in the direct route $A \rightarrow C$ is given by:

$$v_e = \frac{C_B C_M}{L} s \times \frac{kT}{h} \times \frac{(F_{\neq})_{BM}}{F_{BM}} e^{-E_{act}/kT} \tag{9}$$

where C_M is the surface concentration of M, L is the total number of adsorption sites per cm², s the number of direct neighbour sites, surrounding any adsorption site, $(F_{\neq})_{BM}$ the partition function of the activated complex for reaction, per cm², F_{BM} the partition function for the direct neighbouring pairs of B and M per cm² and E_{act} the activation energy for reaction.

Dividing (8) and (9), we obtain:

$$\frac{v_c}{v_e} = \frac{L}{C_M s} \times \frac{F_{\neq}}{F_B} \times \frac{F_{BM}}{(F_{\neq})_{BM}} \times e^{-(E_d - E_{act})/kT} \tag{10}$$

C_M can be written as $L\theta_M$, where θ_M is the degree of occupation of M. Because of the localised character of the adsorption, $F_B = 1$ and $F_{BM} = 1$. $F_{\neq}$ and $(F_{\neq})_{BM}$ need not be unity, but we assume them to be roughly equal, in which case (10) simplifies to

$$\frac{v_c}{v_e} = \frac{1}{\theta_M s} e^{-(E_d - E_{act})/kT} \tag{11}$$

b. *Mobile adsorption of B and M*

If we suppose B and M to be in a mobile adsorbed state, we obtain for the rate v_c the same equation (8) as in the immobile case. However, $F_{\neq}$ and F_B are not equal to unity in this case.

For v_e, we obtain:

$$v_e = C_B \times C_M \times \frac{kT}{h} \times \frac{(F_{\neq})_r}{F_B \cdot F_M} \times e^{-E_{act}/kT} \tag{12}$$

where $(F_*)_r$ is the partition function of the mobile activated complex per cm^2 and F_B and F_M the partition function of B and M, respectively, both per cm^2.

Dividing v_c and v_e, we obtain:

$$\frac{v_c}{v_e} = \frac{1}{C_M} \times \frac{F_* \times F_M}{(F_*)_r} e^{(-E_d - E_{act})/kT} \tag{13}$$

For C_M we write again $L\theta_M$ and we assume $F_* = (F_*)_r$.

Equation (13) then simplifies to:

$$\frac{v_c}{v_e} = \frac{F_M}{L\theta_M} e^{-(E_d - E_{act})/kT} \tag{14}$$

c. *Comparison between equations* (11) *and* (14)

The pre-exponential factor in equation (11) contains, apart from θ_M, the number s, which may be 3, 4 or 6. The pre-exponential factor in equation (14), however, contains, apart from θ_M, the proportion F_M/L. L is of the order of magnitude of 10^{15} cm^{-2}, whilst:

$$F_M = \frac{2\pi m_M kT}{h^2} \times (F_M)_{rot} \times (F_M)_{vib} \tag{15}$$

where m_M is the mass of a molecule M and $(F_M)_{rot}$ and $(F_M)_{vib}$ are the partition function of the rotational and vibrational degrees of freedom, respectively.

If the molecular weight of $M = 20$ and $T = 300°$ K, (15) gives:

$$F_M = 20 \times 10^{16} \ (F_M)_{rot} (F_M)_{vib}$$

and the pre-exponential factor of (14) may be roughly 10^3 times the pre-exponential factor of (11). Even if $M = H$ (hydrogen atom), as may well be the case in hydrogenation reactions, $F_M = 10^{16}$ at 300° K and $F_M = 1.5 \times 10^{16}$ at 450° K (rotational and vibrational contributions can be neglected) and the pre-exponential factor is still 40 to 60 times higher in the case of mobile adsorption.

5. Influence on selectivity

If the intermediate product B is the desired product and C is an undesired by-product, k_1 should be large and, both, k_2 and k_3 should be low. A low value of k_3 is obtained if v_c is high with respect to v_e.

If, in equation (11) or (14), $E_d = E_{act}$, the proportion v_c/v_e is only governed by the pre-exponential factor of both equations. In such a case localized (immobile) adsorption would hardly give any selectivity, but mobile adsorption would result in an appreciably high degree of selectivity. Mobile adsorption is promoted by raising the temperature and by choosing a catalyst not adsorbing too strongly.

It is a remarkable result of these considerations that raising the temperature should promote selectivity. This, of course, would be more pronounced if $E_d - E_{act}$. If, therefore, the activation energy for desorption

of the intermediate B is smaller than the activation energy of the further reaction of this intermediate, selectivity is certainly promoted by raising the temperature. At the same time, the condition $E_d < E_{act}$ points to the selective character of a less active catalyst.

Both equations (11) and (14) contain θ_M in the denominator. Any factor lowering θ_M, therefore, also promotes the selectivity.

Selectivity by suppressing the rate constant k_3 can, therefore, be obtained by:

a) higher temperature,
b) a less active catalyst,
c) a lower concentration of the substance M on the catalyst.

6. The selective hydrogenation of linoleic ester as an example

Literature shows that the selectivity of this hydrogenation reaction to form oleic ester, and preferably not stearic acid, is promoted by the following factors:

a) higher temperature. Waterman [2] showed that the high temperature hydrogenation (180° C) could be represented by equation (5), hence by scheme (α). It means that, at that temperature, reaction k_3 is practically suppressed;
b) a less active catalyst; Ni is a more selective catalyst than Pt;
c) a lower concentration of hydrogen on the catalyst, which may e.g. be obtained by a lower hydrogen pressure.

If we take the selectivity factors $S = k_1/k_2$ for higher temperatures from the figures of Waterman [2] and, if we denote $S = k_1/(k_2 + k_3)$ for lower temperatures, where k_3 is still significantly high and we calculate S from the figures, given in the previous publication [1], we obtain the following table, which illustrates the relations very well.

TABLE I

Catalyst	Temp. ° C	Hydrogen pressure atm	S
10 % Pt-carbon	30	1	1.55
	20	100	0.7
	180	1	6
2 % Ni-guhr	90	1	3.4
	180	1	~25
	180	100	~ 2

7. The special case of scheme (γ)

If [1]) scheme (γ) is a special case of scheme (β), step $B \rightarrow C$ is suppressed, which means that adsorption of B from the bulk phase does not lead to

[1]) A scheme (γ) can also be visualized if the two reactions are quite independant from each other. We only consider here the special case that the step $A \rightarrow C$ takes its course via absorbed B.

reaction. A poisoning of the catalyst in such a way that B cannot be adsorbed properly may lead to such conditions. If the other conditions are such that also k_3, hence step $A \rightarrow C$ is suppressed, ideal selectivity will be found. It is reported in literature that sulphur-poisoning of a nickel-catalyst may suppress the hydrogenation of oleic ester completely [6].

Another method of suppressing step $B \rightarrow C$ may be applied by adding an indifferent substance with an adsorbability in between those of A and of B. Step $B \rightarrow C$ will then be suppressed, but not step $A \rightarrow C$. Other measures, such as choosing a higher temperature, or desactivating the catalyst, or a lower concentration of hydrogen (in hydrogenation reactions) may be applied to that end. It is not improbable that some very special catalysts, used in the pharmaceutical industry operate along these lines [6].

8. Other factors

It must finally be pointed out that the kinetic expressions, leading to equation (1) are derived, assuming that the all-over rate reactions can be described as first order reactions. This may in practice often be done.

Diffusion rates are not taken into consideration. In liquid media the bulk diffusion may influence the results of practical experiments. When microporous catalysts are used diffusion in the pore system may influence selectivity problems seriously. The influence of these factors on the selectivity problems discussed in the present paper, will be the subject of later studies.

LITERATURE

1. Borg, R. J. A. M. van der, Proc. Kon. Ned. Ak. v. Wet. B 62, 299 (1959).
2. Waterman, H. I., Anal. Chim. Acta 18, 395, 498 (1958); Correlation between Physical Constants and Chemical Structure, Elsevier Publ. Cy, Amsterdam, London, New York, Princeton 105 (1958).
3. Wheeler, A., Adv. in Catalysis III, p. 249, Academic Press, Inc., New York (1951).

4*a*. Boer, J. H. de, The Dynamical Character of Adsorption, The Clarendon Press, Oxford, 31 (1953).

4*b*. ———, Adv. in Catalysis VIII, 85, Academic Press, Inc., New York (1956).

5. Glasstone, S., K. J. Laidler and H. Eyring, The Theory of Rate Processes, Academic Press, Inc., New York. 1941.
6. Bailey, A. E., Industrial Oil and Fat Products, Interscience Publ., Inc., New York (1945).
7. Boer, J. H., Chemistry and Industry 1959, p. 934.

ON THE POWER TRANSFER BETWEEN PARAMAGNETIC SPINS AND CRYSTAL LATTICE. Ia

BY

B. BÖLGER

(Communicated by Prof. C. J. GORTER at the meeting of June 27, 1959)

INTRODUCTION

The establishment of equilibrium between a system of paramagnetic moments and the crystal lattice can be characterized by a spin-lattice relaxation time τ_1. This has been the object of many investigations and recently the interest and that for related problems has gained new impetus due to the application of paramagnetic materials in low noise microwave amplifiers, so called "solid state masers".

In the usual method to determine the spin-lattice relaxation time an alternating field is applied parallel to the static magnetic field and the complex susceptibility measured as a function of the frequency. With the aid of the thermodynamical model of CASIMIR and DU PRÉ [1], τ_1 can then be found. A survey of the experimental data up to 1947 has been given by GORTER [2].

Apart from a few exceptions, the theory of VAN VLECK [3] describes the experimental results for the magnetically diluted salts fairly well. For the concentrated salts, on which most of the early measurements were carried out, the agreement at liquid helium temperatures is miserable.

With the advent of paramagnetic resonance new techniques have become available to measure the spin-lattice relaxation behaviour. The system of magnetic moments can be heated, owing to an inadequate power transfer to the lattice, by absorption of microwave power. The study of the magnetic temperature as a function of the absorbed power in the stationary state, yields a value of the power transfer constant closely related to τ_1. This method is called the saturation method. Data obtained by ESCHENFELDER and WEIDNER [4] seemed to indicate a large discrepancy between the results obtained by the two methods.

It has been the purpose of the investigations described in this work to study the spin-lattice relaxation behaviour in a number of paramagnetic salts by the saturation method. A comparison is made between the results obtained by theory and by the relaxation and the saturation method. For the work carried out in connection with the construction of a maser reference is made to [5] and [6]. Only the results of that work pertaining to relaxation properties has been used.

REFERENCES

1. CASIMIR, H. B. G. and F. K. DU PRE, Physica **5**, 507 (1938); Comm. Kamerlingh Onnes Lab. Leiden, suppl. no. 85 a.
2. GORTER, C. J., Paramagnetic Relaxation. Elseviers Publ. Co. Amsterdam (1947).
3. VAN VLECK, J. H., Phys. Rev. **57**, 426 (1940).
4. ESCHENFELDER, A. H. and R. T. WEIDNER, Phys. Rev. **92**, 869 (1953).
5. BÖLGER, B., B. J. ROBINSON and J. UBBINK, To be published in Physica and Commun.
6. ———— and ————, Arch. des Sc. Geneve **11**, 187 (1958); and Commun. Suppl. 114 i.

ON THE GENERAL THEORY OF PARAMAGNETIC RESONANCE AND RELAXATION

[1.1] *The energy levels of paramagnetic ions*

Paramagnetic resonance deals with the transitions caused by a magnetic high frequency field between the lowest group of energy levels of a paramagnetic ion. The splittings between these levels will first be discussed.

The case of free ions is relatively simple. The fact, however, that in crystals the energy levels are displaced by interactions with the surroundings makes paramagnetic resonance a fruitful source of problems in solid state physics.

In this thesis we shall restrict ourselves to crystals in which the effect of the crystal field is small compared to that of the Coulomb interactions of the electrons with the nucleus and with each other, so that the self consistent field method can be used to describe the ionic wave functions. In ionic crystals this condition is fulfilled to a high degree.

We shall only consider the elements belonging to the iron transition group.

[1.1.1] The Hamiltonian used to describe a paramagnetic ion in a crystal lattice can be divided into:

a. the orbital energy $\mathscr{H}_O$ due to the coulomb energy of the electrons. This energy is mainly due to the influence of the nearest atoms. The direct effect of ions at a larger distance is negligible and their influence is mainly felt via coupling with the nearest neighbours.

b. The spin orbit coupling $\mathscr{H}_{OS}$ will be taken to be (cf. [1]) $\mathscr{H}_{OS} = \lambda \mathbf{L} \cdot \mathbf{S}$ where $\mathbf{L}$ and $\mathbf{S}$ are the total angular momentum vectors of orbit and spin.

A tensor type of interaction between $\mathbf{L}$ and $\mathbf{S}$ has been considered by Pryce [2].

c. The Zeeman energy

$$\mathscr{H}_Z = \beta(\mathbf{H} + \mathbf{h})\,(\mathbf{L} + 2\mathbf{S}) \tag{1.01}$$

where β is the Bohr magneton. $\mathbf{H}$ the applied static field and $\mathbf{h}$ a radio frequency field.

d. The dipole-dipole interaction between two ions i and j can be written as

$$\mathscr{H}_d = \frac{\boldsymbol{\mu}_i \cdot \boldsymbol{\mu}_j}{r_{ij}^3} - 3\,\frac{(\boldsymbol{\mu}_i \cdot \mathbf{r}_{ij})(\boldsymbol{\mu}_j \cdot \mathbf{r}_{ij})}{r_{ij}^5} \tag{1.02}$$

where $\mathbf{r}_{ij}$ is the radius vector between ions i and j with magnetic moments $\boldsymbol{\mu}_i$ and $\boldsymbol{\mu}_j$.

e. The exchange interaction

$$\mathscr{H}_{ex} = 2J_{ij}\mathbf{S}_i \cdot \mathbf{S}_j \tag{1.03}$$

is due to the overlap of the wave functions of ion i and j; in this expression superexchange may be included. In more general considerations one has to add anisotropic exchange terms.

The interactions of the electronic spin with the nuclear spin moment have been omitted as they are generally small and are not of interest in the present work.

The terms d. and e. determine the coherence effects between the spins and will be discussed later.

As the interactions $\mathscr{H}_O$, $\mathscr{H}_{OS}$ and $\mathscr{H}_Z$ are generally far more important than the coupling of the spins with each other, it is possible to consider the spins of different ions as being separate entities in a first approximation.

[1.1.2] The perturbation calculation starts with the largest term $\mathscr{H}_O$. The crystal field around an ion is expanded in Legendre polynomials and one considers how the orbital degeneracy is removed by going successively to lower orders of field symmetry. This has been done by the methods of group theory by Bethe, Mulliken and Jahn [3] [4] [5] and we will use their notation of designating the levels.

For the case that the lowest eigenvalue of $\mathscr{H}_O$ is non-degenerate, the perturbation calculation can be carried out by a method given by Pryce [6], by chosing a representation for $\mathbf{L}$, diagonalizing $\mathscr{H}_O$ and the so-called spin Hamiltonian contains the operator $\mathbf{S}$ and the matrix elements of $\mathbf{L}$ in the specified representation, corresponding to the lowest multiplet. It is now possible to define an effective spin operator $\mathbf{S}'$ so that $2S'+1$ is the degeneracy of the ground state. The spin Hamiltonian can be expressed in terms of the operator $\mathbf{S}'$. For the case of a degenerate lowest orbital level reference is made to the literature [7] [8].

For ions with $L=0$ one has to go to a high order perturbation, but for other ions the second order is usually sufficient. In the derivation one makes use of a general theorem that $\mathbf{L}$ has no diagonal elements for a singlet orbital state.

The spin Hamiltonian, when spin-spin interactions (d and e) are neglected, has the following form: (cf. [7])

$$\left\{\begin{aligned}\mathscr{H}_S &= 2\beta\mathbf{H}\cdot\mathbf{S} - (2\lambda)^{-1}(\beta\mathbf{H} + \lambda\mathbf{S})(g-2)(\beta\mathbf{H} + \lambda\mathbf{S}) - \\ &= \bar{\bar{g}}\beta\mathbf{H}\cdot\mathbf{S} + \mathbf{S}\cdot\bar{\bar{D}}\cdot\mathbf{S} - \beta^2\mathbf{H}\bar{\bar{A}}\mathbf{H}.\end{aligned}\right. \tag{1.04}$$

If the ground state orbital wave function is denoted by $\langle o|$ and the higher ones by $\langle n|$ then

$$(\bar{\bar{g}}-2) = \sum_n \frac{2\lambda}{E_n - E_0}\langle o|\mathbf{L}_i|n\rangle\langle n|\mathbf{L}_j|o\rangle \qquad i,j = x,y \text{ or } z. \tag{1.05}$$

The factor $\bar{\bar{g}}$ is a tensor and so are $\bar{\bar{D}}$ and $\bar{\bar{A}}$.

In the third part of (1.04), the Zeeman energy is given by the first

term, the second term gives the zero field splitting caused by the crystal field and the third term represents the temperature independent paramagnetism. The total spin Hamiltonian must of course show at least the same symmetry as the crystal field. One advantage of using this method is that the resonance properties of an ion can be described by a small number of constants. For a more detailed discussion of the spin Hamiltonian and the values of the constants found experimentally in the various substances, reference is made to the review articles of BLEANEY and STEVENS [7] and of BOWERS and OWEN [8].

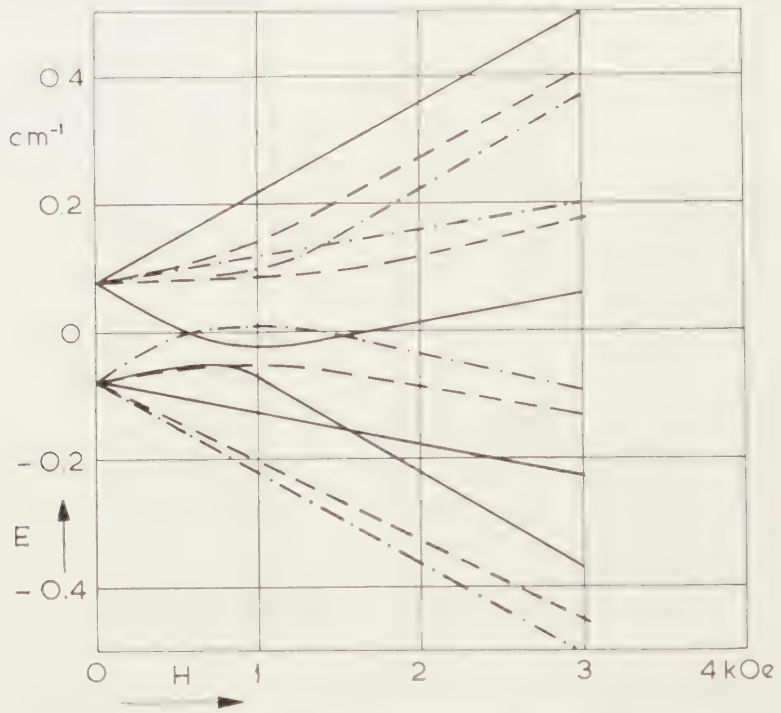

Fig. 1.1. Energy levels of $K_3Cr(CN)_6$ as a function of **H**.
– – – **H** // x-axis. –·–·– **H** // y-axis. ——— **H** // z-axis.

[1.1.3] As an illustration we give in fig. 1.1 the energy levels of Cr^{+++} in $CrK_3(CN)_6$ diluted with the Co salt as a function of the applied magnetic field **H** along the different crystal axes, as calculated from the spin Hamiltonian. Cr^{+++} has a $S=3/2$ and in this substance $\mathscr{H}_S$ has the following form

$$\mathscr{H}_S = g\beta \mathbf{H}\cdot\mathbf{S} + D[S_z^2 - 1/3 S(S+1)] + E(S_x^2 - S_y^2) \tag{1.06}$$

where g is almost isotropic and equal to 1.99. The values of the other constants are $D=0.083$ cm^{-1} and $E=0.011$ cm^{-1}. The magnetic axes are slightly rotated with respect to the crystal axes. There are two Cr^{+++} ions in a unit cell with the ac-plane as a symmetry plane.

To find the paramagnetic spectrum at 4000 MHz (or 0.133 cm^{-1}) for instance, one has to adjust the field so as to fit this energy between two energy levels. To show the anisotropy, a rotation diagram (fig. 1.2) in the ac-plane for the frequencies 1420, 3850 and 8500 MHz has been drawn for some of the transitions. This diagram represents the loci of the field vector for which resonance takes place as a function of the angle α of **H** with the a-axis.

The transitions are labeled by the corresponding energy levels, numbered from the lowest.

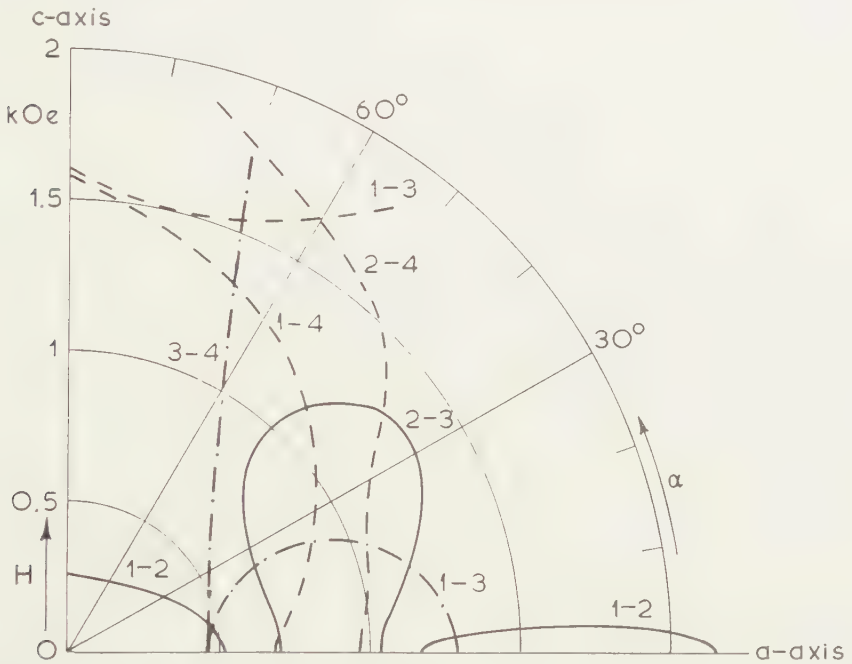

Fig. 1.2. Rotation diagram of $K_3Cr(CN)_6$, **H** in ac-plane. Corresponding energy levels next to loci, lowest is 1.

——— 1420 MHz. —·—·— 3850 MHz. – – – 9400 MHz.

[1.1.4] The terms of the Hamiltonian of the paramagnetic ion depending on the position of the ion in the lattice such as in $\mathcal{H}_O$, through a perturbation calculation, and in $\mathcal{H}_d$ and $\mathcal{H}_{ex}$ through the ion distances $\mathbf{r}_{ij}$ in (1.02) and (1.03), may be developed into a power series of the deviations $\mathbf{u}_k$ and $\mathbf{u}_j$ of ion k and j from their equilibrium positions. Limiting ourselves to terms of second order, this gives

$$\mathcal{H} = \mathcal{H}_0 + \sum_k \mathcal{H}_{1k}(u_k) + \sum_{kj} \mathcal{H}_{2kj}(u_k u_j). \tag{1.07}$$

For the first term $\mathcal{H}_0$, due to the ions in their equilibrium positions, we take the spin Hamiltonian (1.04) with the spin-spin interactions added, the second and third terms are respectively linear and quadratic terms in the displacement vectors $\mathbf{u}_k$. They give rise to the coupling of the

spin system with the thermal motions of the lattice. Their influence is several orders of magnitude smaller than $\mathscr{H}_0$ and they can be regarded as small perturbations. To a first approximation the spins can be regarded as being decoupled from the lattice.

[1.2] *Macroscopic equations*

[1.2.1] A classical description of nuclear and paramagnetic resonance has been given by Bloch [9] for spins without zero field splitting. Consider an assembly of N spins, all with the same gyromagnetic ratio $\gamma = g\beta/\hbar$.

If the spin system is in thermal equilibrium with the lattice at a temperature T, the magnetization $\mathbf{M}$ will have the value given by the Curie law,

$$\mathbf{M} = \frac{C\mathbf{H}}{T} = \frac{N\gamma^2\hbar^2 S(S+1)\mathbf{H}}{3kT} \tag{1.08}$$

where $\mathbf{H}$ is the applied magnetic field.

The equation of motion of $\mathbf{M}$ without interactions with the surroundings is

$$\frac{d\mathbf{M}}{dt} = \gamma(\mathbf{M}\times\mathbf{H})$$

which expresses the fact that $\mathbf{M}$ precesses around $\mathbf{H}$ with the Larmor frequency:

$$\boldsymbol{\omega}_L = \gamma\mathbf{H}.$$

Bloch introduced damping terms in the equation of motion of $\mathbf{M}$. Due to the interactions the different electrons will precess at slightly different frequencies. The components of $\mathbf{M}$ perpendicular to $\mathbf{H}$ will therefore get out of phase after a time τ_2, the so-called transverse relaxation time. Then

$$\frac{d|M_{x,y}|}{dt} = -\frac{|M_{x,y}|}{\tau_2} \tag{1.09}$$

where $\mathbf{H}$ is taken along the z-axis.

The relaxation time τ_1 of the component of $\mathbf{M}$ parallel to $\mathbf{H}$ will in general have a larger value than τ_2, as a change in the z-component entails a change of the Zeeman energy and this can only happen through a coupling with the surroundings.

$$\frac{dM_z}{dt} = -\frac{M_z - M_0}{\tau_1}. \tag{1.10}$$

We shall now write down the equations of motion when a linearly polarized radio frequency field $\mathbf{h}$ perpendicular to $\mathbf{H}$ is applied to the sample.

$$\begin{cases} \dfrac{dM_{x,y}}{dt} = \gamma[\mathbf{M}\times\mathbf{H}]_{x,y} - \dfrac{M_{x,y}}{\tau_2} \\ \dfrac{dM_z}{dt} = \gamma[\mathbf{M}\times\mathbf{H}]_z - \dfrac{M_z - M_0}{\tau_1} \end{cases} \tag{1.11}$$

with $H_x = h/2\,(e^{i\omega t} + e^{-i\omega t})$; $H_y = 0$; $H_z = H$.

The steady state solution has the following form

$$(1.12)\qquad \begin{cases} M_x = \dfrac{M_z\gamma^2 H h\tau_2^2[(\omega_L^2+1/\tau_2^2-\omega^2)-(2i\omega/\tau_2)]e^{i\omega t}}{4\omega^2+\tau_2^2[\omega_L^2+1/\tau_2^2-\omega^2]^2} \\ M_y = \dfrac{M_z\gamma h[i\omega+1/\tau_2]e^{i\omega t}}{(i\omega+1/\tau_2)^2+\gamma^2H^2} \\ M_{z_{av}} = M_0\dfrac{4\omega^2+\tau_2^2(\omega_L^2+1/\tau_2^2-\omega^2)^2}{4\omega^2+\tau_2^2(\omega_L^2+1/\tau_2^2-\omega_2^2)^2+{}^1/_2\gamma^2h^2\tau_1\tau_2(\omega_0^2+1/\tau_2^2+\omega^2)} \end{cases}$$

where the high frequency motions of M_z have been eliminated by averaging over many Larmor periods.

Near the resonance frequency $\omega^2=\omega_L{}^2+1/\tau_2{}^2$, slightly displaced because of the damping, we have

$$(1.13)\qquad M_x = \frac{M_0}{2}\frac{\gamma h\tau_2(\Delta\tau_2+i)\,e^{i\omega t}}{1+(\Delta\tau_2)^2+{}^1/_4\gamma^2h^2\tau_1\tau_2}$$

where

$$\omega_L{}^2-1/\tau_2{}^2-\omega^2=2\omega\Delta.$$

Introducing the complex susceptibility $\chi=\chi'-i\chi''$ so that $\mathbf{M}=\chi\mathbf{H}$, and relating this to the power P absorbed by the system from the r.f. field, one obtains

$$(1.14)\qquad P={}^1/_2\omega\chi''h^2={}^1/_2\omega\mathbf{h}\cdot\mathrm{Im}\,\mathbf{M}.$$

From (1.13) we find

$$(1.15)\qquad P=\frac{\mathcal{N}(\hbar\omega)^2\gamma^2h^2\tau_2S\cdot(S+1)}{12kT[1+(\Delta\tau_2)^2+{}^1/_4\gamma^2h^2\tau_1\tau_2]}.$$

Upon increasing h we have initially $P\propto h^2$ as expected, but for values of $h^2>\frac{1}{{}^1/_4\gamma^2\tau_1\tau_2}$ (at resonance), P starts to saturate (cf. fig. 1.3) and reaches

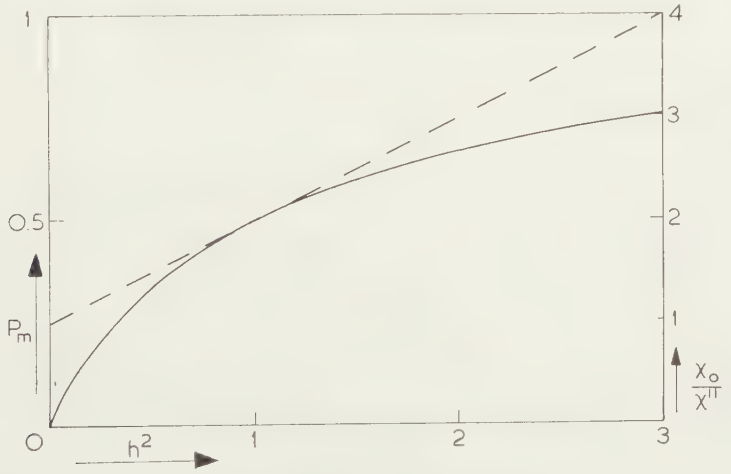

Fig. 1.3. P_m and χ_0/χ'' as a function of h^2.
——— P_m ---- χ_0/χ''

asymptotically the value

$$P_\infty = \frac{N(\hbar\omega)^2 S\cdot(S+1)}{3kT\tau_1}. \tag{1.16}$$

At 4° K and $H = 3000$ ø typical values for the relaxation constants are $\tau_2 \approx 10^{-9}$ s. and $\tau_1 \approx 10^{-3}$ s. requiring a r.f. field of about 0.1 ø to reach half the expected saturation.

[1.3] *Microscopic theory*

We shall now approach the subject from a microscopic viewpoint. Suppose we have an assembly of spins of which the spin Hamiltonian (1.04) is known, and that the eigenvalues and eigenfunctions have been calculated.

When a radio frequency field $h_x \sin \omega t$ is applied as a perturbation

$$\mathscr{H}_{\text{rf}} = \gamma\hbar h_x(\omega) S_x \sin \omega t, \tag{1.17}$$

then the transition probability induced by this perturbation will be proportional to the square of the modulus of the matrix elements $\langle i|S_x|j\rangle$, taken between the eigenstates i and j of the spin Hamiltonian.

The transition frequencies $\omega_{ij} = \frac{E_i - E_j}{\hbar}$ will have a certain width due to spin interactions and lifetime limiting processes. The shape of the transition will be characterized by the normalized shape function $g(\omega - \omega_{ij})$ where

$$\int_{-\infty}^{+\infty} g(\omega-\omega_{ij})\frac{d\omega}{2\pi} = 1. \tag{1.18}$$

If the transition frequencies ω_{ij} have a separation much larger than their width, the induced transition rate W_{ij} can be written as

$$W_{ij} = {}^1/_4\gamma^2\hbar^2(\omega)\, g(\omega-\omega_{ij})|\langle i|S_x|j\rangle|^2 \tag{1.19}$$

with

$$W_{ij} = W_{ji}. \tag{1.20}$$

These results follow from normal time dependent perturbation theory (cf. [10]).

If the population of the ith level is called n_i, then the power absorbed by the spin system due to transitions from i to j will be

$$P_m = (n_j - n_i)\hbar\omega_{ij} W_{ij}. \tag{1.21}$$

The populations will change, partly due to transitions induced by the r.f. field and partly due to transitions induced by the lattice vibrations. (Spontaneous emission can be neglected.)

We shall now consider a two-level system and call the lattice induced transition rate U_{12}, level 1 being the lowest in energy.

Multilevel systems will be considered later as they lead to rather large formulae, masking the effects we want to discuss here.

For the rate of change of the population difference we find

$$\frac{d(n_1-n_2)}{dt} = 2(-n_1U_{12}+n_2U_{21})-2(n_1-n_2)W_{12}. \tag{1.22}$$

Because of the fact that the energy exchange between the spins and the lattice, which is in the thermal equilibrium at a temperature T, takes place in quanta $\hbar\omega_{12}$, we have

$$\frac{U_{12}}{U_{21}} = e^{+(\hbar\omega_{12}/kT)} = \frac{n_{2_0}}{n_{1_0}} \tag{1.23}$$

where n_{1_0} and n_{2_0} are the equilibrium populations, having their normal Boltzmann ratio.

The exponential may be expanded as in most cases $\hbar\omega_{12} \ll kT$, and (1.22) can be rewritten using the relation $n_1+n_2=n_{1_0}+n_{2_0}$ as:

$$\frac{d(n_1-n_2)}{dt} = -[(n_1-n_2)-(n_{1_0}-n_{2_0})]\,2\bar{U}_{12}-(n_1-n_2)\,2W_{12} \tag{1.24}$$

where

$$\bar{U}_{12} = \frac{U_{12}+U_{21}}{2}.$$

The steady state solution of (1.24) is

$$n_1-n_2 = \frac{n_{1_0}-n_{2_0}}{1+W_{12}/\bar{U}_{12}}. \tag{1.25}$$

If N is the total number of spins we find with (1.19)

$$n_{1_0}-n_{2_0} = \frac{N}{2S+1}\frac{\hbar\omega_{21}}{kT} \text{ and } \frac{1}{\bar{U}_{12}} = 2\tau_1$$

$$\left.\begin{aligned} P_m &= (n_{1_0}-n_{2_0})\frac{\hbar\omega_{21}W_{12}}{1+W_{12}/\bar{U}_{12}} = \\ &= \frac{N}{2S+1}\frac{(\hbar\omega_{12})^2}{kT}\frac{{}^1/_4\gamma^2\hbar^2(\omega)\,g(\omega-\omega_{12})|\langle 1|S_x|2\rangle|^2}{1+{}^1/_2\gamma^2\hbar^2(\omega)\,g(\omega-\omega_{12})\tau_1|\langle 1|S_x|2\rangle|^2}. \end{aligned}\right\} \tag{1.26}$$

[1.4] *Spin-spin equilibrium and the resonance line shape*

[1.4.1] Spin-spin equilibrium. There have been many theories and experiments on the internal equilibrium in spin systems. The main body of the experimental work has been carried out by Gorter e.a. [11], using their relaxation methods. The spin system has many degrees of freedom, more or less coupled through the spin-spin interactions. If such a system is in internal equilibrium one can assign a temperature T_S to it and by using its density matrix

$$\varrho_S = \frac{\exp -\mathcal{H}_S/kT_S}{\sum \exp -\mathcal{H}_S/kT_S}$$

the equilibrium properties can be described. In most cases one does not have to take the total density matrix of spin system plus lattice because the spin and lattice degrees of freedom are independent, apart from a small term causing spin lattice relaxation. To obtain ϱ_S one can sum the total density matrix over all lattice states.

That the spin system is in internal equilibrium does not merely mean that the populations of the energy levels are in accordance with the Boltzmann factors. It means also that the non-diagonal elements of the density matrix are zero. Or, macroscopically, the transverse magnetization is zero.

Let us consider what happens macroscopically in the Bloch picture when at a certain time the magnetization **M** is not along the magnetic field (cf. [9] and fig. 1.4). Because of the coherence disturbing effects the

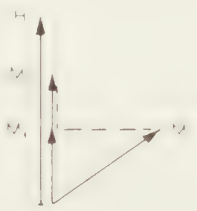

Fig. 1.4. Time behaviour of **M** according to Bloch.

transverse magnetization decreases according to (1.09) with a time constant τ_2. During this process the internal energy $\mathbf{M}\cdot\mathbf{H}$ remains constant, as in the Bloch picture a change in the spin-spin interactions is neglected. After a time of about τ_2, **M** will reach the value M_1 and the spin system will be in internal equilibrium at a temperature T_S which corresponds to its internal energy and the size of M_1.

According to Curie's law (1.08) we have

$$\mathbf{M}_1 = \frac{C\mathbf{H}}{T_S} \text{ where } \frac{T_S}{T} = \frac{n_1 - n_2}{n_{1_0} - n_{2_0}}. \tag{1.27}$$

If in paramagnetic resonance the r.f. field is much smaller than the coherence disturbing internal fields, it is still legitimate to describe the situation by means of a spin temperature. To describe the saturation behaviour one has to put in (1.26):

$$T_S = T[1 + {}^1\!/_2\gamma^2\hbar^2 g(\omega - \omega_{ij})\tau_1|\langle i|S_x|j\rangle|^2]. \tag{1.28}$$

At r.f. fields higher than the internal fields, or for times shorter than τ_2 after a shock excitation of the spin system, it is not possible to speak of a spin temperature. Phase coherence effects then play an important rôle and the state of the spin system cannot be described in terms of phaseless constants.

The studies of Gorter **e.a.** in this field have been mainly concerned

with the spin absorption at low frequencies which is closely connected with resonance line shapes, although no completely satisfactory analysis has yet been presented to relate them [12] [13]. Especially in the case of multilevel spin systems, as will be discussed in [1.6], and systems with exchange the theory is far from complete.

There have been many discussions as to whether it is allowed to split the spin system into a Zeeman part and an interaction part each with its own internal energy and temperature. This procedure has been followed by Bloembergen e.a. [14], Yokota [15] and Abragam e.a. [16]. The difficulty is that the degrees of freedom are not independent. In the case of large exchange interaction they may be considered to be commuting, which is not sufficient to justify their assumptions.

According to a theory of Kronig and Bouwkamp [17] the rate of spin transitions due to the spin interactions in a two-level system, is

$$U_S = \omega_d \, e^{-\omega^2/2\omega_d^2} \tag{1.29}$$

where $\hbar\omega$ is the energy required for the spin transition and ω_d a frequency characterizing the dipole-dipole interactions, which will be introduced later (cf. (1.35)). One may regard the exponential as the probability that the internal field just compensates the applied field, or as the amplitude of the Fourier component at frequency ω of a gaussian random fluctuating internal field. This probability readily becomes a very small quantity as ω is increased, one of the reasons why this theory was originally rejected by Broer [18].

[1.4.2] The resonance line shape. Comparing the results of the quantum theory and the classical picture, it is found that (1.26) corresponds with (1.15) when

$$g(\omega-\omega_L) = \frac{2\tau_2}{1+(\omega-\omega_L)^2\tau_2^2}.$$

This is a Lorentz line shape with a half width at half power of $1/\tau_2$. It is not surprising that the classical description leads to a Lorentz line shape, as it was introduced by assuming (1.09). This is one of the main drawbacks of the Bloch picture as experimentally one finds mostly an almost gaussian line shape in the absence of exchange interactions.

The shape of a paramagnetic resonance line will partly be determined by the lifetime broadening due to spin lattice relaxation. That contribution will have a Lorentz shape with a half width $1/\tau_1$. There are many salts in which this is the main contribution to the line width at the higher temperatures e.g. TiCs alum [19], $FeNH_4$ tutton salt etc.

This situation arises also in salts containing ions of the rare earths group, but for the iron group we have for the ions with an odd number of spins in general $\tau_1 \ll \tau_2$, making the lifetime broadening negligible.

To calculate the contribution of the spin-spin interactions to the line width two widely different methods have been used. Van Vleck applied

the method of moments to the case of identical spins [20]. He calculated

$$\int (\omega-\omega_L)^4 g(\omega-\omega_L)d\omega \quad \text{and} \quad \int (\omega-\omega_L)^2 g(\omega-\omega_L)d\omega$$

by a diagonal sum and showed that $\mathscr{H}_{ex}$ has no influence on the second moment of the absorption line, because of the commutation properties of $\mathscr{H}_{ex}$, $\mathscr{H}_Z$ and $\mathscr{H}_{rf}$. There are two contributions to the fourth moment, however, the first one due to dipole-dipole coupling alone, the second due to the rate of change of this coupling which, as we shall see later, is determined by $\mathscr{H}_{ex}$.

Anderson [21] and Kubo and Tomita [22] have developed a mathematical model which allows one to calculate the actual line shape. They assume the system to absorb a single frequency, which varies in a random way over a certain range determined by the dipole-dipole interactions, but at a rate controlled by the motions or exchange coupling. This concept was first proposed by Gorter and Van Vleck [23].

We will first split up the dipolar interaction (1.02) into terms depending on their influence on M_z

$$(1.30)\quad \begin{cases} \mathscr{H}_d = \sum_{i>j} A S_{zi} S_{zj} + B(S_i^+ S_j^- + S_i^- S_j^+) + C(S_i^+ S_{zj} + S_{zi} S_j^+) + \\ \qquad + D(S_i^- S_{zj} + S_{zi} S_j^-) + E\, S_i^+ S_j^+ + F\, S_i^- S_j^- \end{cases}$$

where $S^{\pm} = S_x \pm iS_y$ and A, B, C, D, E and F are dependent on the polar coordinates of ion i with respect to ion j.

Abragam called these terms stop-stop, flip-flop, flip-stop etc., according to their effect on M_z.

For large static fields the terms A and B will broaden the absorption line at the Larmor frequency ω_L, while the terms C, D, E and F introduce weak satellite lines at frequencies around 0, $2\omega_L$ and $3\omega_L$ (cf. fig. 1.5) [24]. The absorption near zero frequency has been the subject of many experimental studies by Gorter e.a. [11] [25] [26].

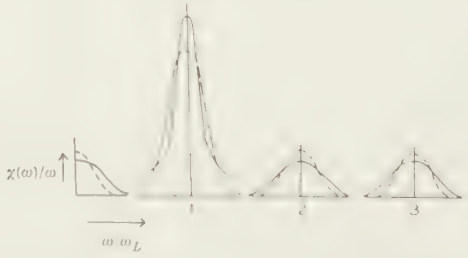

Fig. 1.5. $\chi''(\omega)/\omega$ as a function of ω/ω_L.
——— $\omega_d < \omega_{ex} < \omega_L$ — — — $\omega_{ex} < \omega_d$.

[1.4.3] The influence of exchange coupling. A brief outline of Anderson's theory [21] [27] will now be given.

We take as the Hamiltonian

$$(1.31)\qquad \mathscr{H} = g\beta H \sum_j S_{zj} + \mathscr{H}_d + 2 \sum_{j>k} J_{jk}\, \mathbf{S}_j \cdot \mathbf{S}_k + g\beta h \sum_j S_{xj}.$$

The absorption spectrum as measured by the last perturbing term is given by the Fourier integral of the time dependent operator $S(t)$

$$I(\omega) = \text{Trace } |\int S_x(t)\, e^{i\omega t} dt|^2 \tag{1.32}$$

where

$$i\hbar \frac{dS_x}{dt} = [\mathscr{H}, S_x]. \tag{1.33}$$

Since $\mathscr{H}_{ex}$ commutes with $\mathscr{H}_Z$ and with $\sum_j S_{x_j}$, the exchange interaction causes no broadening as it does not directly change the energy levels nor interrupt the radiation, but we do have

$$i\hbar\, \dot{\mathscr{H}}_d = [\mathscr{H}_Z + \mathscr{H}_{ex}, \mathscr{H}_d] \approx [\mathscr{H}_{ex}, \mathscr{H}_d]. \tag{1.34}$$

The omission of $\mathscr{H}_Z$ in the commutator expresses the assumption that $\mathscr{H}_d$ is so small as to have no appreciable matrix elements between the eigenstates of $\mathscr{H}_Z$ and also that we are only interested in the line near the Larmor frequency.

This assumption is the much discussed truncation and only valid when

$$\mathscr{H}_{ex} \ll \mathscr{H}_Z \text{ and } \mathscr{H}_d \ll \mathscr{H}_Z.$$

We thus retain only the secular terms A and B of $\mathscr{H}_d$ which results in a frequency shift of the resonance. This shift has a time variation due to (1.34) at a rate of the order of $\mathscr{H}_{ex}/\hbar$, to the effect that $\mathscr{H}_d$ is partly averaged out during the time that resonance is observed.

The assumption now is that this time variation is a gaussian random one.

The results of calculations on this basis are that the second moment has for a simple cubic lattice the value

$$\omega_d^2 = \langle|\omega - \omega_L|^2\rangle_{av} = 12.3\,\gamma^4\hbar^2 S\cdot(S+1)\,(\lambda_1^4+\lambda_2^4+\lambda_3^4-0.187)\,cd^{-6} \tag{1.35a}$$

and the fourth moment for **H** along the (100) axis.

$$\langle|\omega - \omega_L|^4\rangle_{av} = 3\omega_d^4\left[0.742 + c^{-1}\left\{0.098 \quad \frac{0.021}{S(S+1)}\right\} + \frac{\pi}{6}\left(\frac{\omega_{ex}}{\omega_d}\right)^2\right] \tag{1.35b}$$

where d is the lattice constant, c the magnetic concentration and $\lambda_{1,2,3}$ the cosines fixing the direction of **H** with respect to the crystal axes. The half width at half power of the resonance line becomes

$$\begin{aligned} \Delta\omega &= \frac{\omega_d^2}{\omega_{ex}} \quad \text{for} \quad \omega_d \ll \omega_{ex} \ll \omega_L \\ \Delta\omega &= \omega_d \quad \text{for} \quad \omega_{ex} \ll \omega_d \end{aligned} \tag{1.36}$$

with

$$\omega_{ex}^2 = \frac{8{,}48}{3}\left(\frac{J}{\hbar}\right)^2 S(S+1). \tag{1.37}$$

For the case that $\omega_{ex} \gg \omega_L$ the truncation performed in (1.34) is no longer permitted as the energies for transitions induced by the non-

secular terms of $\mathscr{H}_d$ are now available from the interactions. In the calculation of $\mathscr{H}_d$ retaining all the terms of (1.30) multiplies (1.35a) by the factor $\frac{10}{3}$.

We get

$$\Delta\omega = \frac{10}{3}\frac{\omega_d^2}{\omega_{ex}} \quad \text{for} \quad \omega_{ex} \gg \omega_L. \tag{1.38}$$

[1.4.4] Inhomogeneously broadened lines. It may be that, upon diluting a substance magnetically, $\mathscr{H}_d$ becomes smaller than variations from ion to ion in the zero field splitting or static local fields, due to ions of another kind or field inhomogeneities. For the so-called inhomogeneously broadened lines then occurring one has to modify the absorbed power (1.26). For $g(\omega-\omega_{ij})$ the single ion absorption shape is taken, but as the ions are spread over a wider line, one has to multiply the whole expression (1.26) by $\frac{g^*(\omega-\omega_0)}{g(\omega-\omega_L)}$, the ratio of the observed shape $g^*(\omega-\omega_0)$ to the single ion shape, and integrate over the distribution of the Larmor frequencies of the different ions. If $g^*(\omega-\omega_0)$ only varies slowly over the region where $g(\omega-\omega_L)$ is appreciable, then the magnetic absorption becomes:

$$P_{\text{inh}} = \frac{N}{2S+1}\frac{(\hbar\omega)^2}{kT}\frac{1/4\gamma^2\hbar^2\langle 1|S_x|2\rangle^2 g^*(\omega-\omega_0)}{\sqrt{1+1/2\gamma^2\hbar^2 g(0)\tau_1\langle 1|S_x|2\rangle^2}} \tag{1.39}$$

where g is assumed to have a Lorentzian shape [28] [29].

(To be continued)

ON THE POWER TRANSFER BETWEEN PARAMAGNETIC SPINS AND CRYSTAL LATTICE. Ib

BY

B. BÖLGER

(Communicated by Prof. C. J. GORTER at the meeting of June 27, 1959)

[1.5] *On the theory of the relaxation rates*

The energy transfer from a spin system to its environment has been the subject of many controversies, and the different mechanisms that have been proposed will be reviewed in this chapter. We shall limit ourselves to the case of non-conducting ionic crystals.

[1.5.1] Spontaneous emission. An excited spin can return to its ground state by spontaneous emission, in which case it gives a quantum $\hbar\omega$ to the radiation field. For the case of a single excited spin in free space the Einstein coefficient A for spontaneous emission is:

$$A = \frac{4\omega^3}{\hbar c^3} |\mu_{mn}|^2 \tag{1.40}$$

where μ_{mn} is the matrix element of the component $\gamma\hbar S_x$ of the magnetic moment perpendicular to the static magnetic field **H**. At frequencies $\omega/2\pi$ around 10^{10} Hz the value of A is about 10^{-12} giving a lifetime of 10^{12} s. or 10^5 years.

In resonance experiments, however, the conditions for the calculation of A are not fulfilled, and this rate will be enhanced for two reasons.

The first is that the spins are not in empty space but in an electromagnetic resonator with a quality factor Q and a volume V_c. PURCELL [30] has pointed out that in this case the energy density of the field per unit frequency range and unit volume is increased by a factor $\beta = \lambda^3 Q/8\pi^2 V_c$ making the rate for spontaneous emission

$$W_{em} = \frac{4\pi Q}{\hbar V_c} |\mu_{mn}|^2. \tag{1.41}$$

In our experiments β ranged from 50 to 500.

The second reason is that we are not dealing with a single spin, but a great number of spins, constricted within a space with dimensions smaller than the velocity of light c divided by the frequency width $\Delta\omega/2\pi$ of the transition band. In such aggregates of spins coherence effects become important and states exist with radiation rates far greater than normal [31] [32]. However, the factor by which the radiation is increased is for paramagnetic materials in saturation experiments of no importance.

[1.5.2] Lattice induced transitions. For the lattice vibrations there are two ways to influence the magnetic moment. One way is through modulation of the spin-spin interactions, the other through modulation of the electric crystal field near a magnetic ion.

In spin lattice relaxation, one spin quantum is used to excite lattice states, and as these states have a continuous spectrum, one can apply time dependent perturbation theory; the calculations differ from spin-spin relaxation ones, in which one cannot describe the relaxation mechanism in terms of a coupling between one spin and the spin system as a whole.

Waller [33] has pointed out that two essentially different processes are possible by which the lattice vibrations can take or give up the energy for the spin transition. When the spin jumps from level i to level j the energy

$$E_i - E_j = \hbar\omega_{ij} \tag{1.42}$$

is in the direct process compensated by the emission or absorption of one elastic quantum $\hbar|\omega_{ij}|$ and is induced by the part of the spin Hamiltonian linear in the displacement vectors u_k, the term $\mathscr{H}_{1_k}$ in (1.07).

In indirect processes two lattice quanta play a rôle. One $\hbar\omega_l$ is absorbed while another $\hbar\omega_k$ is emitted so that

$$\hbar|\omega_{ij}| = \hbar\omega_k - \hbar\omega_l. \tag{1.43}$$

This is called a quasi Raman process and has its origin in the quadratic terms $\mathscr{H}_{2_{kl}}$ in (1.07).

The lattice will be considered to behave according to the Debye theory. We are interested in the part of the frequency spectrum below 1/200th of the Debye temperature when dealing with the direct process. So this assumption is not a real restriction. For the indirect processes the whole frequency spectrum plays a rôle, and so the optical branch as discussed by Blackmann [34] may have an important influence at the higher temperatures.

In the Debye theory, according to the procedure of Sommerfeld and Bethe [35], the normal modes of the lattice are quantized. The lattice states are described by a set of quantum numbers p_k for each of the kth modes of the elastic vibrations. The energy of the mode is given by

$$E_k = (p_k + 1/2)\hbar\omega_k. \tag{1.44}$$

The normal coordinates q_k will have matrix elements

$$\langle p_k|q_k|p_k+1\rangle = \left\{\frac{\hbar(p_k+1)}{M\omega_k}\right\}^{1/2} \tag{1.45}$$

where M is the total mass of the crystal. As Van Vleck remarked [36] this is a weak point in the theory as it assumes that the amplitude of vibration is the same for all atoms regardless of their mass, although in

first approximation one can neglect the particle structure for long phonon wave lengths.

The number of oscillator modes in a frequency interval between ω and $\omega+d\omega$ for the longitudinal waves with velocity v_l is given by

$$\varrho_l(\omega)d\omega = \frac{\omega^2 V d\omega}{2\pi^2 {v_l}^3} \tag{1.46}$$

and for the transverse waves with velocity v_t by

$$\varrho_t(\omega)d\omega = \frac{\omega^2 V d\omega}{2\pi^2 {v_t}^3} \tag{1.47}$$

where V is the volume of the crystal. These formulae are valid for $\omega \ll \omega_c$, the cut-off or Debye frequency.

If N is the number of atoms in the crystal, there are N longitudinal and $2N$ transverse modes of vibration, so

$$\int_0^{\omega_{c_l}} \varrho_l(\omega)d\omega = N \text{ and } \int_0^{\omega_{c_t}} \varrho_t(\omega)d\omega = 2N$$

giving

$$\omega_{c_l} = \left(6\pi^2 v_l \frac{N}{V}\right)^{1/3} \quad \text{and} \quad \omega_{c_t} = \left(6\pi^2 v_t \frac{N}{V}\right)^{1/3}. \tag{1.48}$$

We can write the displacement vectors $\mathbf{u}_i$ as a linear combination of the normal modes $\mathbf{q}_k$ of the lattice,

$$\mathbf{u}_i = \sum_k a_k \mathbf{q}_k \sin \omega_k(t - r_i/v_a + \varphi_k)$$

where $v_a = v_l$ for the longitudinal modes and equals v_t for the transverse ones.

The relative displacement between the atoms i and j for waves propagating along $\mathbf{r}_{ij}$, if the wave length $\lambda_k \gg |r_{ij}|$, is

$$\mathbf{u}_{ij} = \mathbf{u}_i - \mathbf{u}_j = \mathbf{r}_{ij} \sum_k a_k \frac{\omega_k}{c} \mathbf{q}_k \cos \omega_k(t - r/v_a + \varphi_k). \tag{1.49}$$

For the direct process we are interested in matrix elements of the linear part of (1.07) corresponding to the creation or destruction of one phonon:

$$\langle p_k, i | \mathscr{H}_1(\mathbf{q}_k, \mathbf{S}_l, \mathbf{S}_m) | p_k + 1, j \rangle \tag{1.50}$$

with the condition (1.42) due to conservation of energy.

The rate U_{ij_d} at which transitions are induced in the spin system by this direct process will be

$$U_{ij_d} = \int_0^{\omega_c} \varrho(\omega_k) |\langle \mathscr{H}_1 \rangle|^2 d\omega_k \propto \int_0^{\omega_c} (\hbar\omega_k)^\alpha |\langle \mathscr{H}_1' \rangle|^2 g(\omega_k - \omega_{ij})(p_k + 1)_{\text{av}} d\omega_k \tag{1.51}$$

where the exponent α gives the frequency dependence of $\varrho(\omega_k)|\langle \mathscr{H}_1 \rangle|^2$, and $\langle \mathscr{H}_1' \rangle$ contains the matrix elements of the spin operators in $\langle i | \mathscr{H}_1 | j \rangle$.

The integrant of the second integral, which extends over all possible lattice vibrations, contains the distribution function of the spin transition centered at ω_{ij}.

If the lattice is in equilibrium at a temperature T, then the average number of phonons at a frequency ω is

$$\langle p_k \rangle_{\text{av}} = \frac{1}{e^{\hbar\omega/kT} - 1}. \tag{1.52}$$

Combining (1.51) and (1.52) one obtains for $\omega_{ij} \gg \omega_d$

$$U_{ij_d} \propto \omega_{ij}^{\alpha-1} \cdot T \text{ for } \hbar\omega_{ij} \ll kT. \tag{1.53}$$

thus at very low temperatures, the zero point vibrations determine the relaxation rates.

For the indirect process we are interested in the matrix elements of $\mathscr{H}_2$ in (1.07), quadratic in the normal coordinates:

$$\langle p_k, p_l, i | \mathscr{H}_2(\mathbf{q}_k, \mathbf{q}_l, \mathbf{S}_m, \mathbf{S}_n) | p_k + 1, p_l - 1, j \rangle \tag{1.54}$$

with (1.43) as a condition. The transition rate due to this indirect process will be

$$U_{ij_{\text{ind}}} = \int_0^{\omega_c}\int \varrho(\omega_k)\,\varrho(\omega_l)\,|\langle \mathscr{H}_2 \rangle|^2\, g(\omega_k - \omega_l - \omega_{ij})\, d\omega_k\, d\omega_l. \tag{1.55}$$

The main contribution to this integral will come from phonons around kT or $\hbar\omega_c$, depending on which is smaller. One has to go to a higher order perturbation calculation but the decrease in the matrix element is more than offset by the large increase in the number of lattice vibrations that can take part in the process at higher temperatures.

We substitute $\omega_k - \omega_l = \omega$ into (1.55) and find:

$$U_{ij_{\text{ind}}} \propto \int_0^{\omega_c}\int_0^{\omega_c} \omega_k^{\alpha}\, g(\omega - \omega_{ij})\, |\langle \mathscr{H}_2' \rangle|^2 \langle p_k + 1 \rangle_{\text{av}} \langle p_k \rangle_{\text{av}}\, d\omega_k\, d\omega \tag{1.56}$$

where $\langle \mathscr{H}_2' \rangle$ contains the matrix elements of the spin operators in $\langle \mathscr{H}_2 \rangle$.

With (1.52) one finds for (1.56)

$$U_{ij_{\text{ind}}} \propto T^2 \text{ when } kT \gg \hbar\omega_c \tag{1.57}$$

$$U_{ij_{\text{ind}}} \propto T^{\alpha+1} \text{ when } kT \ll \hbar\omega_c. \tag{1.58}$$

The case $\omega_{ij} > \omega_c$ can be neglected.

[1.5.3] The energy transfer by means of modulation of the spin-spin interactions has first been considered by Waller [33] for systems without exchange interactions. One may include the exchange interactions by considering the magneto-elastic interactions as a perturbation which causes spin transitions because of lattice strains (magnetostriction).

The dipolar coupling $\mathscr{H}_d$ (1.02) depends on the radius vector $\mathbf{r}_{ij}$ between ion i and j and will therefore be affected by the lattice vibrations.

In (1.07) the linear part becomes proportional to $\gamma^2\hbar^2/r_{ij}^4$ and the quadratic part to $\gamma^2\hbar^2/r_{ij}^5$. The non-secular terms of these perturbations come from the corresponding ones in $\mathscr{H}_d$ in (1.30), and are derivatives of the terms C, D, E and F, which can cause transitions in the spin system. WALLER arrived at values for the relaxation rate of about 10^{-1} s^{-1} at liquid air temperatures and $10^{-11}\cdot H^2$ s^{-1} in the liquid helium range. As the observed values for a typical salt such as CrK alum are 10^6 s^{-1} and 10^2 s^{-1} resp. this mechanism is too weak to explain the observed values. When there are inequivalent ions in the unit cell, as is the case for most salts, the terms A and B will also contribute to the relaxation. This, however, does not much reduce the large discrepancy.

The exchange integral J is a sensitive function of the radius vector $\mathbf{r}_{jk}$. If ions j and k are equivalent, however, the exchange interaction between them commutes with the Zeeman energy and $\mathscr{H}_{ex}$ will not be able to change the magnetization.

In [1.4.3] and the subsequent discussion we have seen that the exchange produces a random frequency modulation of $\mathscr{H}_d$, and one could therefore imagine a perturbation $\mathscr{H}_Z \to \mathscr{H}_d \to \mathscr{H}_{ex} \to$ lattice. I have made an estimate of the relaxation probability due to this process, assuming that the exchange constant J_{ij} in (1.03) is an exponentially decreasing function of the distance r_{ij} between i and j, and that $\omega_{ex} < \omega_L$.

The amplitude of the Fourier component at frequency ω_L in $\mathscr{H}_d$, due to the modulation of $\mathscr{H}_{ex}$ by the lattice vibrations, can be calculated by using (1.34), (1.49) and the above-mentioned assumption. The effect of this Fourier component on the spin operators is found by using (1.33). For the direct effect it is found that $U_{ij_d} \propto \omega_{ex}^2 T$ where ω_{ex} is defined by (1.37). For $\omega_{ex} \approx 3.10^{10}$ s^{-1} a rough estimate makes $U_{ij_d} \approx 10^{-5}$ s^{-1} at 1° K. As this rate is quite slow, this mechanism seems not to be the most important one.

BLOEMBERGEN and WANG [14] indicated that another situation arises, however, when the exchange frequency (cf. 1.37) is much larger than the Larmor frequency. For this case the 10/3 effect comes into play. The energy for a spin transition is now available in the dipole term because of the strong modulation by $\mathscr{H}_{ex}$. An analogous situation arises in the case of nuclear resonance, where the dipole term is modulated by the random velocities of the nuclei. Up to a cut-off frequency $\bar{\omega}$ one finds a white spectrum there and τ_1 becomes about equal to τ_2 if $\bar{\omega} \gg \omega_L$.

When $\omega_{ex} \gg \omega_L$ the energy exchange between "exchange system" and lattice is at a high rate, as it can take place in large quanta $\hbar\omega_{ex}$. The bottleneck for the energy transfer will presumably be between the "Zeeman" and "exchange" system. With respect to the random frequency modulation picture cf. [1.4.3] and the above-mentioned analogy, BLOEMBERGEN e.a. expect $\tau_1 \approx \tau_2$.

An example of this case is the free radical diphenyl pycril hydrazyl. BLOEMBERGEN and WANG report a value of τ_1 of 6.4×10^{-8} s. at 300° K and 77° K with $\tau_2 \approx 6\times10^{-8}$ s, while MEYER [37] found $\tau_1 \approx 10^{-7}$ s. at 4.2° K. VERSTELLE (to be published) has recently studied this effect in more detail.

As this type of relaxation is determined by the spin-spin interactions and independent of the lattice vibrations one would expect U not to depend on temperature.

[1.5.4] The influence of spin orbit interactions. Relaxation probabilities due to the modulation of the crystal electric fields are essentially single ion processes. HEITLER and TELLER [38] considered the case of substances with a spin splitting at zero magnetic field. The lattice vibrations modulate the value of D in the spin Hamiltonian (1.04) and induce transitions in the spin system accordingly. They considered only the direct process. FIERZ [39] extended these calculations to the case of indirect processes. Their results are similar to those of WALLER's when $g\beta\mathbf{H}$ is replaced by $2D$ and they find for the direct process

$$U_{ij} \approx 3.3\times10^{6}\,\omega_{ij}^{2}kT/\hbar\omega_c^{3}.$$

KRONIG [40] was the first to recognize the important possibility for heat transfer via the orbit lattice coupling. VAN VLECK [36] independently carried out similar, more detailed calculations for the special cases of Cr and Ti alum.

In the alums the paramagnetic ions X are surrounded by a near octahedron of watermolecules Y.

VAN VLECK [41] considers the influence of the normal modes of vibration Q_i of the cluster XY_6 and their effect on the orbital momentum $\mathbf{L}$ of X. The modes Q_i can again be developed into linear combinations of the lattice modes $\mathbf{q}_\ell$.

The crystal field of the cluster XY_6 around the center ion X will generally contain only terms quadratic in the Q's. Our case differs, however, from the general situation in two ways. If an orbital state of the central ion is degenerate, the Jahn Teller theorem [42] states that the octahedron will become distorted, so as to lift this degeneracy. The atoms around the cluster will partly oppose this distortion. Through this Jahn Teller effect terms linear in the Q's with even symmetry will appear in the field.

Another way to obtain linear terms is by the so-called indirect effect of atoms not belonging to the cluster XY_6. In an early analysis VAN VLECK [43] comes to the conclusion that the direct effect of distant atoms is not very important, but the influence of them on the octahedron of watermolecules is quite large and will bring linear terms in the field acting on X. More recently many paramagnetic resonance experiments have shown that this indirect effect can be large. The constants in the spin Hamiltonian

of a paramagnetic ion are found to depend on temperature, magnetic dilution, pressure and the size of the other ions present. It may be that this indirect effect of distant atoms is coupled with the Jahn–Teller effect. Only the even normal modes produce linear terms in the crystal field. They are (cf. [41]) Q_1 (total symmetric vibration, representation Γ_{1_g}), Q_2 and Q_3 (tetragonal distortion, Γ_{3_g}), Q_4, Q_5 and Q_6 (trig. dist. Γ_{5_g}) and Q_{19}, Q_{20} and Q_{21} (rotation, Γ_{4_g}).

Considering (1.04) and (1.05), there are two different ways for the lattice vibrations to influence the g-factor:

A. The adiabatic terms.

These are present when considering the change in the orbital wave functions $|n\rangle$ by the Q's only. The perturbation calculation can be carried out by keeping **S** and Q as operators, but as $(E_n - E_0)$ in (1.05) retains the same value, the second order perturbation becomes zero because of the Hermitian property of any element and the pure imaginary values of the matrix elements of $\mathscr{H}_{SO}$, while those of $\mathscr{H}_{OL}$ are real.

Van Vleck [36] showed that one has to go to a third order perturbation to get non-vanishing terms. A good example of these terms being predominant is Cr^{+++} in CrK alum. In equilibrium the water octahedron is slightly distorted along a body diagonal of the cubic alum crystal, thus producing a crystal field of trigonal symmetry with this diagonal as a symmetry axis. By taking the x, y, z-axes along the principle cubic axes, Van Vleck finds for the interaction between **S** and Q

$$(1.59)\quad \begin{cases} \mathscr{H}_{SL} = \varepsilon_1[Q_3(2S_z^2 - S_x^2 - S_y^2) + \sqrt{3}\, Q_2(S_y^2 - S_z^2)] + \\ \qquad + \varepsilon_2[Q_4(S_xS_y + S_yS_x) + Q_5(S_xS_z + S_zS_x) + Q_6(S_yS_z + S_zS_y)] \end{cases}$$

where ε_1 and ε_2 are constants proportional to $\lambda^2/(E_n - E_0)^2$.

After expressing the normal coordinates of the cluster in the normal modes of the lattice and multiplying the square of the modulus of the matrix elements by the phonon density, the relaxation rates become:

$$(1.60)\qquad U_{ij_d} = 1/\hbar^2 \langle \varrho(\omega_{ij}) | \mathscr{H}_{SL}(i p_k, j(p_k + 1)) |^2 \rangle_{\mathrm{av}}.$$

With (1.51), (1.52) and (1.53) one has $U_{ij} \propto T\omega_{ij}^2$. At low fields and at $T = 1.4\ ^\circ\mathrm{K}$ it is found that $U \approx 50\ \mathrm{s}^{-1}$.

To obtain the power which the spin system is able to transfer towards the lattice from the values of U_{ij}, one has to take a suitable average over all energy levels.

We will postpone this calculation to [1.7] where a more general discussion of the power transfer will be given.

The values of $U_{ij_{\mathrm{ind}}}$ calculated with (1.55) are independent of ω_{ij}. The value of the exponent $\wedge$ for the adiabatic processes equals 6, made up of an ω^4 dependence of the number of lattice vibrations taking part in the process, and an ω^2 factor due to (1.49).

One of the underlying assumptions for calculating $U_{ij_{\text{ind}}}$ is that the phonon wave length is large compared to the dimensions of the water octahedron, a condition which is only fulfilled at temperatures well below the Debye temperature, which is about 80° K for the alums.

B. The non-adiabatic terms.

If one takes into account the contribution of the energy of the phonon or spin jump $\hbar\omega_{ij}$ to the energy difference in the denominator of (1.05), the second order perturbation of the lattice vibrations on the spins does not become zero, and can be relatively large in cases where the energy difference of the orbital levels between which **L** has non-vanishing matrix elements, is small so that one cannot neglect $\hbar\omega_{ij}$ compared to $E_n - E_0$.

An example of this case is TiCs alum where this splitting is about 400 cm^{-1} which is small compared to the corresponding value of about 23000 cm^{-1} for Cr^{+++} in CrK alum.

When developing the energy denominator, in which because of energy conservation the phonon frequency has to be ω_{ij}, one finds for the matrix element of $\mathcal{H}_{SL}$ by perturbation with the orbital levels n

$$\langle 0, i, p_k|\mathcal{H}_{SL}|0, j, p_k+1\rangle = \\ = \sum_n \frac{-2\hbar\omega_{ij}}{(E_n-E_0)^2}\langle 0, i|\mathcal{H}_{SO}|n, j\rangle\langle n, p_k|\mathcal{H}_{OL}|0, p_k+1\rangle. \tag{1.61}$$

The relaxation rate will have the same form as in (1.59), but due to the appearance of ω_{ij} in (1.60), one finds $U_{ij} \propto \omega_{ij}{}^4 T$ for $\hbar\omega_{ij} \ll kT$.

For the indirect processes the exponent α in (1.56) will be 8, which is 2 higher than for the adiabatic terms for the same reason why ω_{ij} appeared in (1.61).

For Cu^{++} in CuK tutton salt calculations have been made by Nagaoka [44] on the same basis as those of Van Vleck. The five orbital levels in the lowest multiplet are, in a cubic crystal field, split into a lower lying doublet and a triplet with a separation Δ of 15500 cm^{-1}.

The rhombic component in the electric field splits the doublet with a separation of say Δ'. This last splitting has no influence on the g-factor in first order, but does influence the relaxation rates. The adiabatic and non-adiabatic terms seem to be of about equal importance. Nagaoka expects a highly anisotropic $1/T_1 \propto H^4$ depending on $(\Delta'/\Delta)^2$. This rate is expected to become extremely small when **H** is parallel to one of the axes of the crystal field.

[1.5.5] The Temperley effect. It has been known for a long time that the discrepancies between these theories and experiments are quite serious in the liquid helium range. The relaxation rates in that range for the concentrated salts are usually found to be a decreasing instead of an increasing function of ω_{ij} while the temperature dependence

is stronger than expected for the direct process, but not strong enough for the indirect ones. So for undiluted CrK-alum it is found that $U \propto T^3$ and for undiluted $FeNH_4$-alum $U \propto T^5$. The diluted salts seem to behave more according to VAN VLECK's theory.

TEMPERLEY [45] attempted to explain these discrepancies by supposing that by spin-spin interactions a number of spins jump at the same time, creating a phonon with the total energy. This effect could explain the field dependence of the relaxation probabilities. To explain also the temperature dependence one has to assume that a large number of spins jump together making the excited phonon frequency $\omega \gg kT/\hbar$.

VAN VLECK [36] doubted whether this effect is large enough. We shall discuss it later in more detail.

[1.6] *Equilibrium and saturation of multilevel spin systems*

[1.6.1] The attainment of equilibrium in spin systems with $S > 1/2$ can be different from the case of $S = 1/2$ in this respect, that in addition to the processes considered there, the separations of the energy levels may be such as to allow flip-flip or flop-flop processes requiring no energy. These processes become possible because of energy splittings at zero magnetic field.

GORTER, DREWES and VERSTELLE [12] used this picture for the description of their experimental results, but did not work it out so that it explains the experimental results quantitatively.

BLOEMBERGEN e.a. [46] considered the possibility that a multiple effect of the spin-spin interactions is important. The idea is that at points where the resonance lines of different spin transitions overlap, flip-flop processes ($\propto B^2$ in (1.30)) between neighbouring ions occur. They call the rate at which this takes place the cross relaxation rate U_{cr}.

Jumps in which more than two spins take part, may sometimes increase U_{cr} considerably, and for LiF it is possible to explain the short times required to establish spin equilibrium [47] by considering triple spin processes.

For the overlap they take the product of the shape functions of the two resonance lines. If these lines are far apart compared to the line width, this overlap will be small, reducing the cross relaxation rate considerably.

When saturating a single resonance line of the absorption spectrum U_{cr} becomes important when comparable with the spin lattice relaxation rate. Calculations for similar processes have been made by ANDERSON [21] when he considered the effect of the exchange on the fine structure of resonance lines. The jump rates he considered were of the order of ω_d. At this moment we are interested in much smaller rates, of the order of $10^{-6}\ \omega_d$.

The resonance transitions can be considered as weakly coupled oscillators. In the case considered by ANDERSON the coupling is strong

and one therefore gets an appreciable distortion of the initial resonance lines. In the case considered here, however, the distortion will be too small to be observable. The exact values of U_{cr} will be difficult to calculate, but there is no doubt that in concentrated salts the interactions are usually so large as to produce saturation of the total spin system when saturating a single resonance line with a radio frequency field.

[1.6.2] No cross relaxations. We will consider first the case of low magnetic concentrations without cross relaxation. At times much longer than the spin spin relaxation time τ_2 after applying a r.f. magnetic field to a sample in a static magnetic field, the transverse magnetization will be damped out, and the spin system can be described by the population densities n_i of levels i. There are $2S+1$ levels and we have always

$$\sum_{1}^{2S+1} n_i = N \tag{1.62}$$

the total number of ions present. We shall discuss the rates of change of n_i and the influence on n_i of radio frequency fields at the various resonances. This can be done by setting up equations of the type (1.22).

The transition rates from level i to level j due to interaction with the surroundings are called U_{ij} and those due to r.f. fields W_{ij} the sum being $V_{ij} = U_{ij} + W_{ij}$.

Because of (1.23) we have

$$U_{ij} = U_{ji}\, e^{\hbar\omega_{ij}/kT} \tag{1.63}$$

with $\hbar\omega_{ij} = E_i - E_j$ and also we have $W_{ij} = W_{ji}$.

We will now use a treatment analogous to that of Lloyd and Pake [48].

$$\frac{dn_i}{dt} = \sum_{j}{}' -n_i V_{ij} + n_j V_{ji} \qquad (i, j = 1 \ldots (2S+1)) \tag{1.64}$$

where the prime means that the sum is taken for all values of $j \neq i$. Of the $2S+1$ equations (1.64) there are $2S$ independent ones, from which one variable can be eliminated with (1.62). We are left with $2S$ simultaneous differential equations with $2S$ independent variables.

With a trial solution $n_i - n_{i_0} = A_i e^{-\lambda t}$ for the equations for the deviation from equilibrium one will therefore in general find $2S$ time constants. If n_{i_0} is the equilibrium solution we have in general

$$n_i = n_{i_0} + \sum_{k=1}^{2S} A_{k_i} e^{-\lambda_k t} \qquad (i = 1, 2, \ldots 2S+1) \tag{1.65}$$

where n_{i_0}, A_{k_i} and λ_k are functions of V_{pq}.

If after some time several terms in (1.65) are dominant, it will not be possible to describe the population differences with a single relaxation time.

Experimentally one can measure the population differences between two levels by measuring the resonance signal (1.21).

The steady state solution of (1.64) is obtained by putting $dn_i/dt = 0$. Being interested in the behaviour of the n_i's as a function of the induced transition probability between two specific levels, for which we can take levels 1 and 2 without loss of generality, we shall write out the equations for this case, substituting $n_1 - n_2 = \Delta_{12}$

(1.66)
$$\left\{\begin{array}{l}
-\Delta_{12} \sum\limits_{j \neq 1,2} (V_{1j} + U_{12} + W_{12}) + n_2(U_{21} - U_{12} - \sum\limits_{j \neq 1,2} V_{1j}) + \ldots \\
\qquad\qquad + n_p V_{p1} + \ldots + n_{2S+1} V_{2S+1,1} = 0 \\
\Delta_{12}(U_{12} + W_{12}) \qquad + n_2(U_{12} - U_{21} - \sum\limits_{j = 1,2} V_{2j}) + \ldots \\
\qquad\qquad + n_p V_{p2} + \ldots + n_{2S+1} V_{2S+1,p} = 0 \\
\cdots\cdots\cdots\cdots\cdots\cdots\cdots\cdots\cdots\cdots \\
\Delta_{12} V_{1,2S+1} \qquad + n_2(V_{1,2S+1} + V_{2,2S+1}) + \ldots \\
\qquad\qquad + n_p V_{p,2S+1} + \ldots + n_{2S+1} \sum\limits_{j \neq 2S+1} - V_{2S+1,j} = 0.
\end{array}\right.$$

W_{12} appears in the first column in the first two equations. One of them can be eliminated by replacing for instance the first equation by (1.62) and we then have $2S+1$ independent equations with $2S+1$ unknowns.

With the well-known rule of CRAMER for solving a set of inhomogeneous linear equations Δ_{12} and n_k can be found. Of the determinant D of the coefficients, with W_{12} put zero, we call C_{pq} the cofactor of the pth element in the qth row. The solution is

(1.67)
$$\Delta_{12} = \frac{NC_{11}}{D + W_{12}C_{12}}$$

(1.68)
$$n_k = \frac{NC_{k1} + W_{12}C_{k1,12}}{D + W_{12}C_{12}}$$

$C_{k1,12}$ is the cofactor of the term $U_{12} + W_{12}$ in C_{k1}.

Analogous to (1.25) and (1.26) an average relaxation time can be defined characterizing the saturation of Δ_{12}

(1.69)
$$\frac{1}{\tau_{12}} = \frac{2D}{C_{12}} = 2U_{12} + 2\sum_{k=3}^{2S+1} \frac{C_{1k} V_{1k}}{C_{12}}.$$

For the difference between the populations of level j and k one can write with (1.68)

(1.70)
$$\Delta_{jk} = N \frac{C_{j1} - C_{k1} + W_{12}(C_{j1,12} - C_{k1,12})}{D + W_{12}C_{12}}.$$

The powers absorbed at the various frequencies in the case of well-separated resonances is found from

(1.71)
$$P_{ij} = \Delta_{ij} \hbar\omega_{ij} W_{ij}.$$

Relations between the various cofactors can be obtained by realizing the in equilibrium

$$(\Delta_{jk})_{W=0} = \frac{N}{2S+1}\frac{\hbar\omega_{jk}}{kT}. \tag{1.72}$$

The cases pertaining to the experimental conditions will be calculated in the appropriate places.

[1.7] *The power transfer between spin and lattice systems*

The relaxation rates as discussed in [1.5] enable us to calculate the power transfer between spin and lattice systems. For the case of cross relaxation rates faster than the spin lattice relaxation rate, the spin system will come into equilibrium at a temperature T_S in a time $1/U_{cr}$, short compared to τ_1. The spin lattice relaxation will then take place according to a simple exponential decay e^{-t/τ_1}, and is due to the power transfer of all transitions. To express the power transfer between spins and lattice we will not use the populations n_i of the different levels. This can be done for the case where the spectrum consists of well-separated lines, but if these are overlapping ones, individual level populations lose their meaning.

For the power absorbed from a r.f. magnetic field by the magnetic material, we have (cf. (1.26))

$$P_m = QW/T_S \tag{1.73}$$

where W is the induced transition rate W_{ij}, summed over all possible Larmor frequencies present in the material. The distribution of the spins over their energy levels is described by the density matrix.

$$\varrho_S(E_i) = \frac{\exp -E_i/kT_S}{\sum_i \exp -E_i/kT_S} \tag{1.74}$$

where E_i are the eigenvalues of the spin Hamiltonian $\mathcal{H}_{sp}$ with interactions.

[1.7.1] Direct processes. For the lattice induced transition rates due to the direct processes, we take the integrant of (1.51), without the shape factor. Integration over the shape of the transition as was performed there, is not necessary as we include here the spin-spin interactions in the spin Hamiltonian.

The energy transferred from the spin system in temperature equilibrium to the lattice, by the direct process will be:

$$P_{tr} = \sum_{ij} \hbar\omega_{ij}[U_{ij_d}\varrho_S(E_i) - U_{j i_d}\varrho_S(E_j)]. \tag{1.75}$$

Due to conservation of energy we have $\omega_k = \omega_{ij}$ and with (1.51) formula (1.75) becomes

$$P_{tr_d} = \sum_{ij} (\hbar\omega_{ij})^{\alpha+1} |\langle i|\mathcal{H}_1'(\mathbf{S})|j\rangle|^2 \{\varrho_S(E_i)(p_{ij}+1) - \varrho_S(E_j)p_{ij}\}. \tag{1.76}$$

The factor in brackets contains the part dependent on spin and lattice temperature T_L.

For $T_S \to \infty$ it is seen that, when p_{ij} stays finite, the power transfer becomes independent of p_{ij} and is proportional to the number of ions in the upper state. The power transfer then found could be called spontaneous emission of phonons analogous to the situation with photons.

For the case $\hbar\omega_{ij} \ll kT_L$, (1.76) can be rewritten with (1.52) as:

$$P_{\mathrm{tr}_d} = \sum_{ij} \eta_{ij_d} T_L\left(\frac{1}{T_L} - \frac{1}{T_S}\right) = \eta_d T_L\left(\frac{1}{T_L} - \frac{1}{T_S}\right) \tag{1.77}$$

where the power transfer constant η_d for the direct process equals

$$\eta_d = \sum_{ij} \eta_{ij_d} = \sum_{ij} (\hbar\omega_{ij})^{\alpha+1} |\langle i|\mathscr{H}_1'(\mathbf{S})|j\rangle|^2. \tag{1.78}$$

The summation in (1.78) may be performed by a diagonal sum.

For the case of Cr^{+++} in CrK alum we found (cf. [1.5.4]) that α equals 3 for the adiabatic terms in the direct process. For η_d we then find:

$$\eta_d \propto \mathrm{Tr}[[\mathscr{H}_1' \mathscr{H}_{\mathrm{sp}}]\mathscr{H}_{\mathrm{sp}}]^2. \tag{1.79}$$

The non-adiabatic terms would require the calculation of a sixth moment.

[1.7.2] Indirect processes. To calculate the power transfer due to the indirect processes, the same procedure as above is followed. For the transition rates we take the integrant of (1.55) again without the shape factor $g(\omega - \omega_{ij})$. The power transferred is then found to be

$$\left.\begin{aligned} P_{\mathrm{tr}_{\mathrm{ind}}} - \sum_{ij} \int_0^{\omega_c}\!\!\int \varrho(\omega_k)\varrho(\omega_l)|\langle i|\mathscr{H}_2'|j\rangle|^2 \varrho_S(E_i) \frac{(\hbar\omega_{ij})^2}{k}\left(\frac{1}{T_L} - \frac{1}{T_S}\right) d\omega_k\, d\omega_l = \\ = \sum_{ij} \eta_{ij_{\mathrm{ind}}} T_L\left(\frac{1}{T_L} - \frac{1}{T_S}\right). \end{aligned}\right\} \tag{1.80}$$

The power transfer constant η_{ind} due to the indirect processes becomes

$$\eta_{\mathrm{ind}} = \sum_{ij} \eta_{ij_{\mathrm{ind}}} = \sum A(\hbar\omega_{ij})^2 |\langle i|\mathscr{H}_2'|j\rangle|^2 T_L^{\alpha} \tag{1.81}$$

where A is a constant and α depends on whether adiabatic or non-adiabatic terms are important, and on the integration over the densities of the lattice vibrations (cf. (1.56)). The summation can again be performed by a diagonal sum

$$\eta_{\mathrm{ind}} \propto \mathrm{Tr}[\mathscr{H}_2' \cdot \mathscr{H}_{\mathrm{sp}}]^2. \tag{1.82}$$

[1.7.3] The influence of exchange interactions on the power transfer for the case of $S = 1/2$ is different for the direct and indirect processes. For $S = 1/2$, $\mathscr{H}_1$ and $\mathscr{H}_2$ can only contain the spin operators linearly. In section [1.4] (cf. (1.33)) we have discussed that the fourth moment of the spin operators $\sum_i S_{x,y,z_i}$ is influenced by the

exchange but because of commutation properties the second moment is not. Therefore η_d will be influenced by exchange interactions. If $\omega_{ex} \gg \omega_L$ the lattice vibrations up to the frequency ω_{ex} can be excited.

The value of η_{ind} does not depend on exchange interactions when all ions are equivalent. For $S > \frac{1}{2}$ each salt has to be considered separately.

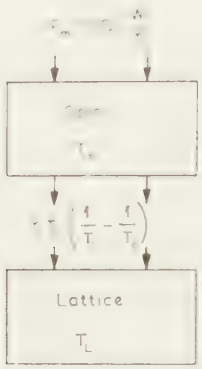

Fig. 1.6. Model for the energy balance.

[1.7.4] The power balance equations are obtained by combining (1.73) and (1.77) or (1.80). The situation is sketched in fig. 1.6. The rate of change of the internal energy U_S of the spin system is:

$$\frac{dU_S}{dt} = \frac{QW}{T_S} - \eta T_L\left(\frac{1}{T_L} - \frac{1}{T_S}\right). \tag{1.83}$$

And the steady state solution:

$$T_S = T_L + \frac{QW}{\eta} \tag{1.84}$$

which with (1.73) results in:

$$P_m = \frac{QW}{T_L + QW/\eta} \tag{1.85}$$

and for the case where (1.26) is valid

$$\tau_{1st} = \frac{Q}{2\eta T_L} = \frac{N(\hbar\omega)^2}{2k(2S+1)\eta T_L}. \tag{1.86}$$

To solve for the transient solution of (1.83) we realize that for **H** kept constant

$$\frac{dU_S}{dt} = \frac{b + CH^2}{T_S^2}\frac{dT_S}{dt} \tag{1.87}$$

where $(b + CH^2)\,T_S^2$ is the spin specific heat at constant magnetic field (cf. [11]), and C is the Curie constant. The term b is made up of the various spin interactions and the zero field splitting.

Solving (1.83) and (1.87) for the case that after $t=0$ the induced transition rate has the value W and at $t=0$ the spin temperature is $T_S(0)$:

$$(1.88) \qquad \left(\frac{1}{T_S(t)}-\frac{\eta}{QW+\eta T_L}\right) \quad \left(\frac{1}{T_S(0)}-\frac{\eta}{QW+\eta T_L}\right) e^{-\frac{QW+\eta T_L}{b+CH^2}t}.$$

The magnetization $\mathbf{M}=C\mathbf{H}/T_S$ will thus show an exponential change towards equilibrium with a relaxation time

$$(1.89) \qquad \tau_{1_{tr}}=\frac{b+CH^2}{QW+\eta T_L}.$$

The ratio between the relaxation times as found by the steady state method using formula (1.26) and by the transient method with $W=0$ is with respect to (1.86) and (1.89)

$$(1.90) \qquad \frac{\tau_{1_{tr}}}{\tau_{1_{st}}}=\tfrac{2}{3}S\cdot(S+1)(2S+1)\gamma^2\frac{(b/C+H^2)}{\omega^2}.$$

At high magnetic fields ($H^2 \gg b/C$) when the relation $\omega=\gamma H$ holds, this factor becomes 1, 4, 10, 20, 35 for $S=1/2$, 1, 3/2, 2, 5/2 respectively.

The background for the difference between $\tau_{1_{tr}}$ and $\tau_{1_{st}}$ lies in the derivation of the equation (1.26) which was obtained by considering only the relaxation probability at the saturated transition, while one actually has to consider the total power transfer between spin system and lattice as was done in formulas (1.77) and (1.83) leading to (1.85).

[1.7.5] For the case $W=0$ the values of $\tau_{1_{tr}}$ in (1.89) due to the direct process are calculated by Van Vleck [36] for CrK alum and are: $\tau_{1_{tr}}=11$; 9; 6.7; and 3 ms for H equal to 0; 0.5; 1 and 3 Kø respectively.

The order of magnitude compares well with the experimental data; however, the temperature and field dependence for concentrated substances are completely different. This will be discussed later. For the indirect processes Van Vleck finds

$$(1.91) \qquad \tau_{1_{tr}}=\tau_0\frac{b+CH^2}{b+pCH^2}.$$

This formula is identical with the formula used earlier by Brons [49] to describe the experimental results at liquid air temperatures. The value of p for CrK alum is expected to be between 0.6 and 0.4, dependent on which of the normal modes Q_i of the water octahedron is the most effective to produce relaxation, but independent of the values assigned to the cubic field splitting of the orbits and the zero field spin splitting. The value of p depends on the commutator (1.82) and is expected also not to depend on temperature. For most salts this is found not to be the case, however (cf. [11]). This discrepancy is rather serious and must not be dismissed lightly. To obtain more insight into the processes involved it seems

advisable to determine experimentally and theoretically the anisotropy of p (or η_{ind}) and the influence of the exchange interactions.

VAN VLECK has averaged his values of the power transfer over a gaussian distribution of the magnetic field, thus taking into account the effect of dipolar fields. It is better, however, to take in the commutators for calculating η, the total spin Hamiltonian with spin-spin interactions, making the calculations exact. This will be considered more fully in Chapter IV.

[1.7.6] Deviations from Curie's law. For the case that the spin splittings become of the order of kT_S, we have to contain the density matrix in (1.76) and (1.80). The magnetic absorption is most easily found by using one of the KRAMERS–KRONIG relations [50] [51]

$$\chi'(\omega_1)-\chi'(\infty)=\frac{2}{\pi}\int_0^\infty \frac{\omega\chi''(\omega)}{\omega^2-\omega_1^2}\,d\omega. \tag{1.92}$$

This relation only holds when the magnetization is a linear function of $\mathbf{h}$, so at low r.f. fields.

For the static susceptibility one finds

$$\chi_0-\chi_\infty=\frac{2}{\pi}\int_0^\infty \frac{\chi''(\omega)}{\omega}\,d\omega.$$

When the line width of the transition is temperature independent we see that the temperature dependence of χ'' and χ_0 are the same.

For many salts the Curie–Weiss law holds

$$\chi_0 \propto \chi'' \propto \frac{1}{T_S-\theta} \text{ for } T_S \gg \theta. \tag{1.93}$$

At higher r.f. fields one can in first approximation insert T_S instead of the bath temperature as is done in (1.93).

When short range order effects are neglected, the curves χ_0/χ'' vs. h^2 as drawn in fig. 1.3 will still be straight lines, with the same slope, but having the ordinate $(1-\theta/T_L)$ at $h^2=0$. So for an antiferromagnetic coupling they are higher, and for a ferromagnetic one lower. We assumed the line width to be temperature independent but this is not realised for $T_L \approx \theta$.

[1.8] *The relaxation method*

When the field applied to a paramagnetic substance is changed, the magnetization will be able to follow this change if the rate is slow enough. At higher rates $\mathbf{M}$ will have a phase lag, with subsequent absorption and dispersion. This provides a method for determining τ_1, the so-called relaxation method. The technique has been developed mainly by GORTER e.a. [11] [52].

The spin system is again regarded as an ensemble in internal equilibrium at a temperature T_S, which was first done by CASIMIR and DU PRÉ [53]. We can start therefore with (1.77) setting $W=0$

$$\Delta U_S = -\eta/T_L \Delta T\, dt. \tag{1.94}$$

We are interested in cases where $T_S \approx T_L$, as the relative variations in H are kept small. Changing H will change the internal energy by an amount

$$\Delta U_S = C_H\left(\frac{\partial T}{\partial M}\right)_H \Delta M + C_M\left(\frac{\partial T}{\partial H}\right)_M \Delta H \tag{1.95}$$

where C_H and C_M are the specific heats of the spin system at constant field and constant magnetization respectively.

On the other hand we have

$$\Delta T = T_S - T_L = \left(\frac{\partial T}{\partial M}\right)_H \Delta M + \left(\frac{\partial T}{\partial H}\right)_M \Delta H. \tag{1.96}$$

From equations (1.93), (1.94) and (1.95) ΔT can be eliminated and one arrives at the following equation

$$\left(C_H + \frac{\eta}{T} dt\right)\left(\frac{\partial T}{\partial M}\right)_H \Delta M + \left(C_M + \frac{\eta}{T} dt\right)\left(\frac{\partial T}{\partial H}\right)_M \Delta H = 0. \tag{1.97}$$

We now superpose on H a parallel sinusoidal component and look for the corresponding component in M and T_S

$$\begin{cases} H = H_c + h\, e^{i\omega t} \\ M = M_c + m\, e^{i\omega t}. \end{cases} \tag{1.98}$$

The static and the complex susceptibility are defined as resp.

$$\chi_0 = \left(\frac{\partial M_c}{\partial H_c}\right)_T \text{ and } \chi = \chi' - i\chi'' = m/h.$$

Inserting these definitions in (1.96) results in the equation for the frequency dependent susceptibility.

$$\chi/\chi_0 = \frac{i\omega C_M + \eta/T}{i\omega C_H + \eta/T} \tag{1.99}$$

or with

$$F = \frac{C_H - C_M}{C_H} = \frac{CH^2}{b + CH^2} \tag{1.100}$$

$$\tau_1 = \frac{C_H T}{\eta} = \frac{b + CH^2}{\eta T} \tag{1.101}$$

one finds

$$\chi/\chi_0 = (1-F) + \frac{F}{1 + i\omega\tau_1}. \tag{1.102}$$

At low frequencies one finds normally $\chi = \chi_0$, and at high frequencies

$$\chi_{ad} = (1 - F)\chi_0 = \frac{C_M}{C_H}\chi_0,$$

the so called adiabatic susceptibility. At these high frequencies the spin system is supposed to be still in internal equilibrium.

(To be continued)

REFERENCES

1. Van Vleck, J. H., The Theory of Electric and Magnetic Susceptibilities, Oxford Univ. Press. (1932).
2. Pryce, M. H. L., Phys. Rev. **80**, 1107 (1950).
3. Bethe, H., Ann. Phys. V **3**, 133 (1929).
4. Mulliken, R., Phys. Rev. **43**, 279 (1933).
5. Jahn, H. A., Proc. Roy. Soc. **164**, 117 (1938).
6. Pryce, M. H. L., Proc. Phys. Soc. A **63**, 25 (1950).
7. Bleaney, B. and K. W. H. Stevens, Rep. Prog. Phys. **16**, 107 (1953).
8. Bowers, K. D. and J. Owen, Rep. Prog. Phys. **18**, 304 (1955).
9. Bloch, F., Phys. Rev. **70**, 460 (1946).
10. Kramers, H. A., Quantentheorie des Elektrons und der Strahlung, Leipzig (1938), P. 216.
11. Gorter, C. J., Paramagnetic Relaxation, Elsevier Publ. Co., Amsterdam (1947).
12. Verstelle, J. C., G. W. J. Drewes and C. J. Gorter, Physica **24**, 632 (1958). Commun. Kamerlingh Onnes Lab. Leiden No. 311*b*.
13. Smits, L. J., H. E. Derksen, J. C. Verstelle and C. J. Gorter, Physica **22**, 773 (1956). Commun. no. 304*d*.
14. Bloembergen, N. and S. Wang, Phys. Rev. **93**, 72 (1954).
15. Yokota, M., J. Phys. Soc. Jap. **10**, 762 (1955).
16. Abragam, A. and W. G. Proctor, Phys. Rev. **109**, 1441 (1958).
17. Kronig, R. and C. J. Bouwkamp, Physica **6**, 290 (1939).
18. Broer, L. J. F., Thesis, Amsterdam (1945).
19. Bleaney, B., G. S. Bogle, A. H. Cooke, R. J. Duffus, M. C. M. O'Brien and K. W. H. Stevens, Proc. Phys. Soc. A **68**, 57 (1955).
20. Van Vleck, J. H., Phys. Rev. **74**, 1168 (1948).
21. Anderson, P. W., J. Phys. Soc. Jap. **9**, 316 (1954).
22. Kubo, R. and K. Tomita, J. Phys. Soc. Jap. **9**, 888 (1954).
23. Gorter, C. J. and J. H. Van Vleck, Phys. Rev. **72**, 1128 (1947), Comm. Suppl. No. 97*a*.
24. Wright, A., Phys. Rev. **76**, 1826 (1949).
25. Volger, J., F. W. de Vrijer and C. J. Gorter, Physica **13**, 653 (1947).
26. Broer, L. J. F. and J. Kemperman, Physica **13**, 465 (1947).
27. Anderson, P. W. and P. R. Weiss, Rev. Mod. Phys. **25**, 269 (1953).
28. Bloembergen, N., Thesis, Leiden (1948).
29. Portis, A. M., Phys. Rev. **91**, 1071 (1953).
30. Purcell, E. M., Phys. Rev. **69**, 681, (A) (1946).
31. Dicke, R. H., Phys. Rev. **93**, 99 (1954).
32. Bloembergen, N. and R. V. Pound, Phys. Rev. **95**, 8 (1954).
33. Waller, I., Z. Phys. **79**, 370 (1932).
34. Blackman, M., Proc. Roy. Soc. A **149**, 117 (1935).

35. Sommerfeld, A. and H. Bethe, Handbuch der Physik, Springer Verlag Berlin (1933) sec. ed. Vol 24/2, p. 500 ff.
36. Van Vleck, J. H., Phys. Rev. **57**, 426 (1940).
37. Meyer, J. W., Thesis, M.I.T. (1955).
38. Heitler, W. and E. Teller, Proc. Roy. Soc. A **155**, 629 (1936).
39. Fierz, M., Physica **5**, 433 (1938).
40. Kronig, R., Physica **6**, 33 (1939).
41. Van Vleck, J. H., J. Chem. Phys. **7**, 72 (1939).
42. Jahn, H. A. and E. Teller, Proc. Roy. Soc. A **161**, 220 (1937).
43. Van Vleck, J. H., J. Chem. Phys. **7**, 61 (1939).
44. Nagaoka, Y., J. Phys. Soc. Jap. **13**, 1328 (1958).
45. Temperley, H. N. V., Proc. Camb. Phil. Soc. **35**, Pt. II, 256 (1939).
46. Bloembergen, N., S. Shapiro, P. S. Pershan and J. O. Artman, Cross relaxations in spinsystems, Harvard Univ. Technical report no. 285.
47. Abragam, A. and W. G. Proctor, Phys. Res. **109**, 1441 (1958).
48. Lloyd, J. P. and G. E. Pake, Phys. Rev. **94**, 579 (1954).
49. Brons, F., Thesis, Groningen (1939).
50. Kramers, H. A., Atti Congr. Fis., Como 545 (1927).
51. Kronig, R., J. Opt. Soc. Amer. **12**, 547 (1926).
52. Marel, L. C. Van der, Thesis, Leiden (1958).
53. Casimir, H. B. G. and F. K. du Pre, Physica **5**, 507 (1938). Comm. Suppl. No. 85*a*.

ON THE POWER TRANSFER BETWEEN PARAMAGNETIC SPINS AND CRYSTAL LATTICE. II

EXPERIMENTAL METHODS AND TECHNIQUES

BY

B. BÖLGER

(Communicated by Prof. C. J. GORTER at the meeting of June 27, 1959)

[2.1] *Introduction*

In this chapter we shall discuss some specific techniques for determining the spin lattice relaxation time by means of paramagnetic resonance. There are two in principle different methods, which have been used up till now. With the first method, the steady state saturation technique, the decrease in relative energy absorption is measured as the microwave field strength is increased. The power transfer constant η or the relaxation time τ_1 is determined by making use of (1.85) and (1.86).

The second method displays with a low power r.f. signal the magnetic absorption and its return to equilibrium after being saturated with a pulse of high r.f. field. With the equations (1.88) or (1.65) the relaxation behaviour can be determined.

Steady state saturation is a heat transfer problem and the spins have a forced motion. The pulse method is more analogous to the relaxation method; a kind of *RC* time is measured. During the time the high power pulse is off, the spins describe a free-running precession. In the pulse method one can choose the saturating frequency to be different from the sensing frequency so that one transition is saturated and its influence on the energy level populations of other transitions is measured. These methods will be discussed at the end of this chapter.

[2.2] *Magnetic losses in resonant structures*

To increase the effects of magnetic resonance the samples are placed in a low loss resonant structure. Maxwell's equations for the electromagnetic field inside the resonator have therefore to be combined with the equations for the magnetization of the sample.

An elegant method of describing the behaviour of resonant structures has been given by PANNENBORG [1], by making use of the scattering matrix. The scattering matrix S of a junction relates the vectors of the incoming to those of the outgoing waves. One of its most important properties is that for a lossless junction S is unitary. By lumping the losses inside a resonator into an extra output line with a matched termination, its scattering matrix becomes unitary. The coupling of this line has to

be made variable when the magnetic losses are changed. When non-linear effects of the magnetization become important, such as in parametric amplifiers etc., one has to go back to Maxwell's equations.

If the modes of vibration of the resonator are well separated, one can make fruitful use of the equivalent circuit method, where all the distributed losses and stored energies are concentrated in resistances and reactances. One of the disadvantages of this method is that one has to assign a specific location to the distributed circuit parameters. At another point along the transmission line, transformation of the impedance Z takes place, due to the finite wavelength and according to the well-known transmission line equations [2]. Therefore all circuit representations will from now on refer to a certain reference plane in the transmission line. For the details of microwave theory we refer to the current handbooks [3].

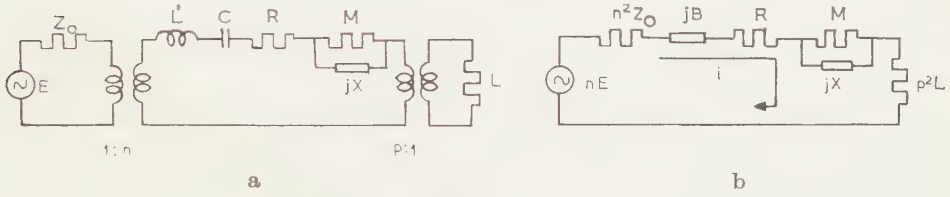

Fig. 2.1. a) Equivalent circuit of resonator with magnetic material.
b) Transformed equivalent circuit.

The resonator without magnetic material can be represented as a simple series RLC circuit (cf. fig. 2.1) with a resistance R due to the losses in cavity walls and dielectric materials present. The reactance at frequency ω equals

$$jB = j\left(\frac{\omega}{\omega_c} - \frac{\omega_c}{\omega}\right) Q_0 R \tag{2.01}$$

where ω_c is the cavity resonance frequency $1/\sqrt{L'C}$ and $Q_0 = \omega L'/R$ the quality factor.

The influence of the magnetic material can be represented by the parallel combination of resistance M and reactance jX, due to the magnetic absorption and dispersion, in series with R.

If the paramagnetic resonance line has a Lorentzian shape we can with (1.13) write for the total impedance of the magnetic material,

$$Z_m = M/1 + j(\omega - \omega_L)\tau_2. \tag{2.02}$$

The cavity is coupled to a generator and a load. This coupling can be represented by transformers with transformation ratios of $1 : n$ and $p : 1$ resp. The generator with voltage E at frequency ω is supposed to be matched to the input transmission line with a characteristic impedance Z_0. The load and the generator mesh can be transformed into the cavity mesh (fig. 2.1b).

Some of the power falling on the cavity will be reflected towards the

generator, some will be transmitted towards the load, both depending on Z_m. This provides two ways of measuring magnetic r.f. susceptibilities. by transmission and by reflection.

Quantities more accessible to physical interpretation than impedances are quality factors. Taking for the energy stored in the volume V_c of the resonator

$$G = \frac{1}{16\pi}\int_{V_c}(\varepsilon' E^2 + \mu' h^2)\,dV = \frac{1}{8\pi}\int_{V_c}\mu' h^2\,dV \tag{2.03}$$

then the quality factors are defined as:

$$\begin{cases} Q_0 = \dfrac{\omega \times \text{energy stored}}{\text{power diss. inside the cav. without magnetic abs.}} = \dfrac{\omega G}{i^2 R} \\ Q_{e_1} = \dfrac{\omega G}{\text{power dissipated in the generator impedance}} = \dfrac{\omega G}{n^2 Z_0 i^2} \\ Q_{e_2} = \dfrac{\omega G}{\text{power dissipated in the load impedance}} = \dfrac{\omega G}{p^2 L i^2} \\ Q_L = \dfrac{\omega G}{\text{total power dissipated without magnetic abs.}} = \dfrac{\omega G}{i^2(n^2 Z_0 + p^2 L + R)} \\ Q_m = \dfrac{\omega G}{\text{power dissipated in the magnetic material}} = \dfrac{\omega G}{i^2 M}. \end{cases} \tag{2.04}$$

As the inverse of the Q's we define $u = 1/Q$ with the same indices. As adding of inverse Q's has often a simple physical meaning (adding of losses) we shall use mainly the u's in the following.

The magnetically dissipated power is according to (1.14)

$$P_m = {}^1\!/_2\,\omega\chi''\int h^2\,dV_m, \tag{2.05}$$

integrated over the volume V_m of the magnetic material and so we have with (2.03) and (2.04);

$$u_m = \frac{1}{Q_m} = 4\pi f\chi'' \tag{2.06}$$

where the filling factor f equals:

$$f = \int_{V_m} h^2\,dV \Big/ \int_{V_c}\mu' h^2\,dV. \tag{2.07}$$

[2.3] *The reflection method*

[2.3.1] The reflection method to detect paramagnetic resonance and saturation will first be dealt with. The reflection coefficient Γ at a certain reference plane is defined as the ratio of the vector of the electric field of the backwards travelling wave to that of the forwards travelling wave, both waves in the same mode of propagation of the transmission line. For a transmission line with characteristic impedance Z_0 terminated by an impedance Z we have by standard microwave theory

$$\Gamma = \frac{Z - Z_0}{Z + Z_0} \tag{2.08}$$

in the plane of Z or equally

$$\frac{Z}{Z_0} = \frac{1+\Gamma}{1-\Gamma}. \tag{2.09}$$

In fig. 2.1b the load impedance can be omitted and is taken zero. For Γ one obtains:

$$\Gamma = \frac{jB+R+M/[1+j(\omega-\omega_L)\tau_2]-n^2Z_0}{jB+R+M/[1+j(\omega-\omega_L)\tau_2]+n^2Z_0}. \tag{2.10}$$

Multiplying numerator and denominator by $i^2/\omega G$, and using the definitions of the u's:

$$\Gamma = \frac{j2\frac{(\omega-\omega_c)}{\omega}+u_0+u_m\{1-j(\omega-\omega_L)\tau_2\}-u_{e_1}}{j2\frac{(\omega-\omega_c)}{\omega}+u_0+u_m\{1-j(\omega-\omega_L)\tau_2\}+u_{e_1}} \tag{2.11}$$

ω_c and ω_L are the cavity resonance and Larmor frequencies respectively.

To determine u_m two measurements are necessary. In the first place a determination of the reflection coefficient Γ_m with the magnetic field adjusted to the centre of the magnetic transition to be studied. Secondly the reflection coefficient Γ_0 with the magnetic field at a high value, making $u_m = 0$. This provides a determination of the relative external loading. When for both measurements the cavity is adjusted to resonance, then Γ_0 and Γ_m are real numbers. In the following this adjustment is always supposed to be made. We keep the sign for Γ, however, and so Γ_0 is negative when $u_e > u_0$ corresponding to an overcoupled cavity, and Γ_0 is positive when $u_e < u_0$ for undercoupling. When u_m is positive we have $\Gamma_m > \Gamma_0$ for both cases.

From the above-mentioned two measurements u_m can be calculated as we have with (2.11);

$$\frac{u_m}{u_e} = \frac{P_m}{P_{\text{ext}}} = \frac{1+\Gamma_m}{1-\Gamma_m} - \frac{1+\Gamma_0}{1-\Gamma_0} = \frac{2(\Gamma_m-\Gamma_0)}{(1-\Gamma_0)(1-\Gamma_m)} \tag{2.12}$$

where P_{ext} is the power dissipated in the external loading of the generator impedance, while there is also magnetic absorption.

Of the power P_i, incident on the iris, the part P_{cav} dissipated inside the cavity is, whilst there is also magnetic absorption,

$$P_{\text{cav}} = (1-\Gamma_m^2)P_i$$

and the reflected power is

$$P_r = \Gamma_m^2 P_i. \tag{2.13}$$

The power dissipated externally can be found from (2.11) if $\omega = \omega_c = \omega_L$ to be:

$$P_{\text{ext}} = \frac{u_e}{u_0+u_m}(1-\Gamma_m^2)P_i = (1-\Gamma_m)^2 P_i. \tag{2.14}$$

If E is the electric field strength of the incident wave, then $(1-\Gamma)E$ is the electric field inside the cavity. As the external loading does not change during the two experiments discussed above, we have with (2.14), (2.03) and (2.04) that $P_{\text{ext}} \sim W \sim h^2$. The proportionality factor between P_{ext} and h^2 is only a geometrical one.

When the r.f. field is uniform over the sample dimensions the final form of the equations becomes:

$$\frac{P_{\text{ext}}}{P_m} = \frac{T_L P_{\text{ext}}}{Q W_{ij}} + \frac{P_{\text{ext}}}{\eta} \tag{2.15}$$

$$\frac{P_{\text{ext}}}{P_m} = \frac{(1-\Gamma_m)(1-\Gamma_0)}{2(\Gamma_m-\Gamma_0)} \tag{2.16}$$

$$P_{\text{ext}} = (1-\Gamma_m)^2 P_i. \tag{2.17}$$

[2.3.2] Determination of η. A fast method of determining the reflection coefficients is to measure the power P_r reflected by the cavity with a microwave bridge. If P_i is the incident power, Γ follows from (2.13).

The first term of the right hand side of (2.15) is independent of h because $W_{ij} \sim P_{\text{ext}} \sim h^2$, giving a straight line for the $P_{\text{ext}}/P_m \sim 1/\chi''$ versus P_{ext} plot if η and T_L are independent of h. The slope is $1/\eta$.

To calculate τ_1 with (1.86) or (1.101) one only has to know, moreover, the weight of the sample and the frequency ω.

For the case of inhomogeneously broadened resonance lines the saturation behaviour becomes different (cf. [1.4.4]).

The determination of τ_1 by the method of Bloembergen, Purcell and Pound reduces to measuring the r.f. field $h_{\frac{1}{2}}$ at which χ'' has dropped to half its initial value. This occurs when the first and second terms on the right side of (2.15) become equal so that $\eta = QW_{\frac{1}{2}}/T_L$ or with (1.26)

$$\tfrac{1}{2}\gamma^2 h_{\frac{1}{2}}^2 g(0) |\langle i|S_x|j\rangle|^2 = \frac{1}{\tau_1}. \tag{2.18}$$

This method involves a calibration of h, — which is difficult to obtain more precise than 30 %, — and knowledge of $g(0)$ the matrix element. A serious disadvantage of Bloembergen's method is that when η or T_L depend on h, of which we shall see examples later, one does not use all the information available in the measurements.

[2.3.3] The polar impedance diagram. We shall briefly sketch what happens in the polar impedance diagram (cf. [2]). This diagram or Smith chart (fig. 2.2) represents the complex Γ plane. The loci of constant resistance and constant reactance form two families of orthogonal circles. The constant reactance circles, dotted dashed in fig. 2.2, have centres on Re $\Gamma = 1$; the constant resistance ones, the solid lines in fig. 2.2, their centres on the real Γ axis.

When varying the frequency of the generator, the impedance presented by an empty resonator without any other resonances nearby will, at

a certain reference plane, be a locus of constant resistance, as only the reactance is varied. The reflection coefficient is the vector drawn from the origin to the locus. Curve (a) corresponds to total reflection, $R=0$, curve (b) $R<Z_0$ corresponds to an overcoupled cavity, curve (c) $R=Z_0$, to a matched cavity and curve (d) $R>Z_0$ to an undercoupled cavity.

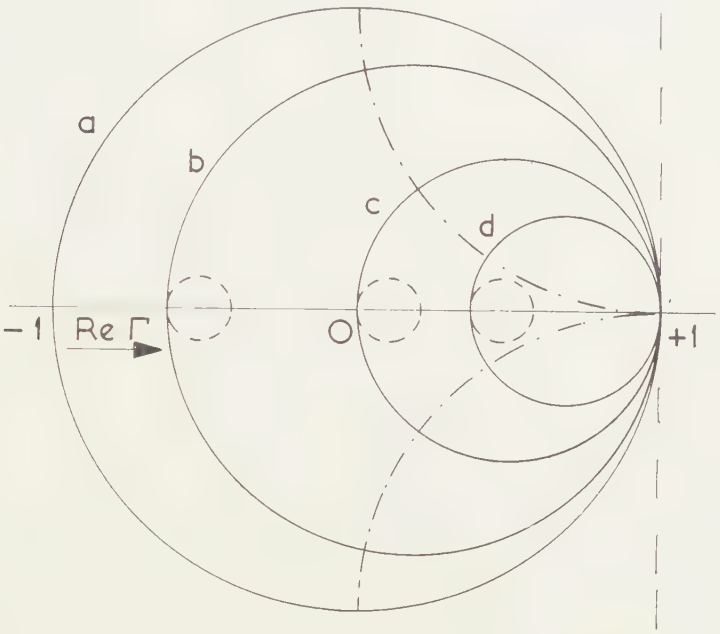

Fig. 2.2. Polar impedance diagram.

———	resistance circles.	a $R = 0$
–·–·–	reactance circles.	b $R < Z_0$
– – –	magnetic effect, H varied.	c $R = Z_0$
		d $R > Z_0$

Suppose now the cavity is at resonance (I' real), then varying ω_L (H) will change Z according to the dashed circles due to the influence of the magnetic material. The reactance part is due to dispersion, the resistance to absorption. One observes that magnetic absorption increases the reflected power for undercoupled and matched cavities and decreases it for overcoupled cavities. As long as the magnetic material is dissipative, its impedance locus has of course to stay inside the cavity locus. Magnetic materials can be brought into an emissive state. Their locus is then inverted with the cavity resonance point as the centre of inversion.

[2.4] *The transmission method*

The calculating labour involved to obtain the saturation curves with the reflection method is quite substantial and we therefore tried to find another method which required less calculating time. We should like a formula like (2.15) where instead of P_{ext} a variable is used, proportional

to the square of the radio frequency field and directly accessible to measurement. Inspecting fig. 2.1 one sees that by inserting for the load a square law detector with detector sensitivity D the signal x becomes:

$$Dx = P_L = i^2 L \propto h^2. \tag{2.19}$$

If x_m is the signal whilst the cavity and magnetization are in resonance, one finds with (2.04) and (2.11):

$$P_{Lm} = Dx_m = \frac{4u_{e_1}u_{e_2}}{(u_L+u_m)^2} P_i \tag{2.20}$$

and without magnetic absorption for the signal X_0:

$$P_L = Dx_0 = \frac{4u_{e_1}u_{e_2}}{u_L^2} P_i. \tag{2.21}$$

Dividing (2.21) by (2.20) gives

$$\frac{x_0}{x_m} = \left(1 + \frac{u_m}{u_L}\right)^2.$$

For the absorbed power we can now write with (2.04)

$$P_m = \frac{u_m}{u_{e_2}} Dx_m = \frac{u_L}{u_2} Dx_m \left(\sqrt{\frac{x_0}{x_m}} - 1\right). \tag{2.22}$$

In these formulae there are two unknown external couplings, one can be eliminated, however, by varying the generator coupling with fixed load coupling so as to maximize P_L (2.21). This makes $u_L = 2u_{e_1}$ and

$$P_L = x_0 D = \frac{u_{e_2}}{u_{e_1}} P_i. \tag{2.23}$$

Together with (2.22) follows

$$\frac{x_m P_i/x_0}{P_m} = \tfrac{1}{2}\left(\sqrt{\frac{x_0}{x_m}} - 1\right)^{-1} \tag{2.24}$$

which is the formula to be used for calculating the saturation graphs. $P_i\, x_0$ is an easily calibrated constant and $x_m \propto h^2$. If the difference $x_0 - x_m = \delta \ll x_0$ we may expand the root:

$$\frac{x_m P_i/x_0}{P_m} = \frac{x_m}{\delta}. \tag{2.25}$$

As δ and x_m are directly accessible to measurement, the calculations take very little time. The power dissipated by the magnetic material is then found to be

$$P_m = \frac{P_i}{x_0} \delta. \tag{2.26}$$

[2.5] *Apparatus for the reflection measurements*

The experiments on the steady state saturation have been carried out at microwave frequencies around 10 KMHz. For the general theory and techniques of microwaves reference is made to the current handbooks on the subject, especially those of the M.I.T. series nos. 8, 9, 10 and 11. Most of the microwave plumbing such as attenuators, tuners, cavities etc. have been designed by us and were made in one of the laboratory workshops. By measuring the power incident on and reflected by a cavity, the reflection coefficient can be obtained from $P_L = \Gamma^2 P_i$. To measure these two powers separately, use is made of a microwave bridge (fig. 2.3). The bridge element was a 3db four outlet directional coupler of the RIBLET and SAAD type [4]. This element consists of pairs of coupling slots and is by far superior to the usual magic Tee because of the inherent directivity of each pair of slots.

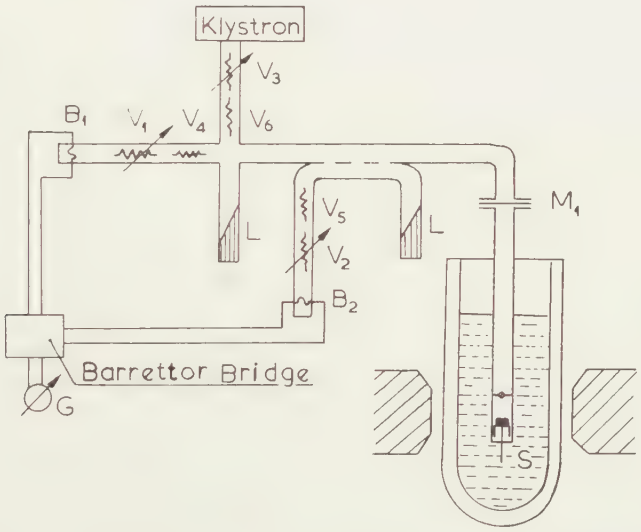

Fig. 2.3. Apparatus for measurements of reflection coefficients.
B_1 and B_2 barrettors; $V_1 \ldots V_6$ attenuators; L matched load; M_1 vacuum seal; S sample in $2\lambda_g$ long cavity.

Initially a magic Tee has been used but sliding screw tuners were needed to obtain satisfactory behaviour of this bridge element.

For the high power microwave source was used a Philips 55395, a two cavity klystron, able to deliver 140 to 200 Watt C.W. power in the X band [5].

Because of the high powers used, special care has to be taken to prevent burning out of attenuators and detectors. For V_3 we constructed a water attenuator, while the fixed attenuators V_4, V_5 and V_6 were made of a ceramic caslode. Their size was chosen so as to keep the power dissipation in the calibrated variable attenuators V_1 and V_2 below the burning out level.

These variable attenuators contained a platinized glass vane as dissipative element. They were calibrated 3 times at three frequencies far apart with the aid of a barrettor bridge and also compared to each other. The reproducibility was within 0.1 db.

The matched terminations were made from double tapered caslode and had a voltage standing wave ratio below 1.1 in the frequency range used. A handy sliding match was made from a long piece of tapered oak just fitting inside the wave guide ($V.S.W.R. < 1.08$).

For power detection we used silicon crystals or barrettors. Barrettors contain as sensitive element a very thin platinum wire which changes its resistance upon heating. Power measurements are made by using the equivalence of heating by microwaves or by a direct current. The barrettors were of the 821 type (Sperry or Narda Co.) with an operating resistance of 200 Ω. For power detection, barrettors compare favourably with crystals because of their good square law and burning out characteristics. They were inserted in one branch of a Wheatstone bridge, which could be balanced by varying the bridge current, causing a change in the barrettor resistance B. This current was measured by a Tinsley potentiometer. The microwave power can be found from

$$P = B(i_0^2 - i^2). \tag{2.27}$$

i and i_0 are the balancing currents required with and without microwave power respectively.

As we are interested in a change in the cavity reflection or transmission, due to saturation of the magnetic losses, when varying the incident power, a null method was used. Two barrettors were placed in neighbouring branches of a Wheatstone bridge (fig. 2.4), passing the same d.c. current. In all measurements the bridge is balanced to zero galvanometer reading and the bridge current measured by the voltage drop over the 1 Ω standard resistance by a Tinsley potentiometer. As the barrettors may need slightly different heating powers one could either give one barrettor an additional heating, by for instance a 100 KHz signal, or take the following procedure. Set switches S_1 and S_2 to the 200 Ω standard resistances R_1 and R_2, adjust G to zero by R_5. Set S_1 to barrettor B_1 and balance with bridge current by R_7 or R_8. This makes B_1 equal to 200 Ω. Set S_2 to B_2 and balance with R_5 keeping the bridge current the same. The bridge is now ready for power measurements. The incident microwave power P_i is measured by B_1 (in fig. 2.3), when setting S_1 to B_1 and S_2 to R_2 and balancing by changing the bridge current. The difference between P_r and P_i is measured by setting S_1 to B_1 and S_2 to B_2 and balancing with the attenuator V_2 in fig. 2.3.

A calibration for the difference in attenuation in the microwave bridge arms and the difference in the detecting sensitivities of B_1 and B_2 is obtained by replacing the cavity with a total reflection. To take measurements in quick succession it is necessary to heat the barrettors also to

about 200 Ω when not passing the bridge current. The time constant involved is of the order of one or two minutes and not at all the generally used time constant characterizing the ability of a barrettor to follow a modulation of the microwave power, which is of the order of 1 ms. The time constant involved here is much longer as it is determined by the establishment of a temperature distribution along the barrettor wire and holder after changing the wire dissipation.

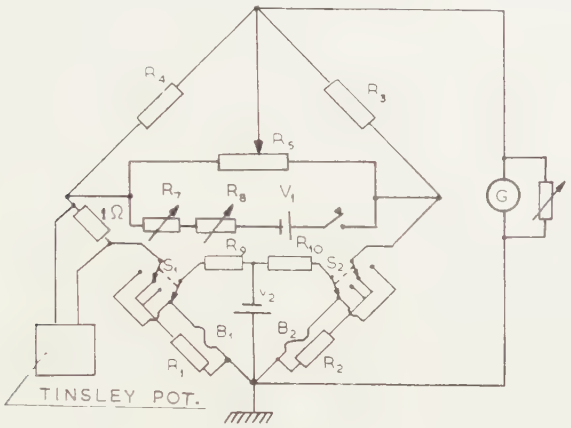

Fig. 2.4. Barrettor bridge. B_1 and B_2 barrettors.

It is more difficult to adjust the frequency of a two-cavity klystron than of a reflex klystron. Therefore the cavities had to be made tunable. Two different cavities with their cryostats were used. For the first cryostat a german silver waveguide, silvered inside, went down into the liquid helium bath, vacuum sealed on top by two thin mica windows $^1/_4\,\lambda_g$ apart. At the end was a rectangular cavity $2\lambda_g$ long with an adjustable iris. The cavity was tunable by a plunger movable from the top of the cryostat. The coupling could be adjusted before cooling to the desired value by placing a small capacitive screw in the middle of the iris. By screwing it in one initially increases the coupling, which decreases again after the iris has become resonant.

As it is not possible to adjust this coupling during a run and as sometimes the plunger stuck because of freezing, a different cavity of about 80 cm, or about 18 λ_g long was constructed. This cavity was tunable with a teflon flap and the iris consisted of a movable copper sheet. Iris and tuner were located above the vacuum seal. Since the filling factor of the paramagnetic sample decreased more than the Q increased, there was a loss in sensitivity, but having ample sensitivity to start with we could spare some in exchange for convenience. The movable iris in this case provided, when closed, the total reflection needed for calibration of the barrettor sensitivities as discussed before. For the first cavity $\Gamma = 1$ was obtained by detuning the cavity far from resonance. That this really

provided a total reflection had been checked before by interchanging the detuned cavity by a total reflection. The unloaded cavity Q's were of the order of 2800. This low value of Q_0 was taken so as to make the whole set up not too frequency-sensitive. To prevent boiling bubbles of the helium inside the cavity to change the resonant frequency, this one was filled with foamplastic. The low temperature techniques used were those customary in our laboratory. The magnet had a resistance of 2 Ω and provided a field of 10 Kø at 100 A current within a gap of about 9 cm and was constructed in the laboratory [6].

[2.6] *Apparatus for the transmission measurements*

The experiments with the transmission method were also carried out at microwave frequencies around 10 KMHz. The apparatus is sketched in fig. 2.5.

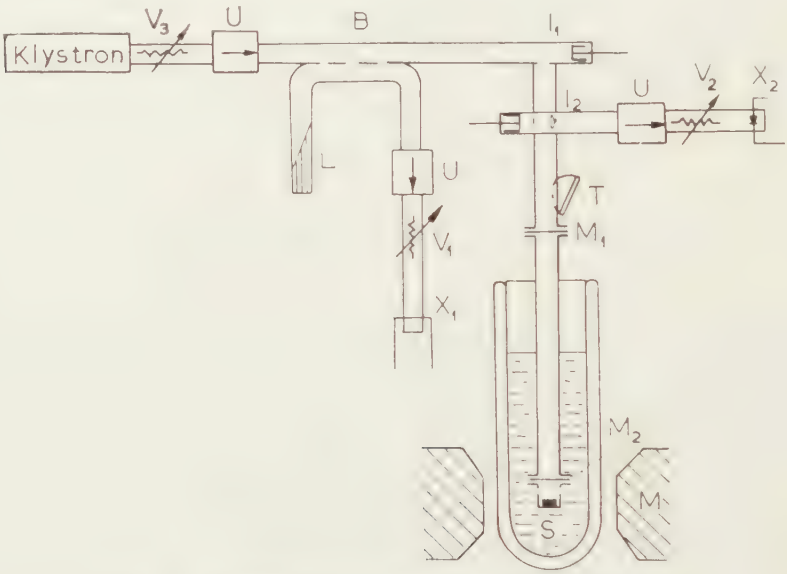

Fig. 2.5. Apparatus for transmission measurements.
B directional coupler; I_1, I_2 input, output coupling; L matched load; M_1, M_2 vacuum seals; S sample; U unilines; V attenuators; X_1, X_2 detecting crystals.

The same power source was used as with the reflection measurements. The power was detected by two carefully selected silicon crystals. The requirements for the selection were: a very close to square law detection and a difference in output between the two of less than 0.1 mV in the range from 0 to 20 mV, the difference being made zero at 20 mV.

In fig. 2.5 the incident power is sampled by crystal X_1, through a 3 db directional coupler [2.5] and the transmitted power by X_2. Their output voltages will be called x_1 and x_2 respectively from now on. The outputs were always kept below or equal to 20 mV and were measured by a Philips d.c. millivoltmeter G.M. 6010.

The cavity was about 80 cm long and tunable by a dielectric vane of teflon ($Q_0 \approx 2800$). The irises had to be made variable, the input iris I_1 in order to match the cavity to the generator, a condition set to the validity of equation (2.24), the output iris I_2 in order to be able to work in a convenient range of V_2.

An easy way of doing this is by a movable shorting plunger in the output waveguide [7] as shown in fig. 2.5. The coupling takes place through the magnetic h.f. fields and for iris I_1 for instance, maximum coupling is obtained when the short is $^1/_4\,\lambda_g$ from the centre of the iris, minimum at $^1/_2\,\lambda_g$ distance. For I_2 the situation is reversed. The two irises were placed before the tuner so that their electrical distance did not change when the insertion of the dielectric was altered.

For a series of measurements the following procedure was used.

At a static magnetic field, chosen high enough to make the magnetic losses zero, the coupling of iris I_1 was adjusted so as to maximize the transmission of the tuned cavity, I_2 being chosen beforehand to a convenient value. The microwave power is now set to make $x_2 = 20$ mV and the difference δ between x_1 and x_2 made zero, by changing V_1. During the rest of this series of measurements the attenuator setting is not changed.

The transmitted power without magnetic absorption is given by x_1, with magnetic absorption by x_2. They correspond to x_0 and x_m respectivily in formulae (2.24) and (2.25) and can be simultaneously measured. This can most conveniently be done by a $X-Y$ recorder. Most of the time we measured $x_2 - x_1 = \delta$ and x_2, as they enter directly into equation (2.25). When the tracking of X_1 and X_2 was not according to the requirements set, a correction was made. The value of the detector sensitivity P_i/x_1 in mW/mV is calibrated by substituting a barrettor for the cavity at the input branch. If this sensitivity is C db, then the input power during a run is $P_i = C + V_1 + 10 \log x_1$ dbm, db above the 1 mW level. V_1 is the attenuator setting in db.

[2.7] *Pulse methods for determining the relaxation times*

The principle of this method has been indicated in [2.1]. The approach of the magnetization towards its steady state value during or after a pulse of saturating power will depend on the transition observed and the initial situation. For the case of non-important cross relaxations, the considerations in [1.6.2] provide the necessary relations for interpreting the observations. For the case of internal spin equilibrium (cf. (1.88)), or one of the time constants $1/\lambda_k$ (cf. (1.65)) much larger than the others, the change of the magnetization is according to a simple exponential.

The magnetization can be observed by a microwave signal of frequency ω_s near the transition to be studied and an intensity so low as not to disturb the system appreciably. We will call this microwave field the sensing or signal field. The magnetization can be made to deviate from its equilibrium value by a pulse of high microwave power, called the

pump power, at frequency ω_p. The pump may saturate the signal transition or one of the others when present. Observation of the fall of the magnetization during the high power pulse may provide information about the cross relaxations.

The situation where $\omega_p = \omega_s$ has been employed by Bowers and Mims [8] and also by Davis and Strandberg [9]. An apparatus for this type of measurements is under test in our group, but only preliminary measurements have been made with it. In our set up $\omega_s/2\pi$ can be changed in steps of about 100 MHz to other cavity resonances in the range of 8.3 to 11 KMHz. The apparatus is essentially the same as used for the transmission measurements. The signal frequency is generated by a low power klystron and is detected by a superheterodyne receiver with a sensitivity of about 10^{-12} W.

Experiments with $\omega_s\, 2\pi$ 1420 MHz and $\omega_p\, 2\pi$ 4000 MHz or 10 KMHz were made in connection with the construction of a low noise microwave amplifier. From the characteristics of some types of these amplifiers it is possible to obtain information about the relaxation processes. We shall therefore mention briefly the principle of a so called three level maser as constructed by our group.

[2.8] *The principle of operation of a three level maser*

[2.8.1] Introduction. In conventional microwave amplifiers (travelling wave tubes and klystron amplifiers) the source of energy is the kinetic energy of an electron beam which introduces a certain amount of noise into the amplifier. Recently it has been found possible to amplify a microwave signal by converting the internal energy of an atomic system directly into microwave energy. When the equilibrium of the system is disturbed in a particular manner it is possible to obtain an emissive condition, and when the medium is stimulated by a microwave signal, the energy thus stored can be emitted coherently. Gordon, Zeiger and Townes [10] have coined the term "maser" to describe such "microwave amplification by stimulated emission of radiation". The small probability of spontaneous emission at radio frequencies (the main source of noise) makes it possible for such an amplifier to have a very low noise figure.

Of the many types of masers (discussed by Wittke [11]) the only one giving continuous emission is the three level maser (Bloembergen [12]) using a paramagnetic material as the working substance.

For a detailed analysis of the characteristics of three level masers reference is made to the papers by Butcher [13] and for the work on this subject by our group to [14].

[2.8.2] Principle of operation. In section [1.6] we discussed the influence of microwave fields on the energy level populations of a multilevel spin system with negligible cross relaxations. Inspecting formula (1.70) it is seen that the difference in population Δ_{jk} of level j and k can

become negative when $C_{k1,12} \gg C_{j1,12}$ and W_{12} (at the pump frequency) is large enough, while levels 1 and 2 have to be non-adjacent ones. The power absorbed by the j to k transition also becomes negative when Δ_{jk} becomes negative (cf. (1.71)) or in other words we have attained emission.

The frequency of the j to k transition will be taken to be the signal frequency ω_s. Suppose the sample is placed in a reflection cavity. When the frequencies in formula (2.11) are so adjusted that $\omega = \omega_L = \omega_s$, it is seen that the reflected power becomes larger than the incident power when $-u_m > u_0$ ($\Gamma_m < -1$) so when the emitted power is larger than that dissipated in the cavity walls ($u = 1/Q$ were defined in (2.04)). For this case we have obtained amplification. The bandwidth can be obtained from the total quality factor (Q_m is negative). Under certain conditions the power emitted by the sample will be so large that the amplifier breaks into oscillation.

Under the conditions of oscillation the signal intensity will build up, until the transition is so far saturated that the power emitted by the sample just compensates for the losses in the cavity and external coupling. The level of oscillation can be obtained from this condition

$$u_m + u_0 + u_e = 0. \tag{2.28}$$

In (1.70) Δ_{jk} is determined by the pump intensity for small signal powers. For large signals, however, Δ_{jk} will also depend on its intensity due to the presence of $V_{jk} = U_{jk} + W_{jk}$ in D and C's in (1.69).
For a spin system with only three levels calculation of (1.70) becomes easy. Numerating the levels from the lowest and pumping between levels 1 and 3 results for high pump powers (W_{13} large) in an induced absorption at ω_{23} of

$$P_{23} = \frac{N\hbar^2\omega_{32}}{3kT} W_{23} \frac{\omega_{32}\bar{U}_{23} - \omega_{21}\bar{U}_{12}}{\bar{U}_{21} + \bar{U}_{23} + W_{23}} \tag{2.29}$$

where $2\bar{U}_{ij} = U_{ij} + U_{ji}$.

The condition for obtaining negative values of P_{23} is seen to be

$$\omega_{21}\bar{U}_{12} > \omega_{32}\bar{U}_{23}. \tag{2.30}$$

At low signal powers ($W_{23} \ll U_{21} + U_{23}$) the ratio of the emitted power when $W_{13} \to \infty$ to the absorbed power when $W_{13} = 0$ is, when W_{23} is the same for both cases:

$$\frac{P_{23_{\mathrm{em}}}}{P_{23_{\mathrm{ab}}}} = \frac{u_{m_{\mathrm{em}}}}{u_{m_{\mathrm{ab}}}} = \frac{\omega_{21}\bar{U}_{12} - \omega_{32}\bar{U}_{23}}{\omega_{32}(U_{21} + U_{23})} \tag{2.31}$$

which depends only on the ratios of relaxation rates and frequencies of transitions 23 and 12, but not on filling factors, cavity Q's, sample weight etc. In case of oscillations, we have mostly $W_{23} \gg U_{21} + U_{23}$. When this

condition is fulfilled over the dimension of the sample the maximum power emitted becomes, still with $W_{13} \to \infty$;

$$P_{23_{\max}} = \frac{N}{3} \frac{\hbar^2 \omega_{32}}{kT} (\omega_{21} \overline{U}_{12} - \omega_{32} \overline{U}_{23}). \tag{2.32}$$

It is noted that this expression does neither depend on line width, when homogeneously broadened, nor on matrix element and filling factor.

[2.8.3] In the experimental arrangement the crystals were placed in cavities resonant simultaneously at the signal and pump frequencies, and cooled by a refrigerant in a Dewar glass. For the best amplifying characteristics the Q_0 of the cavity must be high at the signal frequency and preferably also at the pump frequency. The filling factor f for the signal frequency must be as high as is consistent with the requirement to saturate throughout the crystal with the pump field.

A number of cavities has been used to obtain a variety of field configurations for the different frequencies, needed for the substances tested. Cavities used for 1420 and 3850 MHz were:

(1) A coaxial cavity $\lambda/2$ long at 1420 MHz with a TE_{111} mode at 3850 MHz, and the $3\lambda/2$ coaxial mode for 4260 MHz. This cavity had a high Q_0 but the filling factor was poor. To increase f we tried:

(2) A double reentrant cavity approximately $\lambda/4$ at 1420 MHz and $^3/_4\lambda$ at 3850 MHz. To obtain the right electrical length for both frequencies, a disc of teflon or quartz was inserted at the electrical antinode of the 3850 MHz mode. As the 1420 MHz electric field was small in that region the disc mainly influenced the pump field pattern. Q_0 was 4000 at 1.3 °K. Some unwanted modes were difficult to eliminate, and also because of another experiment to be described, the following cavity was also used.

(3) A resonant strip $\lambda/2$ long at 1420 MHz placed in a rectangular cavity with either a TE_{103} or TE_{104} resonance near 3850 MHz. The strip was supported by two rectangular quartz rods which also shortened the λ_g of the 3850 MHz mode.

The cavity used for 1420 MHz and the pump frequency between 8500 and 10700 MHz was:

(4) A resonant strip $\lambda/4$ long at 1420 MHz at the base of a long rectangular cavity as described in [2.6] (cf. fig. 2.5), carrying a TE_{10n} mode.

In each of the cavities the Q_0 at 1420 MHz was between 5000 and 7000 at room temperature and the filling factors were about 30 %, except for the first one.

[2.8.4] The reflection characteristics were measured with a microwave bridge. The arrangement is sketched in fig. 2.6. The determination of cavity quality factors and amplifier characteristics is most easily performed by using a frequency swept source. This was not available in the laboratory, so we mixed the output of a sweep generator ($f \approx 50$ MHz) with that of a signal generator ($f \approx 1370$ MHz). Ample

signal strength was obtained in this way. The frequency calibration was obtained from markers provided by the sweep generator. For the bridge element a hybrid ring was constructed as described in [15]. The two cross branches with a characteristic impedance of $\sqrt{2}Z_0$ have to be slightly shorter than $\lambda_g/4$ (because of fringing fields). The isolation obtained was 30 db at 1420 MHz. Cavity number 3 is sketched in figure 2.6. Detection took place by a superheterodyne receiver (noise figure 9 db) preceded by a low pass filter F (cut-off 2000 MHz).

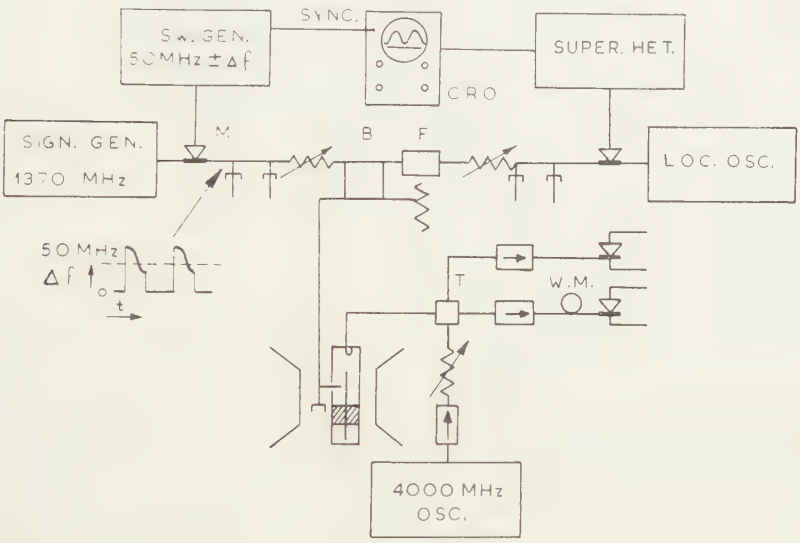

Fig. 2.6. Apparatus for experiments with two different frequencies. B bridge element for 1420 MHz; F filter; T Magic Tee for 4000 MHz.

The 4000 MHz source was a triode oscillator (EC 57) which could be pulse modulated. The rest of the apparatus at this frequency was a straightforward magic Tee bridge.

The 10 KMHz apparatus has been discussed before in [2.6]. The klystron power supply was slightly changed so as to allow pulse modulation.

[2.9] *The temperature behaviour of the quality factors*

The temperature behaviour of the cavity quality factors was peculiar. Fig. 2.7 shows the unloaded Q_0 of a reentrant test cavity, measured as a function of temperature. This cavity was silver plated on the inside. The same behaviour was observed on normally polished copper cavities. Decreasing the temperature from 300 K on, u_0 behaves as expected and decreases also. Below the temperature where the electron mean free path becomes larger than the skin depth, PIPPARD [16] has shown that the u_0 has to stay constant. This temperature is about 70° K for pure annealed copper at 1420 MHz. The increase of u_0 at lower temperatures to about the same value as at 300° K is most unexpected. We should like to explain

this behaviour by supposing that the surface irregularities become larger than the skin depth at lower temperatures, thus increasing the losses. A check on this hypothesis was made by polishing a copper cavity with the finest emery available (0.4 μ). The increase of u_0 was not present anymore and it stayed constant below 20° K (dashed line in fig. 2.7).

Of the cavities tried at low temperatures those made of oxygen free electrolytic copper (no pores) with highly polished surfaces, and with silver soldered joints, had the highest quality factors.

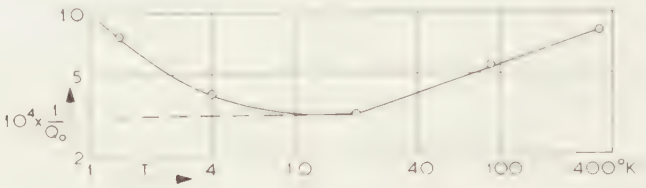

Fig. 2.7. Q_0 as a function of temperature.

[2.10] *Crystal growing*

The small crystals were obtained by normal evaporation in glass discs. In preparing diluted crystals one has to pay attention to the fact that the dilution in the solid state will usually be different from that of the solution from which the crystal was grown. For CrK alum for instance the ratio of the two dilutions may be a factor 4.

For the larger crystals, like those used for the masers, a more sophisticated growing procedure has to be followed. The crystals in question were $K_3(Co(CN)_6$ with a small content of $K_3Cr(CN)_6$ (≈ 1 %). This last substance is rather unstable and the solution may not be heated too much.

The crystals, hanging in the solutions, were rotated back and forth while cooling slowly in a thermostat from 32° C to about 25° C in one week. Rotating the crystals in one direction only, decreased the growing speed considerably. The solutions (without the crystals) had been saturated by placing them in a separate thermostat at about 35° C for some time. The difference between the starting temperature (32° C) and the solution preparation temperature should not be too large, the oversaturation will otherwise become too high and the solution will crystallize out immediately. Crystals weighing about 100 g. were obtained in this way without too much difficulty.

[2.11] *Errors*

The attenuators used were calibrated to within 0.1 db at the frequencies used. The detecting sensitivities of the crystals were calibrated by using a barrettor, the voltage standing wave ratio of which was measured. From repeated measurements the accuracy of this calibration is estimated to be of the order of 0.1 db.

When using the reflection method the value of l'_0 was determined for

every point separately by applying a high magnetic field (10 Kø). The Γ_0 chosen for calculating (2.16) was the average of these values. To prevent boiling of the liquid helium to upset the measurement, the cavity and waveguides inside the Dewar were filled with foam plastic. Nevertheless the changing helium level impaired the accuracy. The resulting accuracy of η or τ_1 from these measurements is estimated to be within 30 %.

In the transmission method more effort was put into eliminating the errors, and the reproducebility of the later measurements (cf. $CoNH_4$ tutton salt) was much better. The main sources of errors were the drift of the cavity resonance, partly eliminated by taking a low Q_0, the drift of the magnetic field and again the changing level of the liquid helium.

The difference in detecting law of X_1 and X_2 was corrected for. The accuracy of the later measurements is estimated to be about 15 %.

The pulse measurements had to be made with low signal powers and thus noise appeared on the pictures. If one takes the upper edge of the observed trace the noise does not necessarily impair the accuracy of the measurements. It is not excluded, however, that not all factors determining the time behaviour of the magnetization (such as pulse length, pump power etc.) have been controlled sufficiently and so some of the results have only a provisional character.

(To be continued)

REFERENCES

1. Pannenborg, A. F., Thesis, Delft (1952).
2. Bronwell, A. B. and R. E. Beam, Theory and Application of Microwaves. McGraw–Hill, New York, (1947) ch. 8.
3. M.I.T. Radiation Lab. series. Vol. **8**, **9**, **10** and **11**. McGraw–Hill, New York.
4. Riblet, H. J. and T. S. Saad, Proc. I.R.E. **36**, 61 (1948).
5. I am very much indebted to the N.V. Philips Gloeilampenfabrieken for the generous loan of this klystron and its power supply.
6. This magnet was designed by Prof. Dr K. W. Taconis.
7. I am very indebted to Ir H. G. Beljers for suggesting this solution.
8. Mims, W. B. and K. D. Bowers, Kam. Onnes Conf. 1958. Physica **24**, 166 (1958).
9. Davis, C. F. and M. W. P. Strandberg, Bull. Am. Phys. Soc. Ser. II **2**, 226 (1957).
10. Gordon, J. P., H. J. Zeiger and C. H. Townes, Phys. Rev. **99**, 1264 (1955).
11. Wittke, J. P., Proc. I.R.E. **45**, 291 (1957).
12. Bloembergen, N., Phys. Rev. **104**, 324 (1956).
13. Butcher, P. N., Proc. I.R.E. **105** B (1958).
14. Bölger, B., B. J. Robinson and J. Ubbink, to be published in Physica.
15. Reed, J. and G. J. Wheeler, Proc. I.R.E. Trans M.T.T. **4**, 246 (1956).
16. Pippard, A. B., Proc. Roy. Soc. **A 191**, 385 (1947).

CONTENTS

PRINTED IN THE NETHERLANDS
DRUKKERIJ HOLLAND N.V., AMSTERDAM